The University
of Manchester

MANCHESTER
1824

Metamaterial Electromagnetic Absorbers and Plasmonic Structures

A thesis submitted to the University of Manchester for the degree of

Doctor of Philosophy

in the Faculty of Engineering and Physical Sciences

2010

Adnan Noor

School of Electrical and Electronic Engineering

Table of Contents

Word Count: 30,977

List of Figures

Abstract

In this thesis metamaterial radar absorbers and plasmonic structures have been investigated. Following a brief overview covering metamaterial structures, and their applications in various areas of Microwave Engineering, a novel thin metamaterial wideband radar absorber, formed by two layers of resistive Hilbert curve arrays, is proposed and analysed numerically in HFSS, revealing a reduction in Monostatic Radar Cross Section (RCS) of more than 10 dB from 9.1 to 18.8 GHz (70% fractional bandwidth) for both polarizations. The structure has thickness of only 0.11λ to 0.24λ at lowest and highest frequencies respectively. The lateral dimensions are only 0.13λ to 0.3λ per unit cell at lowest and highest frequencies respectively which is several times smaller than that of recently reported circuit analogue absorbers operating in the similar frequency band. Furthermore, a wideband terahertz Hilbert curve array is proposed and analyzed both theoretically and numerically, showing an absorption bandwidth of more than one octave. This was followed by study of plasmonic cloak for subwavelength conducting objects. It was demonstrated that a plasmonic cloak designed for a conducting sphere will work for non spherical conducting objects of similar dimensions as well. Finally spoof plasmonic structures were investigated. A novel plasmonic structure based on a modified Apollonian fractal array of cylindrical coaxial apertures in an aluminium sheet was proposed and analyzed. The structure exhibits negative group velocity with less than 3.5 dB attenuation. Plasmonic structure based on Sierpinski array of apertures was also investigated and found to give quite good extraordinary transmission bandwidth.

Declaration

It is hereby declared that no portion of the work referred to in the thesis has been submitted in support of an application for another degree or qualification of this or any other university or other institute of learning.

Copyright Statement

i. The author of this thesis (including any appendices and/or schedules to this thesis) owns certain copyright or related rights in it (the "copyright") and he has given The University of Manchester certain rights to use such Copyright, including for administrative purposes.

ii. Copies of this thesis either in full or in extracts and whether in hard or electronic copy, may be made **only** in accordance with the copyright, Designs and patents Act 1988 (as amended) and regulations issued under it, or where appropriate, in accordance with licensing agreements which the University has from time to time. This page must form part of any such copies made.

iii. The ownership of certain Copyright, patents, designs, trade marks and other intellectual property (the "Intellectual property") and any reproductions of copyright works in the thesis for example graphs and tables ("Reproduction"), which may be described in this thesis, may not be owned by the author and may be owned by third parties. Such Intellectual property and Reproductions cannot and must not be made available for use without the prior written permission of the owner(s) of the relevant Intellectual property and/or Reproductions.

iv. Further information on the conditions under which disclosure, publication and commercialisation of this thesis, the Copyright and any Intellectual property and/or Reproductions described in it may take place is available in the University IP policy (see http:// www.campus.manchester.ac.uk/medialibrary/policies/intellectual-property.pdf), in any relevant Thesis restriction declarations deposited in the University Library, The University Library's regulations (see http://www.manchester.ac.uk/library/aboutus/regulations) and in The University policy on presentation of Thesis.

Dedication

Dedicated to my parents and teachers

Acknowledgement

List of Publications

Journal

1. A. Noor, and Z. Hu "Cloaking of Sub-wavelength Metallic Objects by Plasmonic Metamaterial Shell in Quasistatic Limit," IET Microwaves Antennas & Propagation, Feb 2009, vol. 3, Issue 1, pp 40-46.

2. A. Noor, and Z. Hu, "Dual polarised wideband metamaterial radar absorbing screen based on resistive Hilbert curve array," Electronic Letters, Jan 2009, vol. 45, Issue 2, pp 130-131

3. A. Noor, and Z. Hu, "Study of Wideband, Wide Angle, Polarization Independent Metamaterial Hilbert Curve Absorbing Screen for Terahertz Bolometers," Journal of Infrared, Millimeter and Terahertz Waves (Springer), 2010, DOI 10.1007/s10762-010-9644-x

4. A. Noor, and Z. Hu, "Metamaterial Dual Polarized Resistive Hilbert Curve Array Radar Absorber," IET Microwave Antennas and Propagation. 2010, vol. 4, Issue. 6, pp. 667–673

Conferences

1. A. Noor, and Z. Hu, "Cloaking of Conducting Cone by Plasmonic Shell in Quasistatic Limit," Antennas and Propagation Society International Symposium, 2008. AP-S 2008. IEEE , Jul 2008, pp 1-4

2. A. Noor, and Z. Hu, "Cloaking of Metallic Cube by Plasmonic Shell in Quasistatic Limit," PIERS (Progress In Electromagnetics Research Symposium) 2008, Hangzhou, China, pp 636-639

3. A. Noor, and Z. Hu, "Effects of Spacer Parameters on Resistive Hilbert Curve Array Absorbers, " in APMC (Asia Pacific Microwave Conference) 2009, pp 602-605

4. A. Noor, and Z. Hu, "Effect of Target conductivity on Plasmonic Cloak," in LAPC (Loughborough Antennas & Propagation Conference) 2009, pp 273-276

Chapter 1

Introduction

1.1 Background

Metamaterials are artificial electromagnetic materials, which give electromagnetic properties not available in natural materials [1]. They are usually fabricated using several materials or by making a pattern in a single material to obtain desired properties [1-17].

Most common types of the metamaterials are the Photonic crystals [12-16] (also called EBG, or Electronic Band Gap materials), left handed (simultaneously negative permittivity and permeability) materials [1], Metasurfaces (2D metamaterial)[11] and plasmonic (materials with permittivity less than one) materials[4].

Photonic Crystals are periodic structures and are usually made from dielectrics [12-16]. Photonic crystals allow transmission of electromagnetic waves in certain frequency bands, and block the transmission in others [12-14]. As Photonic crystals block transmission in certain frequency ranges, they are also called EBG (Electronic Band Gap) materials

Left handed materials are materials in which both the permittivity and permeability are negative. Such materials were first studied by Veselago in 1968 [19]. In that paper

Veselago analyzed the properties of such materials and showed that they have negative refractive index, and negative phase velocity.

However at the time of Veselago there was no material known that possessed both negative permittivity and negative permeability. Metals, semiconductors, and ionized gases have negative permittivity, and ferrite materials have negative permeability in a certain frequency range. However there was no known material in which both permittivity and permeability were negative

Finally left handed materials were realized from metallic structures such as arrays of thin metallic wires and open metallic rings (called SRR or Split Ring Resonators)[2]. Thin wires gave negative permittivity, and the split rings provided negative permeability. Later left handed materials were realized by loading a transmission line with inductors and capacitors [7-10].

For many applications such as absorbers the important parameter is the surface impedance. For such applications 2D metamaterials, also called metasurfaces are used to obtain the required surface impedances which are not easily available in the required frequency range [11, 12]. Examples of metasurfaces are the AMC (Artificial Magnetic Conductor) [12], artificial plasmonic surfaces [16], and artificial capacitive sheets for radar absorbers [18].

Plasmonic metamaterials are defined as materials with negative electric polarizability, which means a permittivity of less than one. In nature plasmonic behaviour is found in ionized gases, semiconductors and metals. The reason for the aforementioned

behaviour is that electrons or for that matter any charged particles take finite time to respond to a varying electric field. When an electric field is applied to a conductor, it causes movement of electrons in the conductor, and this movement of electrons generates an internal electric field opposite to the applied electric field [3]. This situation is similar to a simple harmonic oscillator [3]. As the frequency increases the response of electron will lag more and more behind the driving field. At a certain frequency, called the plasma frequency, the electrons will start to oscillate just like it is the case in a simple harmonic oscillator. The frequency at which electrons start to oscillate is called the plasma frequency. Just below the below the plasma frequency the response of the electrons to the applied field lags to such an extent that the resulting permittivity is negative.

Natural plasmonic materials are found only in certain frequency ranges and in the case of gases are not practical to use for many microwave systems. For this reason artificial bulk plasmonic materials and artificial plasmonic surfaces are needed [3]. As mentioned earlier an array of thin wires has negative permittivity below the plasma frequency. An array of thin wires is thus a bulk plasmonic material. The permittivity changes from positive to negative at the plasma frequency.

1.2 Motivation

As mentioned earlier in the discussion, metamaterials provide electromagnetic characteristics not readily available in nature. This makes them very interesting and useful for a wide range of microwave applications, ranging from compact phase shifters to efficient antennas. Because of the aforementioned useful attributes of

metamaterials, it was decided to investigate metamaterial structures for three closely related applications: absorbers, cloaks, and artificial plasmonic structures.

1.3 Aims and Objectives

The work in this thesis mainly concerns with metasurface based wave absorbers and artificial plasmonic surfaces. Aim of this work was to design novel metamaterial structures for use as radar absorbers and artificial plasmonic surfaces, furthermore the investigation of cloaking using plasmonic material was also intended.

Electromagnetic wave absorbers find a wide range of applications from the construction of anechoic chambers to reducing the radar signature of objects. Objective of the work on absorber was to design an absorber which is thin, light weight, doesn't require use of expensive materials and can be used over a wide frequency range i.e. the same concept can be applied to construct an absorber functioning at a different frequency.

Furthermore the objective in the investigation of plasmonic cloaking was to study the effect of geometric shape and the size limit for a simple plasmonic cloak. Moreover it was intended to study artificial plasmonic surfaces and to propose novel plasmonic structures.

1.4 Scope

The work covered metamaterial radar absorbers and plasmonic structures. Three different but interrelated topics were studied in course of this investigation; radar absorbers, plasmonic cloaking, and artificial plasmonic materials. Absorbers and cloaking are closely interrelated as both seek to reduce the radar signature of the object. An absorber accomplishes this by absorbing the incoming radiation, whereas cloaking by guiding the incoming wave around the object. Artificial plasmonic structures support plasmonic waves far below the frequencies at which they are found in nature. Such structures are very useful for studying the behaviour of plasma waves. A lossy artificial plasmonic surface can act as a radar absorber, as has been demonstrated later in this work.

1.5 Approach

The structures in this work were analyzed using HFSS. HFSS is a full wave frequency domain modelling. In the last chapter CST, which is a time domain full wave electromagnetic simulation software was also used along with HFSS.

Various types of traditional and metamaterial absorbers were studies and finally it was concluded that an absorber based on resistive Hilbert curve would be suitable. The advantages of the Hilbert curve absorber proposed in this work are its broad bandwidth and smaller unit cell size. Smaller unit cell size has the advantage of eliminating the unwanted diffraction effects.

A novel metamaterial absorber based on resistive Hilbert curve array was then proposed and numerically analyzed using HFSS [20]. The geometric parameters were optimized using the optimization module of HFSS. In this work instead of using a traditional conducting Hilbert curve, Hilbert curves constructed of graphite were used. The advantage of using a resistive material for the Hilbert curve is the availability of a wide absorption bandwidth. The absorber provided much wider bandwidth than the standard absorbers. Furthermore the concept was then extended to terahertz absorbers and a novel wide band terahertz absorber based on resistive Hilbert curve was presented and analyzed [21].

For the first time cloaking of non spherical subwavelength objects using a plasmonic cloak was investigated. The cloaked structures were numerically analyzed using HFSS. Moreover the cloak was analyzed for increasing wavelength normalized size in order to investigate the limitation of the cloak designed for subwalength spherical targets.

Finally artificial plasmonic surfaces based on the arrays of apertures in a conducting surface were analyzed numerically, including a novel artificial plasmonic surface based on a modified Apollonian fractal. The modified Apollonian fractal surface was observed to give negative group velocity for the wave transmitted through it. Negative group velocity is a very interesting phenomenon as it concerns issue of causality and relativity. Finally a novel plasmonic absorber was proposed and numerically analyzed . The structure gave wide absorption bandwidth for both the normal and oblique incidences.

1.6 Summery

In this work a novel metamaterial absorber based on resistive Hilbert curve array is proposed and analyzed [20]. The structure gave a wide absorption bandwidth [20] unlike traditional conducting Hilbert curve absorber which is narrow band [20]. The structure has a unit cell much smaller than the wavelength hence diffraction effects are eliminated [20]. In addition to the microwave absorber a terahertz absorber based on the same resistive Hilbert curve array concept was proposed and analyzed. The absorber provided much wider bandwidth than the standard terahertz absorbers [21].

Both the microwave and terahertz absorber were also analyzed for oblique incidence and sensitivity to the variations in design parameters. From the results it was observed that the absorber performance is not very sensitive to the variations in the design parameters and has a wide absorption bandwidth even at oblique angles of incidence.

The concept of plasmonic cloak was extended for the first time to non spherical subwavelength objects [22,23] and limitation of subwalength approximation was also investigated. From the results it was concluded that the concept is applicable even to the non spherical geometries as long as the object is smaller than the wavelength.

Furthermore work on artificial plasmonic structure gave interesting results. Wide band extraordinary transmission band was observed for proposed plasmonic structure. Moreover a completely novel artificial plasmonic structure based on array of Apollonian fractal array of aperture in a conducting surface was analyzed and the results showed the interesting phenomenon of negative group velocity. Finally a novel

plasmonic radar absorber was proposed and analyzed and the results showed a wide absorption bandwidth for the plasmonic radar absorber for normal and oblique incidence.

1.7 Thesis Layout

In the next chapter an overview of metamaterials is given. This followed by the design and analysis of the Hilbert curve absorber for microwaves and terahertz frequencies in Chapters 3 and 4. A survey of various types of absorbers was done as described in Chapter3. A metamaterial absorber based on resistive Hilbert curve was then proposed and numerically analyzed using HFSS [20]. The absorber gave much wider bandwidth than the standard absorbers. Furthermore the concept was extended to terahertz absorbers and wide band terahertz absorber based on resistive Hilbert curve was presented and analyzed[21].

Chapter 5 discusses plasmonic cloaking of subwavelength conducting objects[22,23]. The aim was to investigate reduction of the radar signature of objects by using a plasmonic cloak.

In Chapter 6 negative group velocity and extraordinary transmission through artificial plasmonic surfaces is discussed. A radar absorber based on an artificial plasmonic structure has also been proposed and analyzed in Chapter6. Finally in Chapter 7 conclusions and potential for future work are described.

Chapter 2

Theory and Overview of Metamaterials

2.1 Introduction

Wave propagation in a material is controlled by the permittivity, permeability and conductivity of the material. Consider the case of plane wave propagation in an isotropic material with zero conductivity. The complex propagation constant and characteristic impedance are given by the following equations [24]. The dielectric and magnetic losses are incorporated in the values of permittivity and permeability

$$\gamma = \alpha + j\beta = j\omega\sqrt{\mu\varepsilon} \tag{2.1a}$$

$$\eta = \sqrt{\frac{\mu}{\varepsilon}} \tag{2.1b}$$

If both the permittivity and permeability are real and have the same sign, the propagation constant will be purely imaginary, meaning a propagating wave. The impedance will be real in this case.

In the case where one of these constitutive parameters is negative, the complex propagation will be real, and the impedance will be imaginary, i.e. either inductive or capacitive.

The case in which both the constitutive parameters are negative is rather tricky. Due to the square root in (2.1a), the sign of β can either be positive or negative. The ambiguity can however removed through following analysis [24].

$$\vec{k} = \beta \hat{k} \tag{2.2a}$$

$$\vec{k} \times \overline{H} = -\omega \varepsilon \overline{E} \tag{2.2b}$$

$$\rightarrow \hat{k} \times \hat{H} = -\frac{\varepsilon}{|\varepsilon|} \hat{E} \tag{2.3a}$$

$$\rightarrow \hat{k} = \frac{\varepsilon}{|\varepsilon|} \hat{E} \times \hat{H} \tag{2.3b}$$

Similarly

$$\vec{k} \times \overline{E} = \omega \mu \overline{H}$$

$$\rightarrow \hat{k} \times \hat{E} = \frac{\mu}{|\mu|} \hat{H} \tag{2.4a}$$

$$\rightarrow \hat{k} = \frac{\mu}{|\mu|} \hat{E} \times \hat{H} \tag{2.4b}$$

where the hat denotes unit vector parallel to the vector. From the Poynting Theorem for the energy flow vector

$$\hat{S} = \hat{E} \times \hat{H} \tag{2.5}$$

Comparing (2.5) with (2.4) and (2.3) it can be observed that if both the constitutive parameters are positive then the S and k vectors are parallel and we have normal wave propagation. If however both the constitutive parameters are negative than the S and k vectors are antiparallel, meaning the k vector is pointing towards the source. The β is also therefore negative as implied by (2.1). As for the impedance, it will be positive because for any passive system the real part of the impedance has to be positive.

In the case where only one of the constitutive parameters is negative, the propagation constant will be real, and therefore only an evanescent (decaying) wave will exist. The propagation constant has to be positive as the wave is decaying away from the source (using $e^{-\gamma z}$ convention). In the case of the impedance the same problem of ambiguity arises, i.e. is the impedance inductive or capacitive.
.

The ambiguity can be solved by analyzing a standard transmission line. The transmission line can be modelled as series inductors and shunt capacitors. If the permittivity is negative, the shunt capacitance will be negative. Negative capacitance can be modelled as shunt inductance. The transmission line is thus reduced to a network of inductors. It can therefore be assumed that negative permittivity will result in inductive characteristic impedance. By the same reasoning negative permeability will result in capacitive impedance.

2.2 Types of Metamaterials

Metamaterials can be realized from a wide range of structures. Below is an overview of the commonly used metamaterial structures.

2.2.1 Resonant Structures

They are constructed from structures having electrical and magnetic resonance [3, 4]. The operating principle of such resonant structures is as follows: the response of electric plasmas and magnetic dipole lag by about 180° with respect to the Electric and Magnetic fields when the frequency is slightly below the resonance [3-5]. In the case of a magnetic dipole, the magnetic moment will lag by nearly 180° with respect to the H field, which translates into permeability being negative or less than one [4]. By the same reasoning it can be shown that electric resonant structures will provide permittivity less than one, (either negative or positive) at frequencies just below the resonance [3].

Using both electric and magnetic resonant structures it is possible to have both permeability and permittivity negative [2].

Theoretical analyses of low frequency plasma wave structures based thin metallic wires for negative permittivity materials and negative permeability material based on split ring resonators are given in [4, 5]. A later practical negative refractive index medium using thin wires and split ring resonators was first demonstrated in [2]. A brief description of thin wire plasmonic structures and split ring resonators is given bellow.

2.2.1.1 Plasma Waves and Thin Wire Plasmonic Structures

Plasma waves are also called space charge waves. These occur in conductors and semiconductors. These waves arise because electrons or for that matter any charged particles take finite time to respond to a varying electric field.

When an electric field is applied to a conductor, it causes movement of electrons in the conductor, and this movement of electrons generates an internal electric field opposite to the applied electric field [3]. This situation is similar to a simple harmonic oscillator [3].

In ordinary conductors, the plasma frequency ranges from visible to near ultraviolet, whereas in the case of semiconductors, it ranges from millimetre waves to infrared [3]. In order to create low frequency plasmonic material, one would need to increase the effective mass of the electrons [3].

This is accomplished using an array of thin metallic wires [3]. Thin wires have high inductance [18] and the inductance of wires increases the effective mass of electrons [3]. How the inductance increases the effective mass can be explained as follows [3]. Effective mass is the ratio of the applied force to the acceleration of an electron. Acceleration of electrons means change in current, as the current is directly proportional to the drift velocity of electrons. Inductance hinders change in current, and consequently opposes acceleration of electrons, thus increasing the effective mass. Square of plasma frequency is directly proportional to the density and inversely proportional to the effective mass of electron [3]. Using thin wires therefore it is

possible to bring plasma frequency into microwave region. A thin wire array plasmonic structure is shown in Fig. 2.1 [3].
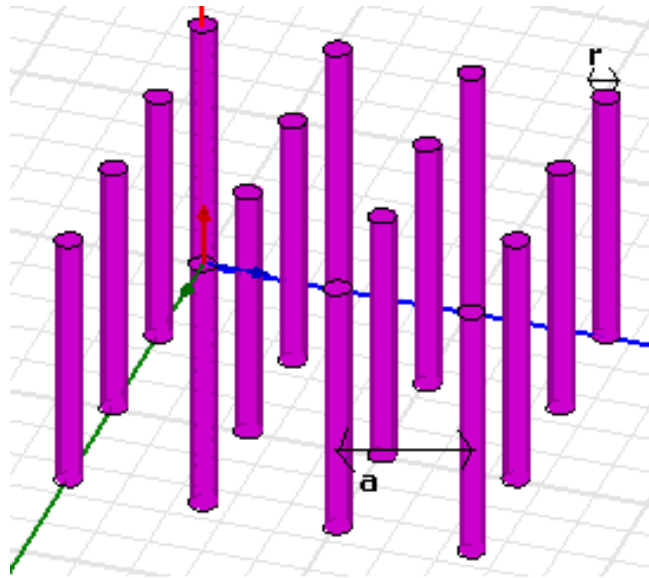
Fig 2.1 Thin wire array for low frequency plasmonic structure.

Plasma frequency and effective permittivity of such a structure is given by following formulas [3]

$$\omega_p = \frac{c}{a}\sqrt{\frac{2\pi}{\ln\left(\dfrac{a}{r}\right)}} \tag{2.6}$$

$$\varepsilon_{eff} = 1 - \frac{\omega_p^2}{\omega\left(\omega + \dfrac{i\varepsilon_0 a^2 \omega_p^2}{\pi r^2 \sigma}\right)} \qquad (2.7)$$

where a is spacing between wires, r is radius of wires, c is velocity of light in free space, and σ is conductivity of the metal used .

2.2.1.2 SRRs (Split Ring Resonators)

A split ring resonator is constructed by having two concentric metallic rings, with a gap in each ring, and the gaps are $180°$ apart. A split ring resonator is shown in the Fig 2.2 [4, 5].
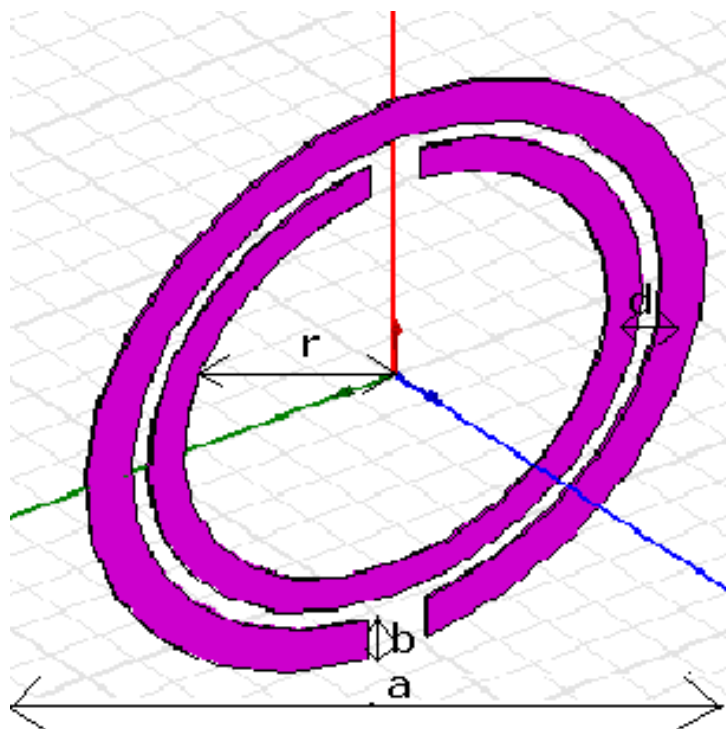
Fig 2.2 A split ring resonator.

An actual negative permeability material is constructed using a 3D array of split ring resonators [4, 5]. The split ring resonator acts as an artificial magnetic dipole [4, 5]. The gap between inner and outer ring acts as a capacitor while the rings themselves act as an inductor, resulting in an LC resonant circuit [5]. Just below resonance, the magnetic dipole due to the split rings will lag the H field by roughly 180 degrees resulting in negative permeability. Permeability of a split ring resonator array is given by the following formula [5],

$$\mu_{eff} = 1 - \frac{\dfrac{\pi r^2}{a^2}}{1 - \dfrac{3lc}{\pi \omega^2 \ln\left(\dfrac{2b}{d}\right) r^3} + \dfrac{2l\sigma}{\omega r \mu_0} i} \tag{2.8}$$

where r is the inner radius of the inner ring, b is thickness of the ring, d is the spacing between rings a is the lattice constant of a 3D SRR in the plane of the rings, l is the lattice constant along the axis of the rings.

Besides bulk metamaterial, an array of split ring resonators can also be used as a metasurface.

2.2.2 Transmission Line Based Structures.

Initially metamaterials were based on resonant structures [3-5]. Resonant structures are lossy and narrow band, as can be deduced from the formulas for their effective

constitutive parameters, which limits their useful application. To solve this problem a new class of metamaterials based on a periodically loaded transmission line was first proposed in [6] .

The concepts described below have been presented in [6-8]. In a standard transmission line, inductance is in series and capacitance in parallel, as shown in the Fig. 2.3.
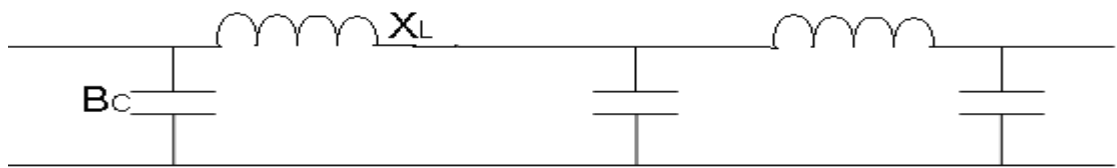
Fig 2.3 Right handed transmission line.

In Fig. 2.3, B_C is capacitive susceptance and X_L is inductive reactance. Susceptance of a capacitor and reactance of an inductor are positive, meaning both per unit length reactance and susceptance are positive. However, if capacitors are inserted in series and inductors in parallel, as shown in the Fig. 2.4, the transmission line (TL) per unit length impedance will become capacitive and admittance inductive (if the values of capacitors and inductors are chosen properly), i.e. both per unit length reactance and susceptance will be negative [6].
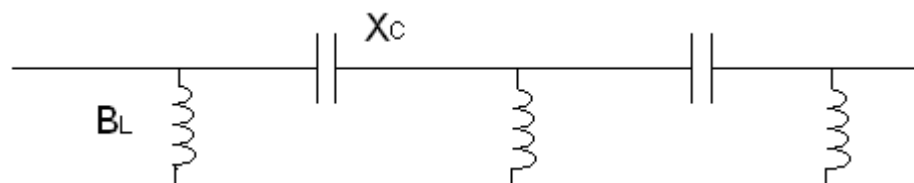
Fig 2.4 Left handed transmission line.

31

The above mentioned loaded TL is equivalent to a standard TL with negative per unit length inductance and capacitance. Negative inductance can in turn be modelled by placing a standard TL in a medium with negative magnetic permeability and negative capacitance by placing the TL in a medium with negative permittivity [6].

It can be concluded from the above discussion that if both per unit length reactance and susceptance are made negative, the TL can be modelled by an unloaded TL placed in a medium with simultaneous negative permittivity and permeability [7].

The TL approach offers the advantage of ease of fabrication (as it is a planar structure, unlike SSR based negative refractive index (NRI) material), low loss, and wider bandwidth of negative refractive index operation [6].

A real TL will always have parasitic shunt capacitance and series inductance. Therefore, in case of a practical periodically loaded TL, the equivalent circuit is shown in the Fig. 2.5 [9].
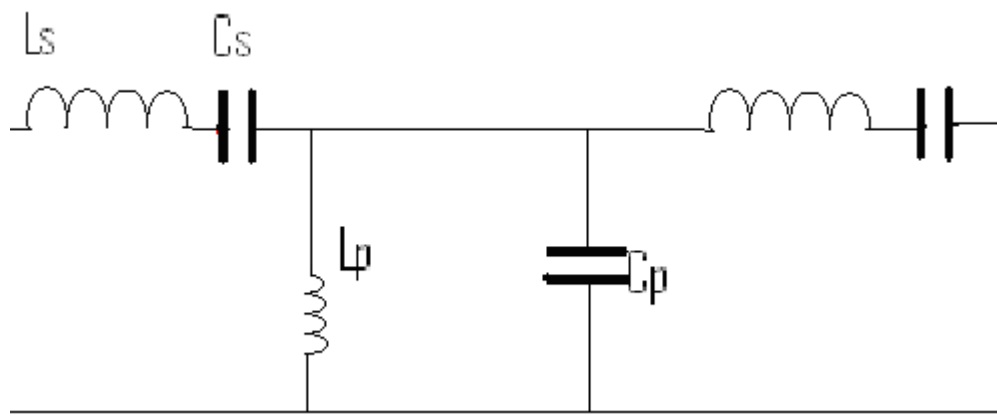
Fig 2.5 CLRH Transmission line

Such TL is called Composite Left/Right Handed (CRLH) TL [10,11].The per unit length impedance and admittance are given by following equations, provided the size of unit cell is considerably smaller than the wavelength of operation [9,24].

$$x = x_L + x_C = \omega L_s - \frac{1}{\omega C_s l} \tag{2.9a}$$

$$b = b_C + b_L = \omega C_p - \frac{1}{\omega L_p l} \tag{2.9b}$$

$$z = jx \tag{2.9c}$$

$$y = jb \tag{2.10d}$$

where x, b, z, and y are per unit length reactance, susceptance, impedance and admittance respectively; L_s and C_p are per unit length intrinsic inductance and capacitance, L_p and C_s are per unit cell shunt inductance and series capacitance of the loading elements added to transmission line, and finally l is length of unit cell.

It can be concluded from (2.9a) and (2.10b) that for frequencies below the resonance of the series branch, per unit length reactance is negative, which means effective per unit length inductance is negative, which in turn means that effective permeability is negative. Using similar arguments, it can be said that for frequencies below resonance of the shunt branch, effective permittivity will be negative [9].

If both permittivity and permeability are negative then, phase velocity is also negative

and the transmission line is left handed. If only one of the effective constitutive parameter is negative, then phase velocity and impedance will be imaginary, corresponding to a stopband of the transmission line. When series and shunt branches have the same resonant frequency, there is no stopband [7,9].

For unit cell size comparable to wavelength, the ABCD matrix of the unit cell has to be calculated. Using the Bloch condition phase velocity and impedances can obtained [18] where ABCD matrix formulation and Bloch boundary condition are used to relate voltage and current of consecutive cells, obtaining set of two equations, one describing the dispersion (ω-k) relationship of TL and other giving characteristic (in this case called Bloch) impedance of the TL for a given frequency [24].

The Bloch theorem deals with solution of differential equations under periodic boundary conditions, and usually it is used in problems of wave propagation in periodic media, which also include problems like calculating the wave function of an electron in a solid [24]. Bloch boundary condition basically means that fields in a unit cell must differ from another unit cell in that periodic structure only by a complex multiple [24].

There are two important characteristics of wave propagation under Bloch boundary condition: the first is; there is the stop band, i.e. there is range of frequency for which propagation constant is real and hence there is no propagation [24]. A signal with frequency in the stop band of a periodically loaded TL will be reflected. The second important characteristic is that the wavevector is negative with respect to group velocity vector, below the stopband [24].

The analogues case in solid state physics is the presence of electronic band gap, and electrons having negative wave vector (with respect to direction of motion) in valence band, which results in valence band having effectively positively charged carriers known as holes [24].

Similar situation occurs in periodically loaded CLRH TLs. There is a stopband, a left-handed (LH) passband below the stopband , and RH passband above the stopband [8-10].There is another interesting feature in CLRH TLs, the phase velocity in the vicinity of the stopband is much higher than velocity of light in the surrounding medium[7-10]. The supraliminal phase velocity results in waves radiating out of the transmission line, and this effect has been utilized to create antennas [10].

When Bloch boundary condition is applied to periodically loaded TL, one gets an equation relating ω and k, the slope of k-ω plot gives the group velocity whereas ω/k gives phase velocity at a given frequency [24]. Group velocity gives the velocity at which a narrow band signal will travel along the TL; this has to be positive as a signal will always travel from source to the receiver [24]. Phase velocity on other hand gives rate of change of phase along TL, and can be either positive or negative , however for normal TLs the phase velocity is always positive [7-9,24]. From ω-k relationship, one can calculate stopbands, RH passbands and LH passband for a periodic structure, such as a periodically loaded TL[7].

If instead of using standard capacitors, varactors are used, one can have a tuneable transmission line. The propagation constant and impedance of the transmission line can be adjusted by changing the biasing of the varactors. Such a tuneable transmission

line was first proposed in [10].

2.2.3 FSS (Frequency Selective Surfaces) and Metasurfaces

A frequency selective surface allows transmission of an incident wave within a certain frequency range. They can be low pass, high pass, band pass or band reject [11]. Metasurfaces are 2D metamaterials and usually based on FSS [12]

A frequency selective surface is usually either a metallic sheet with openings/apertures of certain shapes, or a pattern of metallic patches on a dielectric sheet [11]. Transmission characteristics of a FSS depend on the shape of the openings/apertures in the case of a metallic sheet and the geometry of metallic patches in case of a dielectric sheet [11]. SRR and complementary split ring resonator (CSRR) could be considered as special cases of FSS. FSS based metamaterials are usually constructed by making a periodic array of FSS [11]. Other types of FSS based metamaterials also exist for example a periodic structure with a unit cell of a FSS separated from a PEC layer by a dielectric spacer [12].

FSS based metamaterials can be designed to have a wide range of electromagnetic properties, for example effective negative permittivity, permeability or both i.e. having a NRI [11].

In the case of waveguides, per unit susceptance and reactance are not easy to calculate, so another approach is used to check existence of a NRI frequency band.

In his paper Veselago [19] showed that in NRI material, the phase velocity (ω/k) is opposite to the group velocity (dω/dk). So by calculating the ω-k relationship, bands of positive and negative refractive index can be found. The above approach can also used with any other material, including TLs [7,11].

The procedure can be roughly described as follows [11]. First calculate ABCD matrices for the FSS and the region of free space, dielectric or magnetic material lying between the FSS in each unit cell. The ABCD matrix in this case relates E and H instead of V and I at the input and output of the unit cell [11]. The ABCD matrix of the unit cell is then simply the product of FSS and inter-FSS spacing ABCD matrices. By imposing Bloch's boundary condition on E and H, the band diagram can be calculated in a similar manner as in the case of a periodically loaded transmission line.

The region with negative dω/dk corresponds to DNG (Double negative, i.e. both permittivity and permeability are negative) region, the stopband to either ENG (Electro Negative i.e. negative permittivity) or MNG (magneto Negative), and positive dω/dk represents normal right handed transmission. The above mentioned procedure can also be used for periodic arrays of FSS in free space or a dielectric. FSS loaded waveguide is shown in the Fig. 2.6 [11]
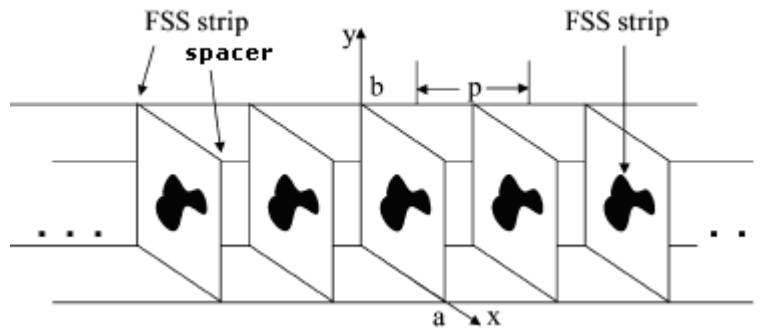
Fig 2.6. FSS loaded waveguide [11]
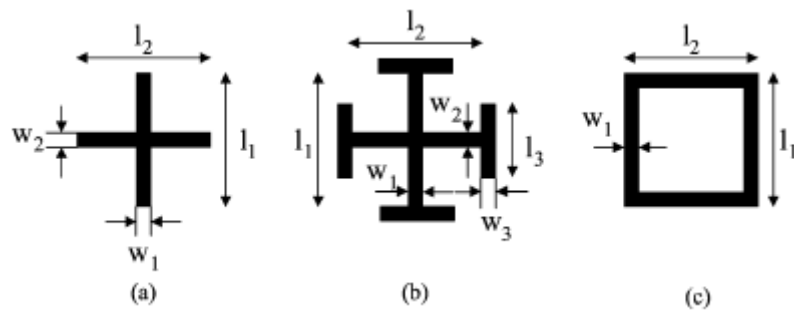
Fig 2.7 Example of FSS: a) Cross, b) Jerusalem Cross, c) Square loop [11]

A Jerusalem cross loaded waveguide is shown in the Fig. 2.8 [11].
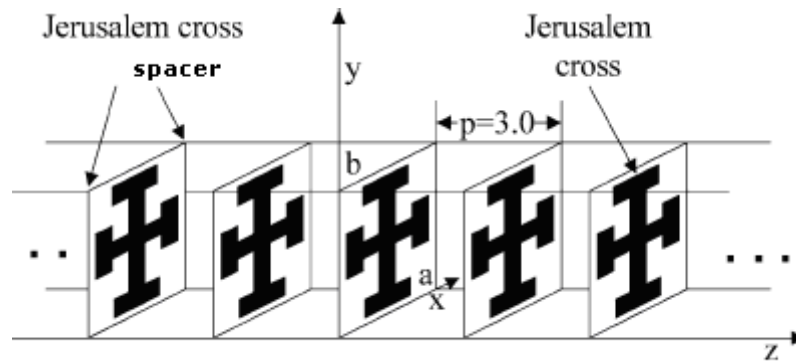
Fig 2.8. Jerusalem cross loaded waveguide [11]

FSS based metamaterials have found several applications. High impedance FSS can be used to design artificial ferrite materials or metaferrite, using just ordinary metals and dielectric [12]. Fig 2.9 shows an FSS based metaferrite
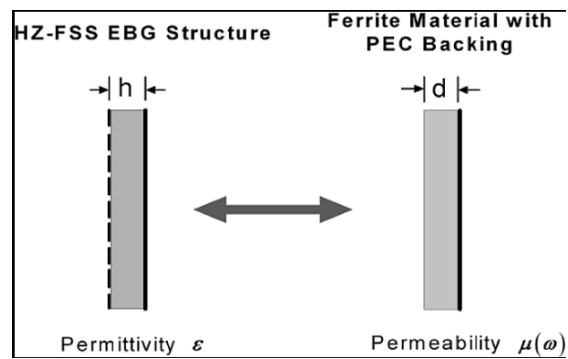
Fig 2.9 FSS based metaferrite (HZ stands for high impedance, EBG for Electric Band Gap) , also compared to an equivalent structure based on natural ferrite [12] .

A very thin radar absorber can be designed by making the FSS based metaferrite lossy [13]. A metamaterial absorber based on a similar metasurface has been proposed and investigated in this thesis.

2.2.4 Photonic Crystal Metamaterials

Photonic crystals are periodic structures made of dielectric, semiconductor or metals. Photonic crystals can be used to get desired electromagnetic properties such as NRI [13-17].

Just like a periodically loaded transmission line, photonic crystals have stop bands and pass bands [16]. Just as in the case of a TL the pass bands with negative ω-k slope will have negative phase velocity. The unit cell of the structure used in [16] and its band diagram (ω-β) are shown in the Fig. 2.10.

(a)   (b)
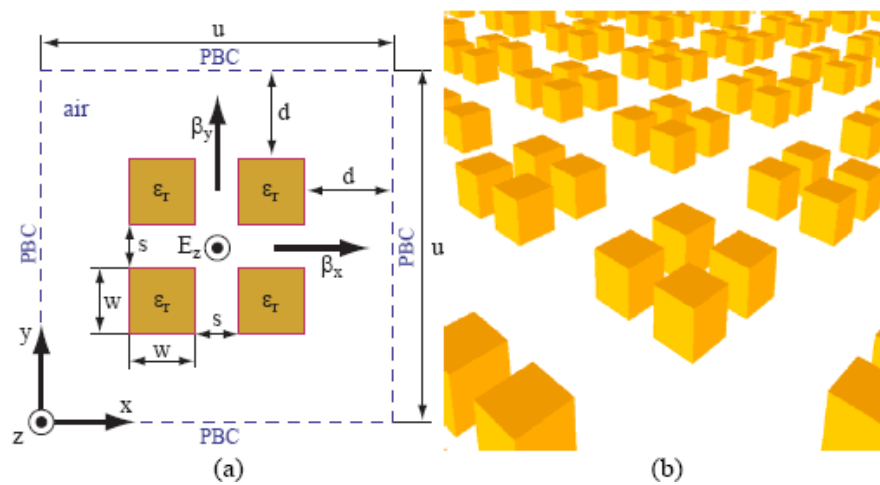
Fig 2.10 a)Unit cell of DNG material based on cluster of dielectric cubes [16]. Height of cubes is 0.5mm, d=0.8mm, s=0.4mm, u=3.2mm, w=0.6mm, and ε_r=100. PBC stands for Periodic Boundary Condition b) Array with the unit cell shown in a)
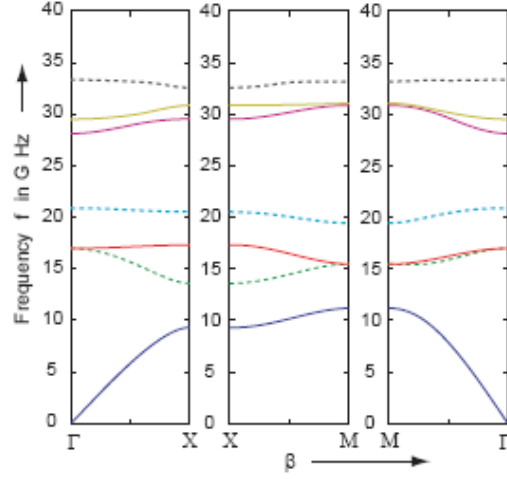
Fig 2.11. Band diagram [16], of the structure studied in Fig 2.10

In Fig. 2.11 β is the component of the k vector along the given axis whereas Γ, X, and M denotes the symmetry points of the reciprocal lattice vector of the periodic structure. Γ, X, and M denotes (β_x,β_y) given by $(2n\pi/u,2n\pi/u)$, $((2n+1)\pi/u,2n\pi/u)$, and $((2n+1)\pi/u,(2n+1)\pi/u)$ respectively, where n is an integer and u is lattice constant [16]. As the E field is along Z axis β_z is always zero. From the band diagram one can see LH pass bands i.e. where slope of the ω-β graph becomes negative, implying vector k and group velocity vector (given by the inverse of derivative of β with respect to ω) being anti parallel. The stop bands represent regions where k is imaginary, and impedance is reactive.

2.3 Applications of Metamaterials

Using metamaterials it's possible to obtain electromagnetic characteristics, such as negative permittivity, negative permeability, high impedance and an arbitrary propagation constant which are difficult or impossible to get using ordinary natural materials. Metamaterials are therefore useful for a wide range of microwave applications. Some examples of these applications are summarized here.

2.3.1 Cloaks and Absorbers

There are basically three ways of reducing electromagnetic scattering and/or reflection by an object; first to absorb the incident wave [25-27], second to cancel out the electric and magnetic fields generated by the object [28], and third to guide incoming waves around the object [29]. The last two techniques are referred to as cloaking the object [25, 29].

Reduction of scattering and reflection by absorption is well established and extensively used [25-27] .The other two techniques are however relatively new [25, 26].

Traditionally radar absorbers have been made using lossy dielectric and magnetic materials [25, 26]. However metamaterial absorbers are being investigated, as one is not limited to the electromagnetic characteristics found in nature [27]. Guiding the electromagnetic waves around the target is essentially through refraction using a cloak with a profile of carefully designed constitutive parameters. Cloaking of an object by guiding the waves around it can be interpreted as transforming the coordinate system [29]. For example if it is required to guide the incoming waves around a sphere using a

hollow spherical cloak, design of the cloak should be such that the inside of the cloak simply doesn't exist for the incoming wave. This is equivalent to transforming the coordinates in such a way that the coordinate points inside the hollow shell cover all the points down to the origin, making the region inside the shell disappear . This transformation can be achieved by converting the Maxwell's equations, written for free space, to the required coordinate system representing the cloak, which results in modification of coefficients of the terms of Maxwell's equations, which in turn could be represented by modified values of the constitutive parameters. Similar method was used at first to solve Maxwell's equation inside non homogeneous materials [30]. Metamaterial cloak based on the concept of coordinate transformation was first proposed in [31].

Cloaking can also be achieved by cancellation of the field generated by the target. This can be achieved by using cloak with electrical and magnetic polarizabilities equal and opposite to that of the target [32, 33].

In the next two Chapters a metamaterial absorber will be proposed and analyzed. Plasmonic cloaking will be studied in Chapter 5.

2.3.2 Phase Shifters

A LH (Left Handed)TL gives great liberty in constructing phase shifters. The reason is that a LH TL gives positive phase shift whereas RH TL gives negative phase shift. By combining a LH TL with a RH(Right Handed) TL it is possible to construct a phase

shifter with arbitrary phase shift [34], such as zero phase shifter which can't be realised using conventional approach..

The major advantage is when a positive phase shift is required. If restricted to a RH TL, one would need a very long TL segment to achieve a positive phase shift for example for phase shift of $+\pi/2$ phase shift a $3\pi/2$ TL segment would be required(a $3\pi/2$ TL gives $-3\pi/2$ phase shift which is equivalent to $+ \pi/2$ phase shift) . Using a left handed TL instead of right handed TL, a phase shift of $+\pi/2$ can be achieved by using TL with a length of only $\pi/2$ instead of $3\pi/2$ required for a right handed TL. The disadvantage however is that the bandwidth might be smaller, as left handed materials are inherently dispersive [19] and thus narrow band.

A phase shifter based on a left handed TL can thus be used to realize a compact phase shifter when the required phase shift is positive. In [34] such a metamaterial phase shifter based on CLRH TL has been reported. The Phase shifters consisting of four unit cells were designed to provide +/- 10° phase shift. In the case of $+10^{\circ}$ degree phase shift, one needs to use a -350° RH TL, however using CRLH TL $+10^{\circ}$ phase shift can be easily obtained. The size of the phase shifter was only about $1/9^{th}$ of the right handed phase shifter.

2.3.3 CLRH Transmission Line for Distributed Amplifier

Distributed amplifier is often used for broad band applications, due to its high gain and wide bandwidth [24, 35].

A distributed amplifier can be constructed using two transmission lines, an output and an input transmission line. The input transmission line is periodically connected to the input of a transistor, usually the gate of an FET. The output transmission line is also periodically connected to the output of the transistor (drain in case of an FET). A standard distributed amplifier based on RH TL is shown in Fig, 2.12 [24].
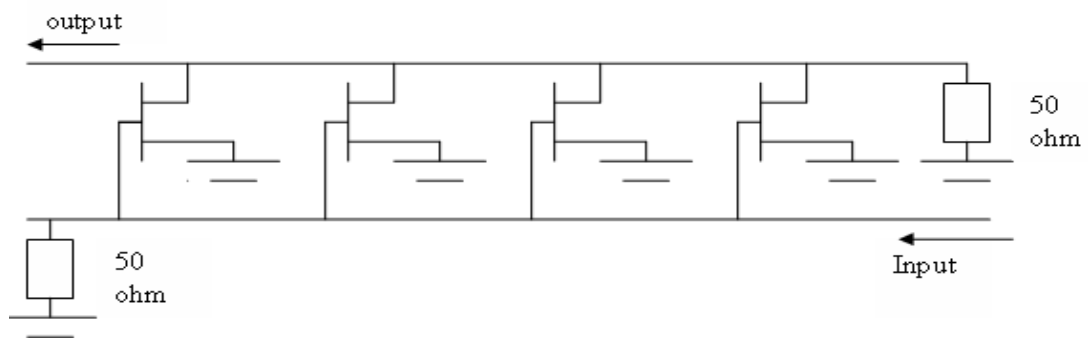
Fig 2.12 A standard distributed amplifier.

Gates and drains of a transistor act a capacitor. Connecting the input and output of the transmission line to the gates and drains of the transistor is equivalent to periodically loading the transmission line with capacitors. If the phase shifts across unit cells (input unit cell consists of the transistor gate and TL section between two neighbouring gates, output unit cell is same but with gate replaced by the drain) of the input and output transmission lines are the same, the current output from all the transistor stages will be in phase. The result is that net output current will be sum of current outputs from all the transistors. For an N stage distributed amplifier, the output current will therefore be N times current output of a single transistor, and total output power will be N^2 times output power of single transistor stage [24]. The number of stages is however limited

by attenuation on the transmission lines. Using distributed amplifier, one can obtain very high gain using medium gain transistors [24].

For a given device technology, gain is directly proportional to the device capacitance, whereas cut-off frequency of any amplifier is inversely proportional to capacitance. So instead of having a very high gain amplifier, one can use low gain transistors to get a medium gain amplifier. The transistor capacitance will be much lower in this case, and thus the amplifier will have a very high cut-off frequency. Furthermore the attenuation constant [18] is directly proportional to the square of capacitance of single transistor stage, so using low gain–low capacitance transistor stages one can have high number of transistor stages.

At high frequency another problem arises. The unit cell of input and output transmission line consists of transmission line segments with gates and drains, acting a capacitive loads connected in shunt. From a Smith chart it can be obsereved that in this case the effective capacitance (capacitive reactance seen from the input port divided by ω) increases with increasing electric length of transmission line segment. This means that with increasing frequency, the effective capacitance per unit cell will increase, further aggravating frequency response and increasing attenuation.

CLRH can be used to solve this problem [36]. Shunt inductance of CLRH will minimize the effect of the gate and drain capacitances, and using CLRH with high phase velocity, electric length of each unit cell can be decreased, thus improving frequency response further. In fact using appropriate value of shunt inductor and series capacitors, the entire structure can be made into set of two CLRH transmission lines

(input and output transmission lines), which can operate at frequencies well above the cut-off of original capacitively loaded transmission lines of traditional distributed amplifier. A CLRH transmission line distributed amplifier is shown below [36].
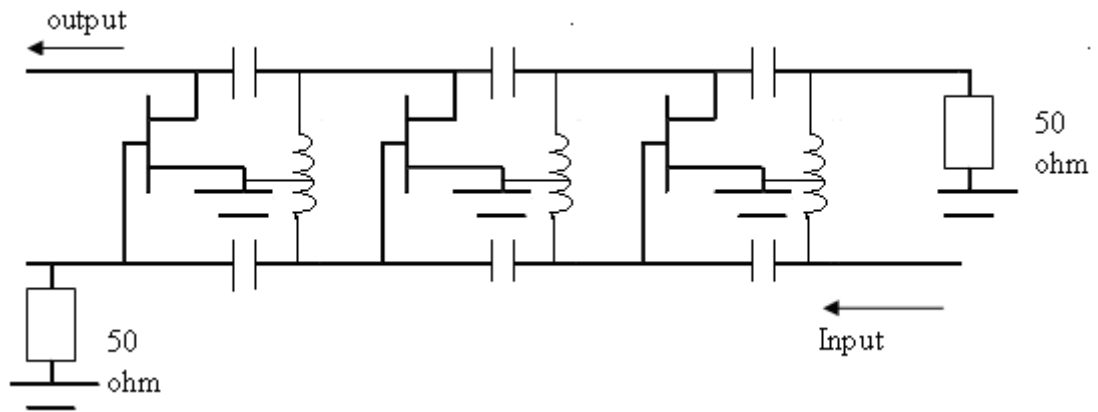
Fig 2.13 A CRLH distributed amplifier.

2.3.4 Metamaterials for Antennas

Metamaterials can be very useful in antenna application. Following are some examples of metamaterial based antennas.

2.3.4.1 Leaky Wave Antennas

In metamaterials, the phase velocity can exceed velocity of light in free space. This creates a very interesting situation in the case of a metamaterial transmission line.

From Maxwell equations, the magnitude of k vector in free space depends only on the frequency, or one can write mathematically [24].

$$k_x{}^2 + k_y{}^2 + k_z{}^2 = k_o{}^2 = \frac{\omega}{c} \qquad\qquad (2.11)$$

A transmission line along Z axis and having only a TEM mode is analyzed in the following discussion to explain the operating principle of a leaky wave antenna. Due to the boundary condition imposed on the interface of two materials, the tangential component of the electric field is continuous, and consequently the tangential component of k vector (k_z) is also continuous [24]. Using cylindrical coordinates (2.11) can be written as below [24].

$$k_z{}^2 + k_r{}^2 = k_o{}^2 = \frac{\omega}{c}$$

$$\Rightarrow k_r{}^2 = k_o{}^2 - k_z{}^2 \qquad\qquad (2.12)$$

In an ordinary right handed transmission line the phase velocity is less than or equal to the velocity of light. This means k_z is greater than k_o (as the wave vector k is inversely proportional to the phase velocity) and therefore k_r is imaginary. Imaginary value of k_r means that the fields are decaying or evanescent in radial direction so there is no radiation in the radial direction.

However if the phase velocity is higher than that of speed light in free space, the situation changes, as k_z is smaller than k_o, and k_r therefore is real. This means radiating fields in the radial direction [36-38]. This phenomenon can be used to construct a leaky

wave antenna [36-38]. The signal is fed to a metamaterial transmission line, in which the phase velocity is greater than velocity of light, and transmission line radiates the signal [36-38].

It must be noted that leaky wave operation can also be achieved for ordinary transmission lines, but only for higher order modes, because in case of ordinary transmission line only for higher order modes can the value of k_z can be smaller than k_o. However in order to have leaky wave operation at TEM mode, metamaterial transmission line has to be used [36-39].

Furthermore using varactors instead of capacitors, one can vary the phase velocity and impedance of the antenna, and consequently its radiation profile [38]. There is another advantage of using CLRH antenna instead of ordinary leaky wave antenna. In RH leaky wave antenna, the radiation is always in the forward direction. However in the case of CLRH it is possible to operate the antenna in both forward radiation and backward radiation mode [38]. The mechanism can be described as follows. Due to the continuity of k_z over transmission line - free space interface, the k_z is negative in vicinity of the leaky wave antenna when it is operating in left hand mode. In free space this means that the Z component of Poynting vector is also negative, as in regular isotropic right handed materials, k vector and Poynting vector point in the same direction. This implies that the antenna is radiating in a backward direction. Backward radiation from left handed transmission line antenna has been verified experimentally in [38].

When using varactor based tuneable antenna one can control the value of the k_z (as it is equal to the propagation constant of the transmission line), while k_0 is constant, thus varying k_z will change the angle of radiation. The radiation angle can be given by following relation [38].

$$\theta = \cos^{-1} \frac{k_z}{|k_o|} \tag{2.13}$$

whereas θ is angle between k_0 and Z axis. Such an antenna with fully steerable radiation angle has been suggested in [38].

2.3.4.2 Zeroth Order Antennas

Many high performance antennas, such as patch antennas and dielectric antennas basically consist of a leaky resonator coupled to a transmission line. The resonator is excited by the input transmission line and the resonator then radiates some of its stored energy [40-43].

As in the case of any resonant structure, here too, the dimension must be at least equal to half wavelength, which places a minimum limit on the size of a resonant antenna. In many applications, such as cellular telephone receivers, or space communications, compact antennas are desirable. Traditionally shorter dimensions used to be achieved by using high permittivity substrate or loading the antenna with reactive elements such as slots [40-43].

However the problem with using above mentioned techniques is generation of surface waves (in case of using high permittivity substrate) and loss of the radiation efficiency [41]. This can be overcome by using metamaterials in resonant antennas [44]. By using left handed materials in combination with the right handed materials it's possible to have k equal to zero, and to have zeroth order excitation of antenna with minimum size of the antenna limited only by minimally small metamaterial structure with required constitutive parameters that can be realized over the operating frequency band [44].

Chapter 3

Metamaterial Electromagnetic Wave absorbers

3.1 Background and Overview of Radar Absorbers

Absorbers are the oldest and most widely used structures for the purpose of reducing radar signatures of targets. Radar absorbers work by absorbing the incoming radiation.

Earliest Radar absorbers, called Salisbury screens have traditionally been constructed by placing a single resistive sheet quarter wavelength from the conducting surface [25,45,46]. To enhance the performance, multiple resistive layer screens, also called Jaumann screens, have been used [47,48]. Instead of alternating layers of dielectric spacer and resistive sheet, radar absorbers can be constructed by using layer(s) of lossy dielectric or magnetic materials [49-62]. Lossy dielectric absorbers are usually constructed by using epoxy /fibre glass composite containing carbon black [53], however other materials such as Silicon carbide foam have also been used [58]. Lossy magnetic absorbers, on the other hand, are usually constructed by using ferrite based composites [61, 62]. A sheet of lossy plasma also acts like a radar absorber [63]

Radar absorbers constructed from metamaterials have been investigated recently [64-74], since one is not constrained by the electromagnetic characteristics of naturally available materials. Metamaterial absorber usually consists of lossy capacitive planar structures placed above the ground plane [65]. A ground plane seen from a distance

less than quarter wavelength is equivalent to an inductive load [24], so using a lossy capacitive sheet it can be matched to free space, suppressing the reflection [65].

The metamaterial absorber reported here is based on an array of resistive Hilbert curves. A Hilbert curve is a type of space filling curve [66]. The advantage of a Hilbert curve, or other space filling curves for that matter, is that they can provide resonance at a lower frequency with a smaller physical foot print [66,75]. However traditional space filling curve absorbers are narrow band, i.e., a few percent at the most [66,75].

Most of the thin broadband absorbers based on lossy capacitive surfaces are constructed using lumped elements and are also called circuit analogue absorbers [67]. however the lateral unit cell sizes reported for such structures are very large. For the similar operating frequency range a large reduction in unit cell size has been achieved during this study. Large unit cell size can give rise to diffraction effects, which result in strong backscatter for certain oblique angles of incidence [76]. Furthermore circuit analogue absorbers also require use of lumped circuit elements, increasing the complexity of fabrication.

For simplicity a linearly polarized plane wave propagating along the z axis is assumed. E and H fields given by Maxwell's curl equations become [24].

$$\frac{\partial E}{\partial Z} = j\omega\mu H$$

(3.1a)

$$\frac{\partial H}{\partial Z} = (j\omega\varepsilon + \sigma) E$$

(3.1b)

The equations given above are similar to following transmission line equations (also known as telegraphic equations, [24].

$$\frac{\partial V}{\partial Z} = zI$$

(3.2a)

$$\frac{\partial I}{\partial Z} = yV$$

(3.2b)

whereas z and y are per unit length impedance and admittance respectively.

Comparing (3.1a&b) and (3.2a&b), and replacing V and I of transmission line equations by E and H respectively, following relationships are obtained [24].

$$z = j\omega\mu$$ (3.3a)

$$y = j\omega\varepsilon + \sigma$$ (3.3b)

$$\eta \equiv Z_0 = \sqrt{\frac{z}{y}} = \sqrt{\frac{j\omega\mu}{j\omega\varepsilon + \sigma}} \qquad\qquad (3.3c)$$

$$\gamma \equiv \alpha + j\beta = \sqrt{zy} = \sqrt{j\omega\mu\sigma - \omega^2\mu\varepsilon} \qquad\qquad (3.3d)$$

From (3.3a)-(3.3d), it can be observed that there is a perfect correspondence between transmission line equations and plane wave equations in an isotropic media[24]. It is therefore possible to apply transmission line theory tools, such as impedance matching, smith chart, S parameters, and ABCD matrices to plane wave propagation problems .

Before moving on further discussion, basic terms used in Radar terminology are defined. For a target located at the origin and the receiver antenna located at (Φ,θ,R). Bistatic cross section is defined as [77]

$$\forall R \to \infty$$

$$\sigma_{\phi\theta} = 4\pi R^2 \frac{P_{\phi\theta}}{P_0} \qquad\qquad (3.4)$$

where P_0 is the incident power density at the target and $P_{\Phi\theta}$ is the power density of the scattered field at the receiving antenna.

Monostatic RCS (Radar Cross Section) is a special case of bistatic RCS [77]. It is defined as bistatic RCS when the same antenna is used for both transmitting and receiving. Monostatic RCS is also known as backscatter [77]. Monostatic RCS is very

important as most of the radar systems use a single antenna for both receiving and receiving[77].

3.1.1 Bandwidth Limitation

Bandwidth limitation of radar absorbers have been discussed by Rosanov[78]. There is a trade off between absorber thickness and maximum achievable bandwidth. For a standard magnetodielectric absorber the upper limit on the bandwidth in terms of the thickness of layer is given by[78].

$$\frac{\Delta\lambda}{d} \approx \frac{32}{\pi} R_0 \operatorname{Re}(\mu) \qquad (3.5a)$$

In eq 3.5 R_0 is absolute value of the required power reflection coefficient, μ and d is the permeability and thickness of the layer respectively, and $\Delta\lambda$ is the absorption bandwidth in terms of λ. Our discussion concerns non magnetic absorbers. The reason for choosing non magnetic absorber is to avoid need for expensive and frequency limited magnetic materials. For a non magnetic absorber and a required absorption coefficient of -10dB eq 3.5a reduces to

$$\frac{\Delta\lambda}{d} \approx 1 \qquad (3.5b)$$

eq 3.5b then gives the upper limit for achievable bandwidth for a given absorber thickness

3.2 Overview of Radar Absorbers

A good overview of radar absorbers has been given by Knott [79, 80]. Following are the major types of radar absorbers

3.2.1 Salisbury Screen

In order to understand its operation, a plane wave incident upon a PEC plane in analyzed. The case of a plane wave incident upon a PEC plane is equivalent to a short circuited transmission line. Impedance seen at any point on a lossless transmission line while looking towards the short circuited end is given by the following equations [24].

$$Z_{in} = Z_0 \frac{Z_l + jZ_0 \tan \beta l}{Z_o + jZ_l \tan \beta l} \tag{3.6a}$$

$$for Z_l = 0$$
$$Z_{in} = jZ_0 \tan \beta l \tag{3.6b}$$

where Z_l is load impedance, which in case of a PEC plane is a short circuit. Using Equations (3.3a)-(3.3d), (3.4b) can be simplified for free space as.

$$Z_{in} = j\eta_0 \tan \beta l \tag{3.7}$$

If βl is equal to $\pi/2$, Z_{in} is infinite, hence at quarter wavelength from the PEC plane, the wave would see an open circuit. If a resistive sheet with sheet impedance equal to the free space impedance is placed at this point the total impedance will be equal to the free space impedance, and therefore there will be no reflection. If the impedance is

close to that of the free space not exactly equal, reflection will still be greatly reduced even if not completely eliminated.

This type of absorbing screen is called a Salisbury screen [25,26,46]. Salisbury screen is very simple however it needs to be a quarter wavelength thick [25,26,46]

3.2.2 Jaumann Screen

Just as in the case of transmission line based networks, where for the purpose of broader matching bandwidth, multiple matching stubs are used [24]; in this case too, multiple resistive sheets could be placed above the PEC plane, to increase the absorption bandwidth. Such absorbers are called Jaumann screens [47,48].

3.2.3 Dallenbach screen

Furthermore, a radar absorber can be constructed by using a lossy dielectric or magnetic material [52-64]. Such screens are called Dallenbach screens. It is possible to use multiple layers of lossy material instead of just a single layer [52].

To understand the working principle of Dallenbach screens, the following analysis can be helpful. A lossy dielectric layer on a conducting surface can be modelled as a short circuited lossy transmission line. The impedance seen at the air/dielectric interface is given by following equation [24].

$$Z_{in} = Z_d \tanh(\gamma l) \tag{3.8}$$

where Z_{in} is the impedance seen at dielectric air interface, Z_d is intrinsic impedance of the dielectric, γ is complex propagation constant inside the dielectric, and l is thickness of the dielectric. Radar absorption can be achieved by making Z_{in} equal to free space impedance. In practice however it is sufficient that Z_{in} is close to free space impedance, in which case the Power reflection coefficient though not zero, will still be very low.

For this absorber to work, the material has to be lossy. The reason is that in absence of losses, γ will be imaginary, and thus the impedance given by (3.6) will always be imaginary, zero or infinity.

There are two types of lossy materials used in Dallenbach screens, dielectric and magnetic lossy materials.

Lossy dielectric materials are usually constructed by dispersing conducting particles in a dielectric matrix. The most common is made from epoxy glass resin containing carbon black [52-55]. The carbon black provides conductivity making the dielectric lossy. Besides carbon black based dielectric, other materials such as Silicon Carbide foam have also been used for radar absorber materials [58].

Lossy magnetic materials are usually constructed by dispersing ferrite powder in a dielectric matrix [61,62]. Moreover a sheet of lossy plasma can also used as radar absorber [63].

3.2.4 Capacitive screens

If the screen thickness of less than quarter wavelength are desired, then the screen impedance should have reactive component as well [64-66]. The reason is explained in the analysis below.

If a screen with surface conductivity G and surface susceptance B, is placed at a distance l from the PEC plane, the net admittance is given by[24,66].

$$Y_t = \frac{1}{Z_{in}} + G + jB \qquad (3.9)$$

Inserting value of Z_{in} from (3.5) in (3.7) the following equation is obtained

$$Y_t = G + j(B - \frac{1}{Z_0 \tan \beta l}) \qquad (3.10)$$

where Y_t is the total admittance seen at distance l from the PEC plane. In order to have no reflection Y_t should be equal to free space admittance [66]. Imposing the aforementioned condition, the following equation is obtained.

$$Y_t = \frac{1}{\eta_0} \supset G + j(B - Y_0 \cot \beta l) = \frac{1}{\eta_0} \qquad (3.11)$$

The real and imaginary component on the left side of the equation should equal to the real and imaginary component on right side respectively. Imposing this condition the following relations are obtained for B and G.

$$B - Y_0 \cot \beta l = 0 \rightarrow B = Y_0 \cot \beta l \qquad (3.12 \text{ a})$$

$$G = \frac{1}{\eta_0} \qquad (3.12 \text{ b})$$

So for βl less than quarter wavelength the PEC plane will appear as an inductive load. In this case a capacitive sheet in parallel with resistive sheet will be required (or alternatively a sheet with complex admittance, with imaginary part being positive).

Such radar absorbers are usually constructed by using lumped circuit elements, mainly capacitors and resisters; or frequency selective surfaces and other metamaterials with lossy dielectrics [64-74].

3.2 The Hilbert Curve Absorber

3.2.1 Introduction

A Hilbert curve is a space filing fractal. 1st, 2nd, 3rd, and 4th order Hilbert curves are given in Fig 3.11 [75].
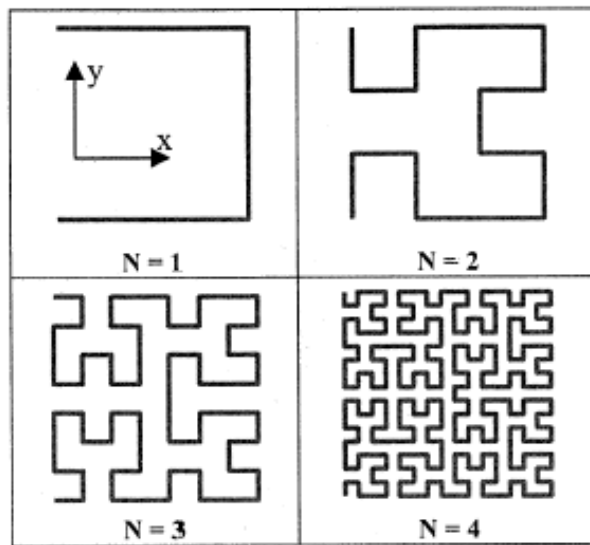
Fig 3.1 1st four orders of Hilbert curve [75]

Hilbert curve order has great effect on its frequency response[75]. From the numerical analysis done in Engheta[75] and it was observed that increasing order of the Hilbert curve reduces the bandwidth. However on the other hand the advantage of using higher order Hilbert curve is that required spacer thickness is reduced. There is therefore a trade off between thickness and bandwidth when the choice of the order of Hilbert curve is to be made. The objective in this work was to realize a wideband absorber, and this objective had a priority over the aim to minimize the thickness, as even in the case of first order Hilbert curve the thickness only $\lambda/6$ and was therefore acceptable. Hence the First order Hilbert curve was chosen for the structure in order to achieve maximum bandwidth.

The novel structure reported here consists of resistive Hilbert curves, whereas a standard Hilbert curve array is constructed of conducting Hilbert curves. Higher resistance of Hilbert curve translates into low Q and thus wider bandwidth, compared to a standard Hilbert curve array.

3.2.2 Hilbert curve-Theory

A Hilbert curve can be modelled as folded dipole, with resonant frequency approximately determined by the following equation [82].

$$m\frac{\eta}{\pi\omega}\log\frac{2d}{b}\tan\beta d+\frac{\mu_0}{\pi}s\left(\log\frac{8s}{b}-1\right)=\frac{k\mu_0\lambda}{4\pi}\left(\log\frac{8k\lambda}{4b}-1\right) \quad (3.12)$$

where m is the order of resonance, η is the free space impedance, k is an integer, β is the propagation constant and b is the diameter of the Hilbert curve wire. s, m, and d are defined below [82]

$$s = \left(2^{2n-1} - 1\right)d \qquad\qquad\qquad (3.13\ a)$$

$$d = \frac{L}{2^{2n-1}} \qquad\qquad\qquad (3.13\ b)$$

$$m = 4^{n-1} \qquad\qquad\qquad (3.13\ c)$$

where n is the order of Hilbert curve and L is the length of Hilbert curve footprint.

If the frequency is below resonance, a Hilbert curve will act as a capacitive element[75], as is the case with a standard dipole. An array of Hilbert curves therefore will act as capacitive sheet. Furthermore if the Hilbert curve is constructed from lossy material, the array admittance will have a real component as well.

As discussed earlier from a distance of less than $\lambda/4$, a PEC plane appears as an inductive load. If a lossy Hilbert curve is placed in front of a PEC surface, it is possible to match the PEC surface to free space, provided the following conditions are met [24].

$$Y_H = \frac{1}{\eta_0} + j \frac{1}{\eta_0 \tan \beta l} \qquad (3.14)$$

where Y_H is the surface admittance due to the Hilbert curve array, η_0 is the free space impedance, β is the free space propagation constant, and l is the distance of the Hilbert curve array from the PEC plane. If the above mentioned conditions are satisfied, then the total impedance seen at the location of Hilbert curve will be equal to that of free space, and therefore there will be no reflection.

In order to get more insight into the behaviour of Hilbert curve, a simplified model will be analyzed. The reason is that it is not possible to get an analytical solution even for the case of simple short wire dipole; and it is the practice to use numerical techniques to obtain fields and currents.

First step in the analysis in model the Hilbert curve as an open circuited transmission line. This model will however give only a qualitative picture, and it cannot give reasonably accurate values for impedances even for the simple case of a wire dipole. The problem with using simple transmission line model is that, unlike a standard transmission line the capacitance and hence the impedance varies along the length of dipole.

For a lossless Hilbert curve. Modelling the Hilbert curve as an open circuited transmission line , the following equation for its impedance and admittance are obtained [24].

$$Z_H = -jZ_{H0} \cot(\beta_H L) \qquad (3.15a)$$

$$Y_H = jY_{H0} \tan(\beta_H L) \qquad (3.15b)$$

where Z_{H0} is the characteristic impedance of Hilbert curve, Z_H is total impedance of Hilbert curve, β_H is propagation constant along the Hilbert curve (which may assumed to be equal to free space propagation constant, and l is length of Hilbert curve. It can be observed from the equations above, that for electric length smaller than quarter wavelength, the Hilbert curve will be capacitive. Furthermore, the susceptance (imaginary component of admittance) of the Hilbert curve will increase with increasing frequency.

If the Hilbert curve is placed at distance from a PEC plane, where the capacitive susceptance of the Hilbert curve would cancel out the inductive susceptance resulting from the PEC plane, and one would get high impedance. Furthermore, a resistive sheet can be placed in parallel with the Hilbert curve to match the structure with free space and reduce RCS.

As evident from the equations above, the admittance of the Hilbert curve increases with increasing frequency; however, the inductive admittance due to the PEC ground

plane decreases with increasing frequency. The cancellation of inductive admittance due PEC plane and that of Hilbert curve will therefore occur only over a narrow band of frequency. Lossless Hilbert curve based high impedance surfaces and absorbers are therefore quite narrow band. This problem can be overcome by using Hilbert curve constructed from lossy material. The reason for broad band performance of lossy Hilbert curve is described in the analysis below.

If the Hilbert curve inclusions are sufficiently lossy, the capacitive susceptance will decrease with increasing frequency, the reason for which will be explained later in the discussion. As evident from (3.2) the inductive susceptance due to PEC plane seen at the position Hilbert curve also decreases with increasing frequency. In the above mentioned case, change in the inductive susceptance due to PEC plane is at least partially compensated by change in capacitive susceptance of Hilbert curve. The result is that a wider absorption bandwidth can be achieved. However if the Hilbert curve is too lossy then the capacitive susceptance will be too low and the condition given in (3.2) will be satisfied only for a narrow band of frequency. The condition given by(3.2) will not be satisfied at all if the losses are too high. There is therefore an optimum range of resistivity of Hilbert curve which will give good broadband performance.

In order to understand why the capacitive susceptance of a Hilbert curve decreases with increasing frequency, the lossy Hilbert curve is analyzed in the same manner as the lossless Hilbert curve. Modelling Lossy Hilbert curve as open circuited lossy transmission line the following equations are obtained [24].

$$Z_H = -Z_{H0} \coth(\gamma_H L) \qquad\qquad\qquad (3.16\,\text{a})$$

$$Y_H = Y_{H0} \tanh(\gamma_H L) \qquad\qquad\qquad (3.16\,\text{b})$$

γ_H is the complex propagation constant along the Hilbert curve. Other symbols have the same meaning as in equations for lossless Hilbert curve.

In order to get a deeper insight, the equations for lossy Hilbert curve can be split into real and imaginary parts. To accomplish this, the complex hyperbolic cotangent is decomposed into real and imaginary parts (similar analysis could be found in standard mathematics text books)

$$\tanh(x + jy) = \frac{\tanh x + j \tan y}{1 + j \tanh x \tan y} \qquad\qquad\qquad (3.17\,\text{a})$$

$$= \frac{\tanh x \left(1 + \tan^2 y\right) - j \tan y \left(1 - \tanh^2 x\right)}{1 + \tanh^2 x \tan^2 y}$$

$$= \frac{\tanh x \sec^2 y - j \tan y \sec h^2 x}{1 + \tanh^2 x \tan^2 y}$$

$$\rightarrow \tanh(x + jy) = \frac{\tanh x \sec^2 y}{1 + \tanh^2 x \tan^2 y} - j \frac{\tan y \sec h^2 x}{1 + \tanh^2 x \tan^2 y} \qquad (3.17\,\text{b})$$

The admittance of a lossy open circuited transmission line can be given as

$$Y_H = Y_{H0} \tan(\gamma L) = (G_{H0} + jB_{H0}) \tanh(\alpha L + j\beta L) \qquad (3.18\ a)$$

$$Y_H = G_H + jB_H \qquad (3.18\ b)$$

$$G_H = \text{Re}\left[\tanh(\alpha L + j\beta L)\right]G_{H0} - \text{Im}\left[\tanh(\alpha L + j\beta L)\right]B_{H0} \qquad (3.18\ c)$$

$$B_H = \text{Re}\left[\tanh(\alpha L + j\beta L)\right]B_{H0} + \text{Im}\left[\tanh(\alpha L + j\beta L)\right]G_{H0} \qquad (3.18\ d)$$

Using equation for hyperbolic tangent for complex numbers, the admittance of lossy open circuited transmission line is given by the following equations.

$$\tanh(\alpha l + j\beta l) = \frac{\tanh(\alpha L)\sec^2(\beta L)}{1 + \tanh^2(\alpha l)\tan^2(\beta l)} + j\frac{\tan(\beta L)\sec h^2(\alpha L)}{1 + \tanh^2(\alpha l)\tan^2(\beta l)} \qquad (3.19\ a)$$

$$G_H = \frac{G_0 \tanh(\alpha L)\sec^2(\beta L) - B_0 \tan(\beta L)\sec h^2(\alpha L)}{1 + \tanh^2(\alpha L)\tan^2(\beta L)} \qquad (3.19\ b)$$

$$B_H = \frac{B_0 \tanh(\alpha L)\sec^2(\beta L) + G_0 \tan(\beta L)\sec h^2(\alpha L)}{1 + \tanh^2(\alpha L)\tan^2(\beta L)} \qquad (3.19c)$$

For lossless line the equations are reduced to

$$B_0 = 0, \alpha = 0, G_0 = Y_0$$

$$\rightarrow G_H = 0, B_H = Y_0 \tan(\beta l) \qquad\qquad\qquad (3.20\ a)$$

$$\rightarrow Y_H = jY_0 \tan(\beta l) \qquad\qquad\qquad\qquad (3.20\ b)$$

This is the same result that was obtained earlier for the lossless case.

From the equation for lossy case, it can be observed that if the value of α is sufficiently high the reactance will decrease with increasing frequency. The reason is $\tanh^2(\alpha l)\tan^2(\beta l)$ term in the denominator and $\sec h^2(\alpha l)$ term in the nominator, as tanh and tan increases and sech decreases with increasing value of the argument, when the argument is less than $\pi/4$. The result is that lossy open circuited transmission line will be able to cancel out the inductive reactance due to PEC plane over much wider bandwidth.

Even though the above analysis is very crude, it gives us the basic picture. It can therefore be expected that the lossy Hilbert curve absorber to have wider bandwidth than a lossless Hilbert curve absorber.

3.2 Structure

The metamaterial absorber structure reported here is a two layer metamaterial resistive Hilbert curve array..

The structure proposed here has a unit cell size of 4.3 mm × 4.3mm. Hilbert curve inclusions and the PEC surface are in the XY plane and the K vector is along negative Z axis. The inclusions are first order Hilbert curves with length of each side equal to 3.7 mm . The inclusions were 2.96mm and 3.4 mm above PEC plane. The width and thickness of the Hilbert curves are 0.18 mm and 0.0196mm respectively and conductivity is $70KSm^{-1}$ (Graphite) giving $40\Omega\ mm^{-1}$ of per unit length resistance. Styrofoam spacer was chosen for its low permittivity, and graphite for being a low cost and easy to process semiconductor. The parameters were optimized using optimization module in HFSS. The unit cell size is only $0.19\lambda \times 0.19\lambda$ at f_o, thus suppressing diffraction effects. A Hilbert curve's resonance depends on polarization. Hence to have a good absorption for both polarizations, two layers of Hilbert curves of mutually orthogonal orientations are required, one for each polarization. The upper and lower inclusions provide resonance for E_x and E_y polarizations, respectively, as is the case of conducting Hilbert curve [81].

The novel absorber structure presented in this work successfully combines the merits of traditional conducting space filling curve based absorbers[66] and circuit analogue absorbers. As discussed earlier a resistive Hilbert curve can be viewed as a lossy high impedance surface equivalent to a high impedance surface in shunt with a resistive layer, resulting in low RCS. This structure eliminates need for a resistive sheet or any

lumped element by combining high impedance surface and resistive layer in one, thus significantly reduce the complexity of the absorbers.

The structure was simulated in HFSS. The unit cell of the proposed structure is shown in Fig. 3.2.
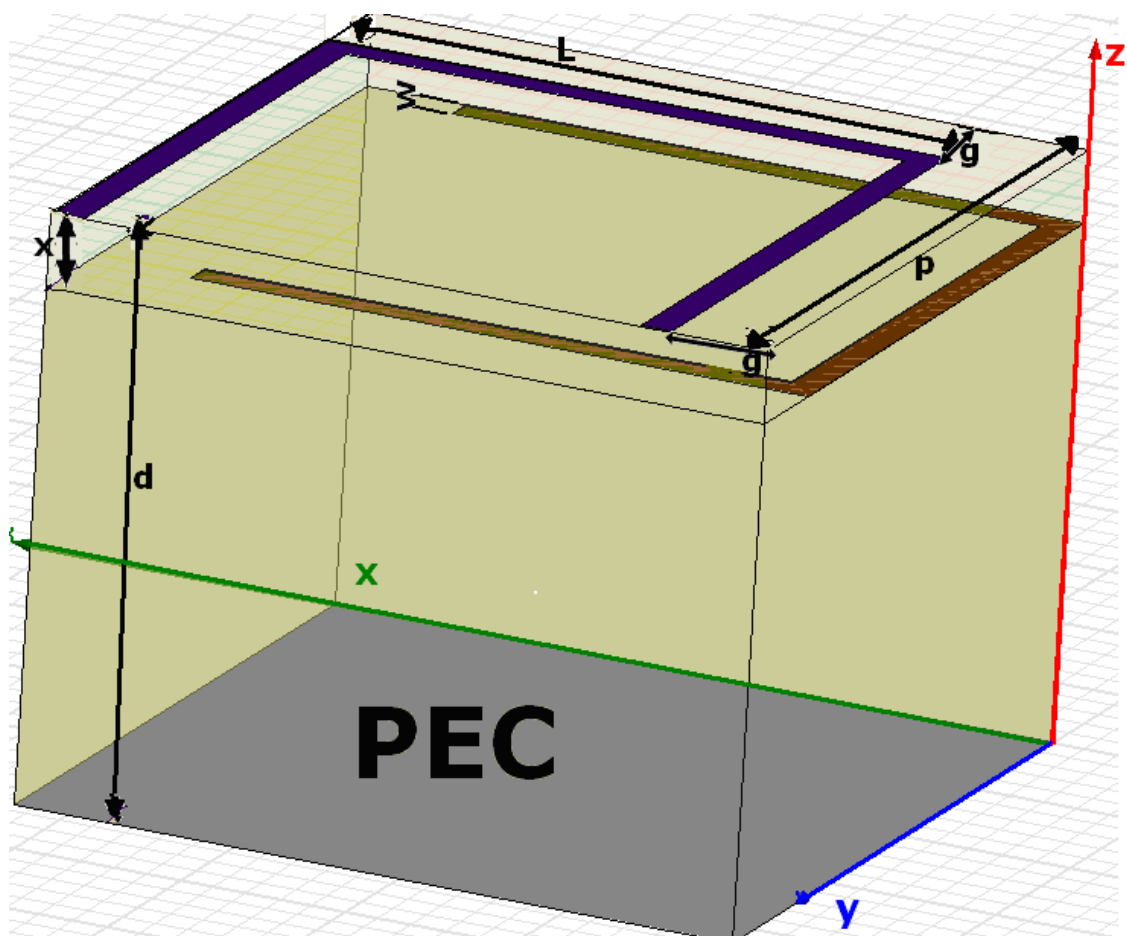
Fig 3.2. Unit cell of Hilbert curve array p=4.3mm, L=3.7mm, g=0.586mm, x=0.424mm

3.3 Simulations and Results

The structure was simulated by imposing periodic boundary condition on a single unit cell. The normalized (to uncovered PEC plane) backscatter is shown in Fig. 3.2. As it

can be observed from Fig. 3.3, the proposed dual polarization metamaterial Hilbert surface provides a good absorption over a wide frequency band. From the HFSS simulation, 10 dB reduction in Monostatic RCS was observed for frequency range from 9.7 to 19 GHz for both E_x and E_y polarizations.
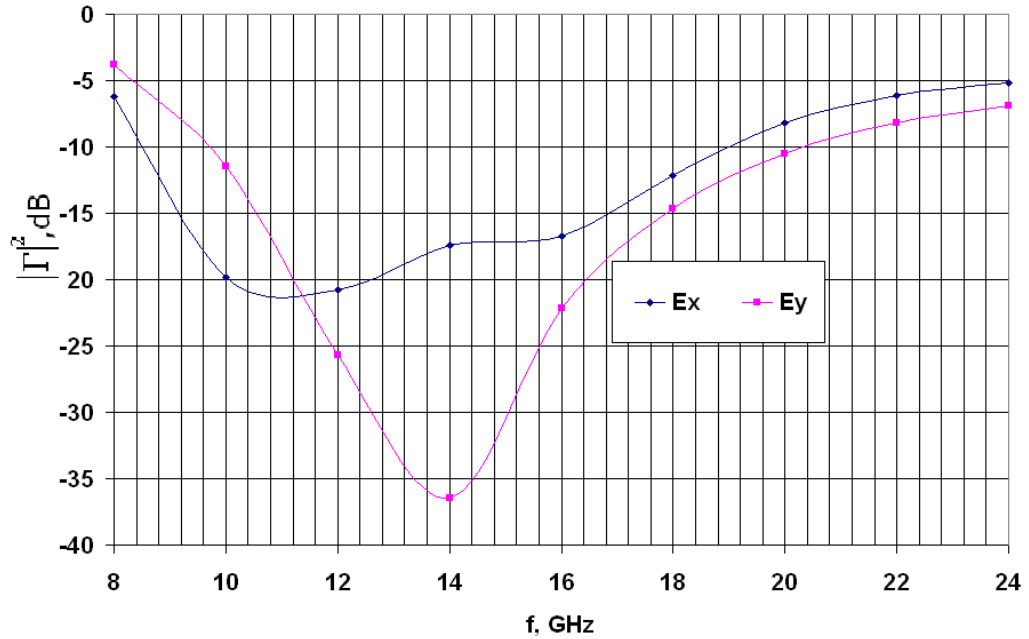
Fig 3.3. Power reflection coefficient for dual polarization metamaterial Hilbert surface.

There is a trade off between thickness of the absorber and the ultimate bandwidth as discussed by Rosanov [80]. For a standard lossy absorber with thickness of $\lambda/6$ (as is the case in the absorber reported here), the maximum achievable bandwidth is only about 15%[79]. Rosanov has defined figure of merit of a radar absorber as dl/d, where d is thickness of the absorber. According to Rosanov absorber maximum bandwidth roughly proportional to thickness. For a given class of absorber the quantity $\Delta\lambda/d$ ($\Delta\lambda$ is the bandwidth in terms of wavelength and d is thickness of the absorber) is given by a certain limit. For Dallenbach absorber -10dB bandwidth limit is given by $\Delta\lambda/d$

limited to roughly 1[78]. The absorber discussed in this work has $\Delta\lambda/d$ ($\Delta\lambda$ is the bandwidth in terms of wavelength and d is thickness of the absorber)of 4.45 for -10dB Power reflection coefficient this more than four times the ultimate limit of 1 given by Rosanov for a single layer Dallenbach absorber. For -20dB absorption $\Delta\lambda/d$ is 0.9 which is nine times the ultimate limit for a Dallenbach screen given by Rosanov[78]. Salisbury screen gives similar and Jaumann wider bandwidth but are much thicker than the absorber presented here[78].

The metamaterial absorbers reported in the literature are usually either narrow band or has unit cell greater than half wavelength which would result in diffraction lobes for oblique incidence[65-74, 79-82]. The structure reported in this work is wideband and has a unit cell size of less than 0.3λ overthe entire frequency range. Suppression of the diffraction effects is evident from good performance at oblique incidence as shown in Fig. 3.4

To investigate the performance of the absorber further, reflection coefficients were evaluated for oblique incidences. The results are shown in Fig 3.4
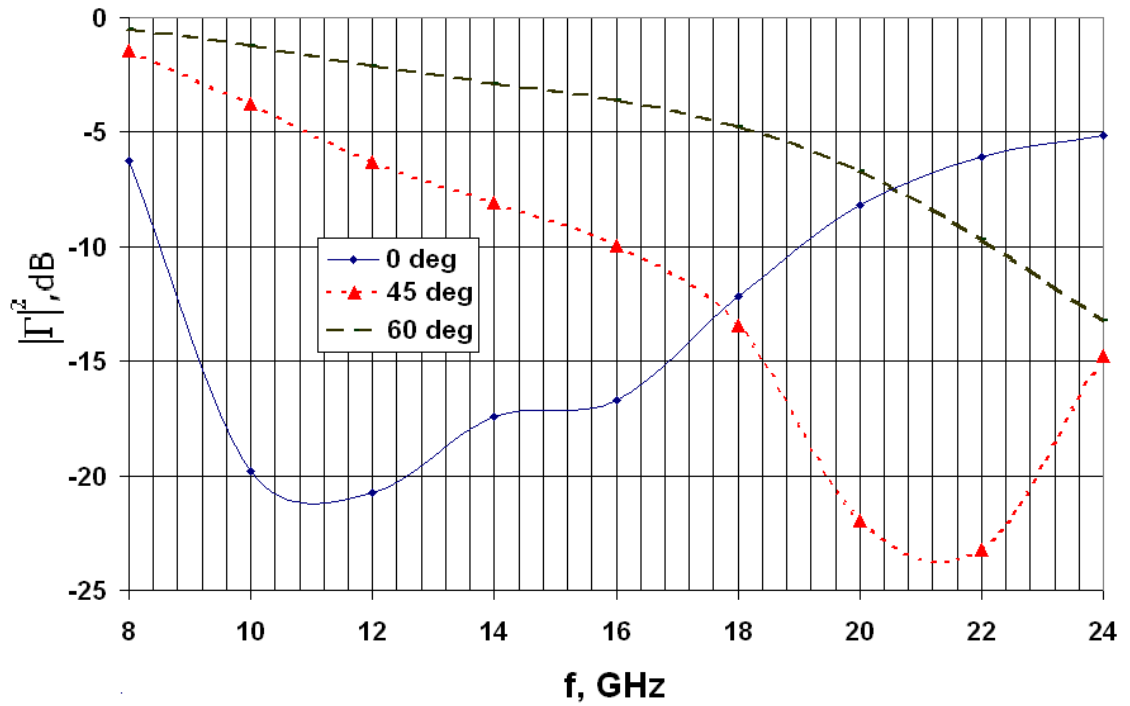
(a)
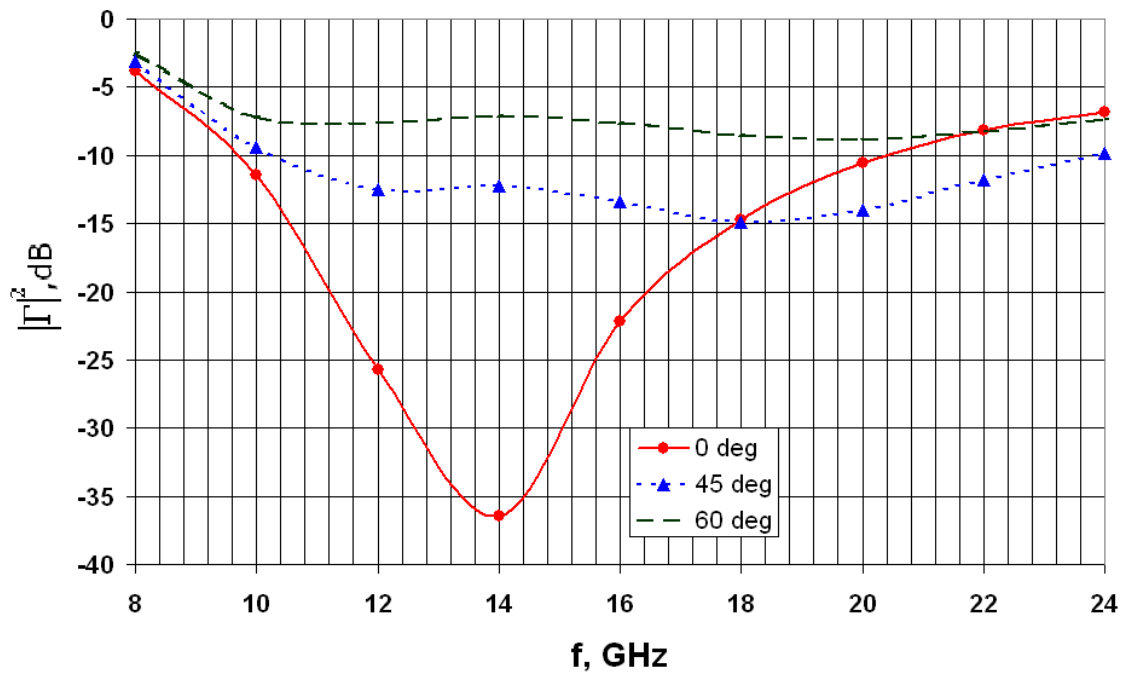
(b)

Fig 3.4 Power reflection coefficient for oblique incidence a)TM b) TE

From the results in Fig3.4 it can be observed that the absorber gives good performance even for oblique angles. Most of the absorbers reported in the literature have been

analyzed for normal incidence. Absorbers reported for oblique incidence have much narrower bandwidth[82].

To get insight into the absorption process, electrical field distribution around the Hilbert curves was also obtained and shown in Fig. 3.4. It can be observed that the electric field is concentrated around the Hilbert curves, implying resonant absorption of the incoming waves. From an equivalent circuit model point of view the resonance occurs because the whole structure with the Hilbert curves placed above ground plane behaves as an LRC parallel resonant circuit (Hilbert curve array acting as lossy capacitive sheet, and the ground plane appearing as inductive load at the plane of Hilbert curve array). In order to make thing clearer, E field surface plots in planes of upper and lower Hilbert curves are shown in Fig . 3.5
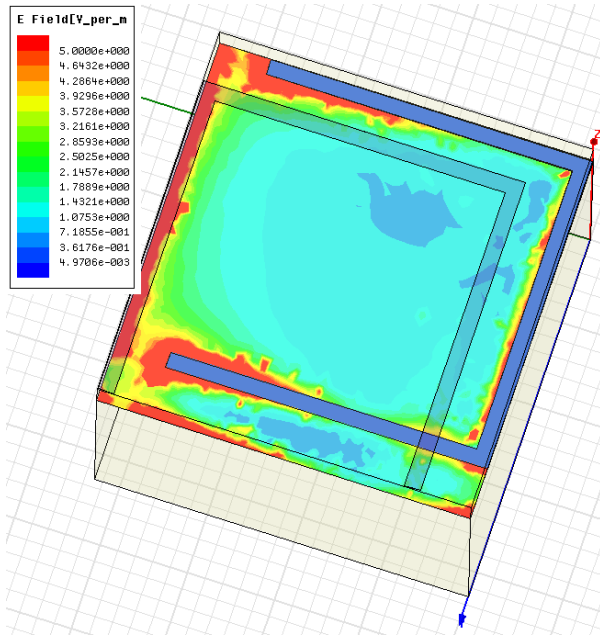
(a)
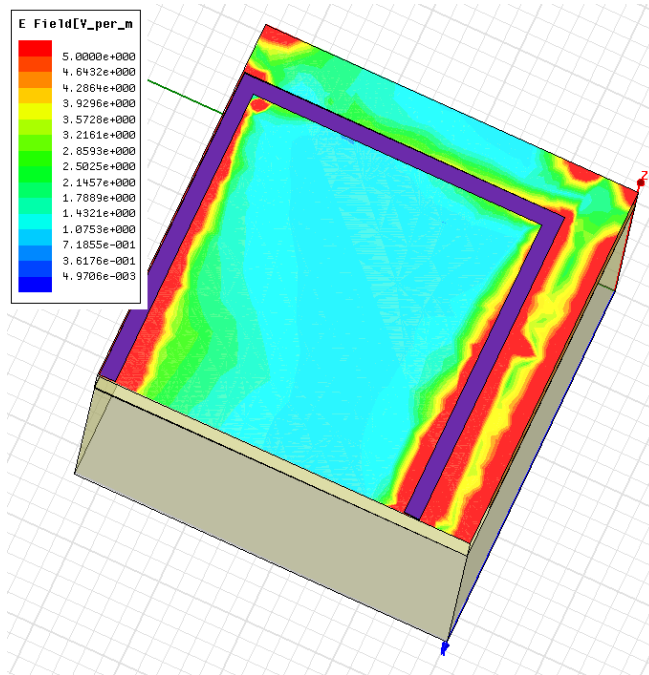
(b)

Fig 3.5 Surface plot of magnitude of E field on the plane of a)lower Hilbert curve b)upper Hilbert curve

3.4 Absorbing Screen for Terahertz Bolometers

A terahertz detector is an important component of a terahertz system. A thermal terahertz detector, also called a bolometer, mainly consists of an absorber layer and a thermopile [83-91]. The absorber layer absorbs the incident radiation and the resultant change in temperature is then detected by the thermopile [83-91]. For high end applications where high speed and/or sensitivity are required more complex types of detectors such as those based on quantum dots or superconductors are used [92-99].

A terahertz absorber is an extremely crucial component of a terahertz bolometer. However, terahertz absorbers reported so far are relatively narrow band [84-87]. A novel metamaterial terahertz absorber based on resistive Hilbert curve array is proposed for wideband terahertz detection in this work. The structure has 100% -3dB fractional bandwidth for normal incidence, and remains wide bandwidth even at oblique angles. For instance at 60° angle of incidence the -3dB bandwidth is 90%. In our case high resistance is achieved by keeping the Hilbert curve extremely thin. Even though the Hilbert curve is made of aluminum, the DC resistance of each Hilbert curve is about 500 Ω, which makes it very different from the conventional conducting Hilbert curve.

3.4.1 Structure

The absorber structure is shown in Fig.3.5, consisting of a 2D resistive Hilbert curve array. Each unit cell is constructed from four coplanar aluminum Hilbert curves. In order to make the structure polarization insensitive at normal incidence each Hilbert curve is rotated by 90 ° with respect to adjacent curves. The array is separated from copper ground plane by a 38 μm thick BCP(Benzocyclobutene) [100] spacer, with

relative permittivity of 2.48 and loss tangent of 0.005[100]. The reason for choosing BCP was its relatively low permittivity [100]. The Hilbert curves have side length of 75 μm, width of 400 nm and thickness of 30 nm. The whole unit cell consisting of four Hilbert curves is 180 μm by 180 μm. At such dimensions the metal (Aluminum) strips have very high resistance. In Fig, 3.6 (a) each Hilbert curve has a DC resistance of about 500 Ω.
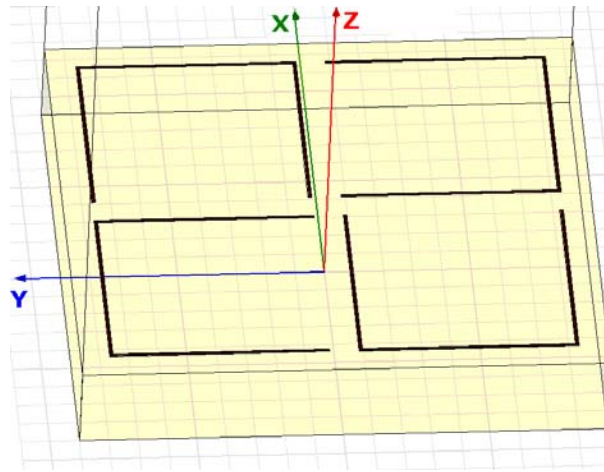
(a)
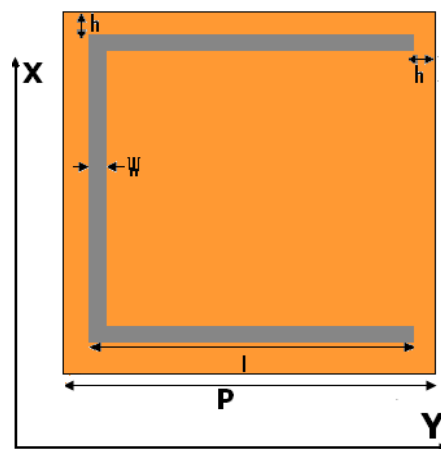
(b)
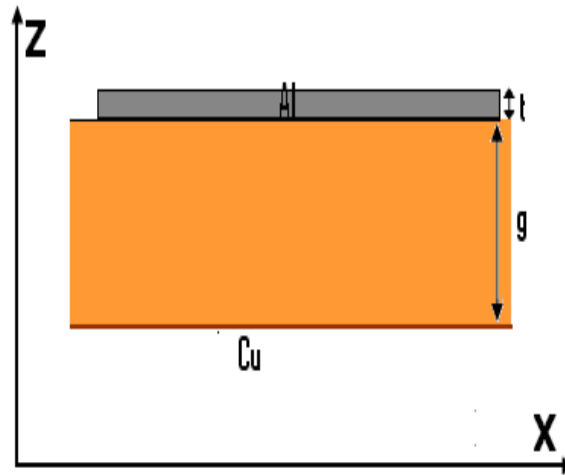
(c)

Fig. 3.6 . (a) Full unit cell of a square Hilbert curve array, (b) top view (top right quarter in (a)), W = 400 nm. h = 10 μm, P = 90 μm, l = 75 μm (whole unit cell is 2P×2P), and (c) side view (top right quarter in (a)), g = 38 μm, t = 30 nm.

3.4.2 Simulations and Results

The structure was simulated using Ansoft's HFSS. Simulation was done considering single unit cell. 2D periodic boundary condition was imposed on the unit cell. Bottom of the unit cell was assigned finite conductivity boundary, with conductivity equal to that of copper in order to simulate the copper ground plane. The incident wave was modeled as a Floquet port above the unit cell. Only the lowest order (n, m=0) Floquet modes were considered in case of incident wave (as the unit cell is smaller than the wavelength). In order to take into account of any possible scattering, coupling of

reflected wave to the higher order modes was also evaluated from the S parameters, but were found to be negligible.
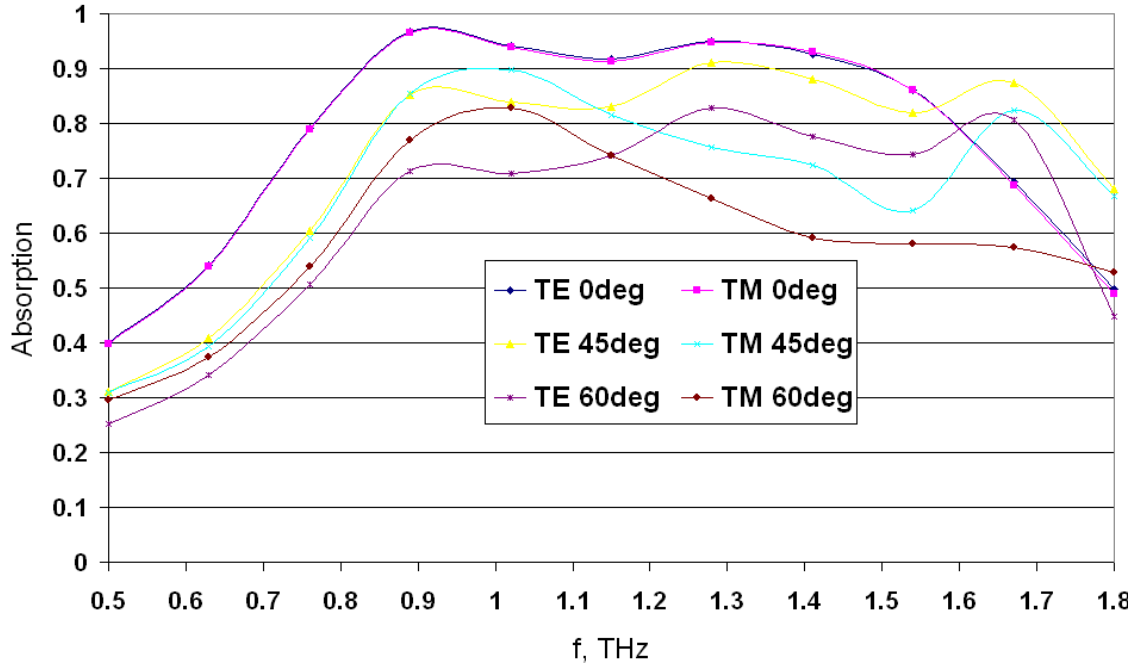
Fig 3.7 Absorption (fractional power absorbed) for the Hilbert curve Terahertz absorber

The structure was also analyzed for normal, 45° and 60° angles of incidence. Fig 3.7 shows the simulation results for absorption from 0.5 THz (600 µm) to 1.8 THz (167 µm). It can be observed that the -3dB absorption bandwidth is 100% for normal incidence, and ranges from 90% to 100% for 45°, and 60° angles of incidence. Peak absorption is 98% for normal incidence and varies from 86% to 94% for oblique incidence. These bandwidths are several times wider than those reported to date [93-95]. It can also be observed that the absorption is polarization independent for normal incidence, as expected from the four fold rotational symmetry of the structure.

To get insight into the absorption process, the electrical field distribution around the Hilbert curves was also obtained and is shown in Fig. 3.8. It is evident that the electric field is concentrated around the Hilbert curves, implying resonant absorption of the incoming wave. From an equivalent circuit model point of view the resonance occurs because the whole structure with the Hilbert curves placed above ground plane behaves as a LCR parallel resonant circuit (Hilbert curve array acting as lossy capacitive sheet, and copper ground plane appearing as inductive load at the plane of Hilbert curve array).
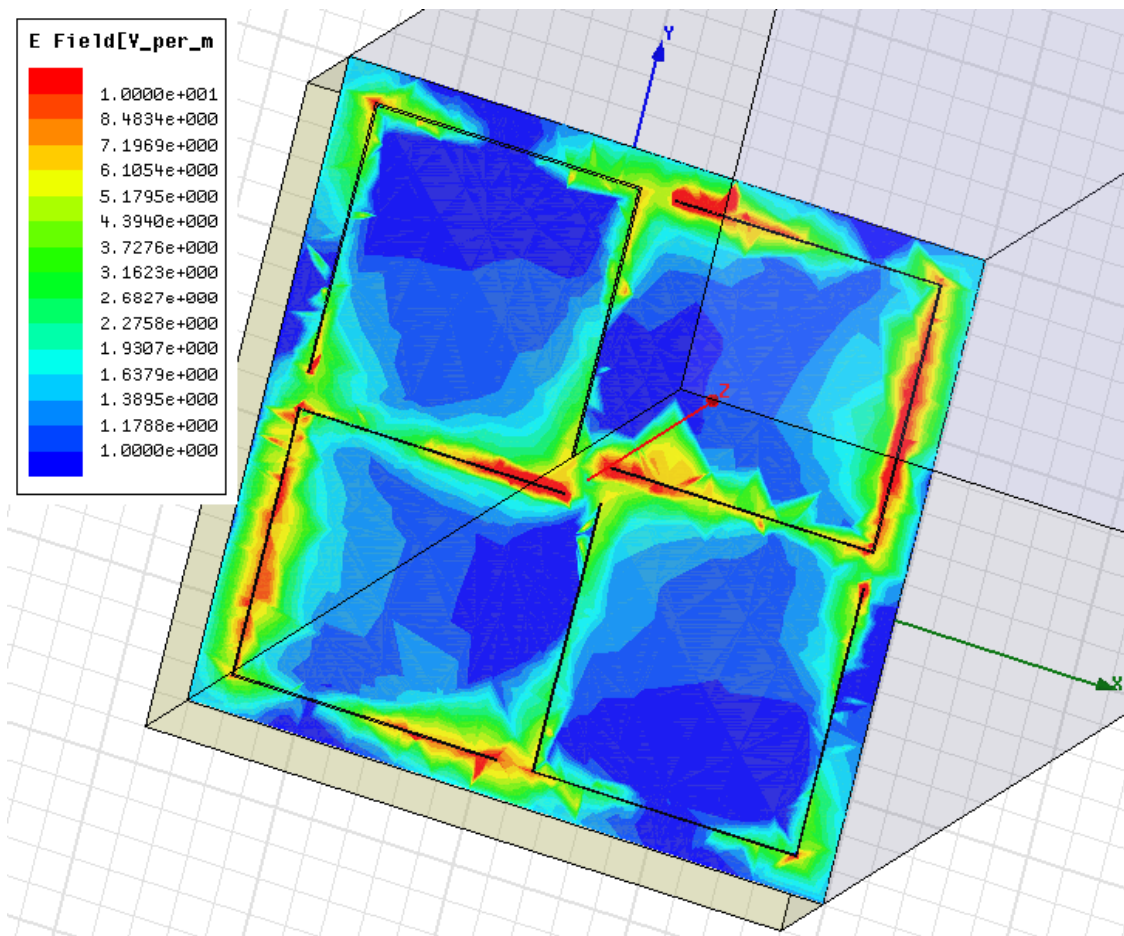
Fig 3.8. Electrical (magnitude) field distribution around the Hilbert curves at 1.2 THz

3.5 Conclusion

It has been demonstrated that a two layer metamaterial Hilbert curve array constructed from resistive/low conductivity materials can act as a thin wideband radar absorbing screen. The advantage of using Hilbert curve over traditional circuit analogue radar absorbing screen is the smaller unit cell size, resulting in reduced coupling to higher order Floquent modes and reduced diffraction effects, which in turn reduces reflection at oblique angles of incidence. The resistive/low conductivity Hilbert curve array gives much wider bandwidth than the one based on conducting ones. Furthermore the structure is simpler than a typical circuit analogue radar absorbing screen.

Furthermore a wideband, wide angle terahertz absorber based on resistive Hilbert curve array was proposed and analyzed numerically. The simulation results show a wide -3dB absorption bandwidth of more than 100% for normal incidence. The structure also works well for oblique incidence. For 60° and 45° angles of incidence, the -3 dB absorption bandwidths are still more than 90%, which is much wider than any other terahertz absorbers reported to date. The peak absorption is also high i.e. 98% for normal incidence and varies from 86% to 94% for oblique incidence

Chapter 4

Parametric Analysis of Metamaterial Hilbert Curve Electromagnetic Absorber

4.1 Introduction

One of the important characteristics of engineering design is its tolerance to the variations in geometric and material parameters from their design values.

In this Chapter the effect of the ground plane-Hilbert curve spacing, inter spacing curve, Hilbert curve cross section geometry, spacer permittivity and ground plane conductivity on the performance of the Hilbert curve electromagnetic wave absorber (discussed in the previous Chapter) is analyzed. Moreover a Hilbert curve absorber for cylindrical targets is also proposed.

4.2 Simulations and Results

4.2.1 Optimization

Inbuilt optimization module of HFSS was used to obtain the optimum values for the geometric parameters. For optimization the first step was to define a suitable optimization goal. In this case the goal was defined as S_{11} to be below -10dB over the

frequency range of 8-18 GHz. In the next step geometric quantities to optimized were fed into the optimization module. The quantities were Hilbert curve thickness, and width, vertical spacing and lateral offset between upper and lower Hilbert curve, and spacer thickness. The optimum value given by the optimization module for Hilbert curve width was 0.18mm, thickness 1.96μm, and spacing between the Hilbert curves was 0.424mm. Thickness of the spacer was 3.4mm and lateral offset between the top and bottom Hilbert curve was 0.585mm along both X and Y direction. Reflection results for the structure are shown in Fig 4.1.
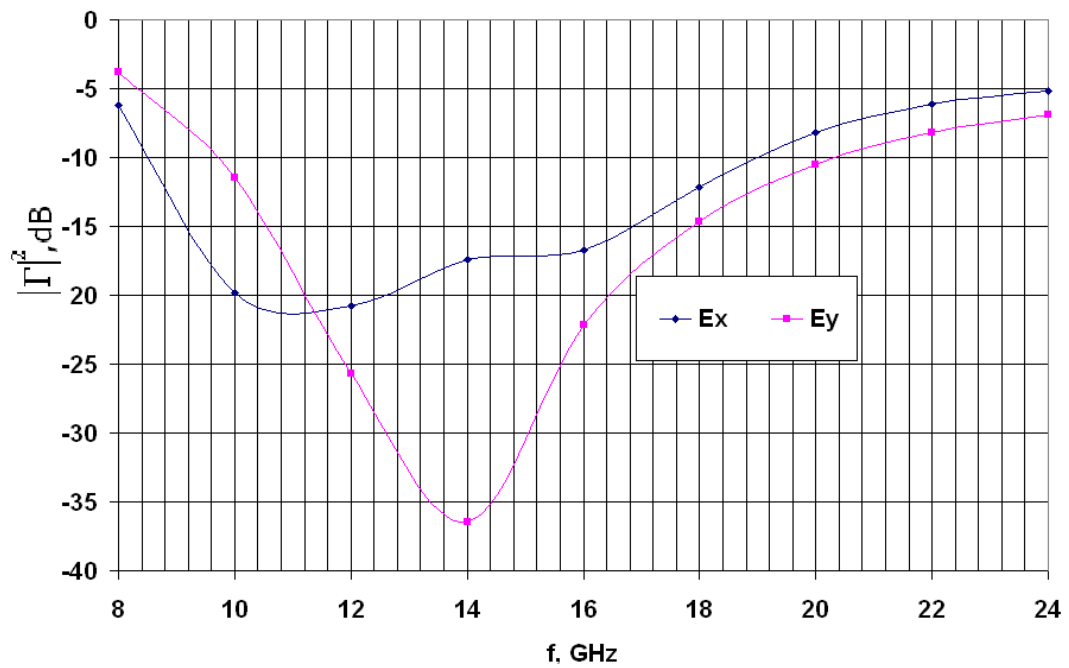
Fig 4.1 Power reflection coefficient for the optimized Hilbert curve array absorber.

4.2.2 Multivariable Sensitivity Analysis

As explained in the previous Chapter, the total reflection depends on the total impedance seen at the plane of the absorber, which is a parallel combination of the inductive susceptance due to the PEC plane and the spacer admittance of the Hilbert curve array.

Absorption will occur for the frequency range over which the capacitive susceptance of the Hilbert curve array has equal or nearly equal magnitude to the inductive susceptance due to the PEC plane and spacer. Our requirement is that the Power reflection coefficient should be less than -10dB. On a Smith chart it would mean the impedance should lie within 0.3r of the centre, where r is the radius of the smith chart[24]. As long as the net impedance of the structure lies within the above mentioned range, the Power reflection coefficient will be less than -10dB

The susceptance due to the PEC plane depends on the distance of the PEC plane from the observation point. Changing the distance of the Hilbert curve array will therefore change the impedance, and thus the absorption profile over a given frequency range, and there will be an optimum value of distance from the PEC plane for which the capacitive susceptance of Hilbert curve will match the inductive susceptance due to PEC plane sufficiently (i.e. keep the net impedance of the structure within the required range) over the broadest frequency range.

The effect of spacing is due to change in coupling between the top and bottom Hilbert curve layers, which in turn will affect the impedance of the Hilbert curve. Impedance of the Hilbert curve will also be affected by the thickness and width of Hilbert curve.

In order to investigate effect of the aforementioned parameters on the performance a multi variable sensitivity analysis was carried out using HFSS. Various combinations of the geometric parameters within 15% of the design values were used for the simulation. Results are shown in Fig 4.2
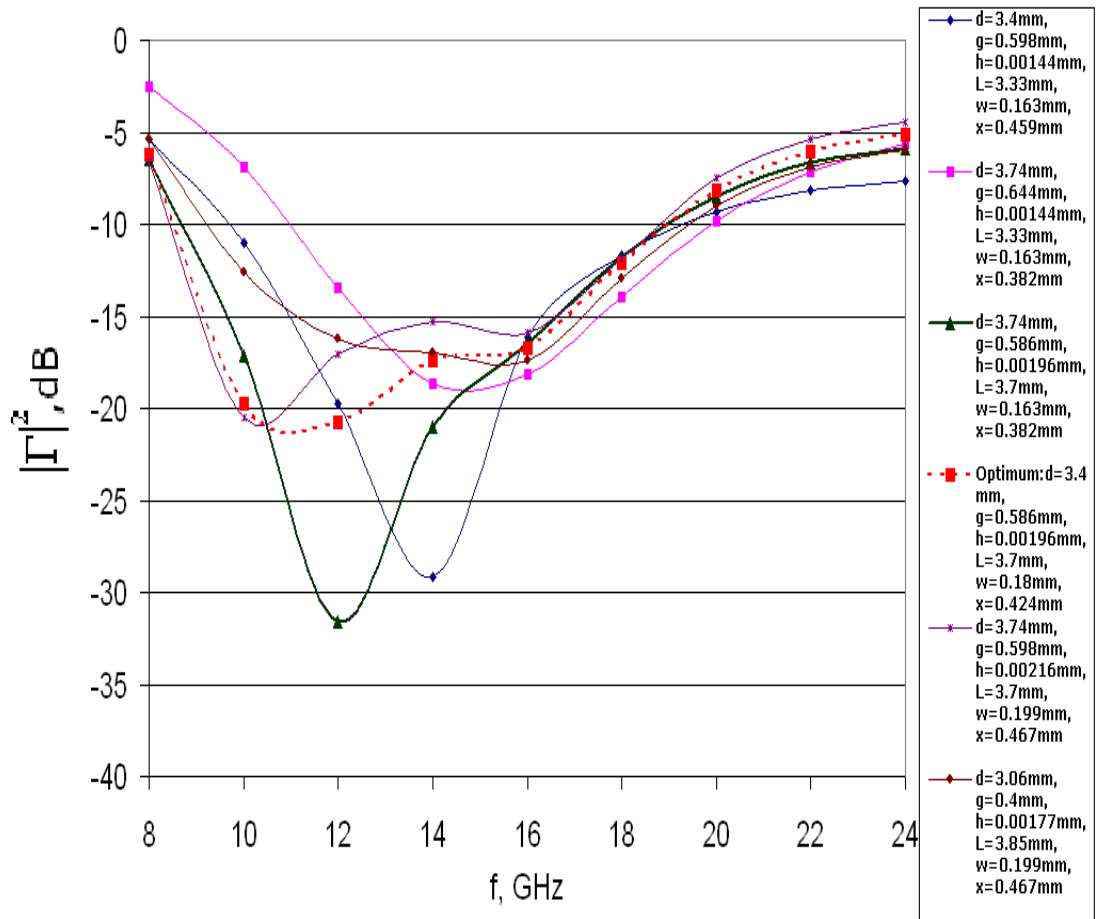
(a)
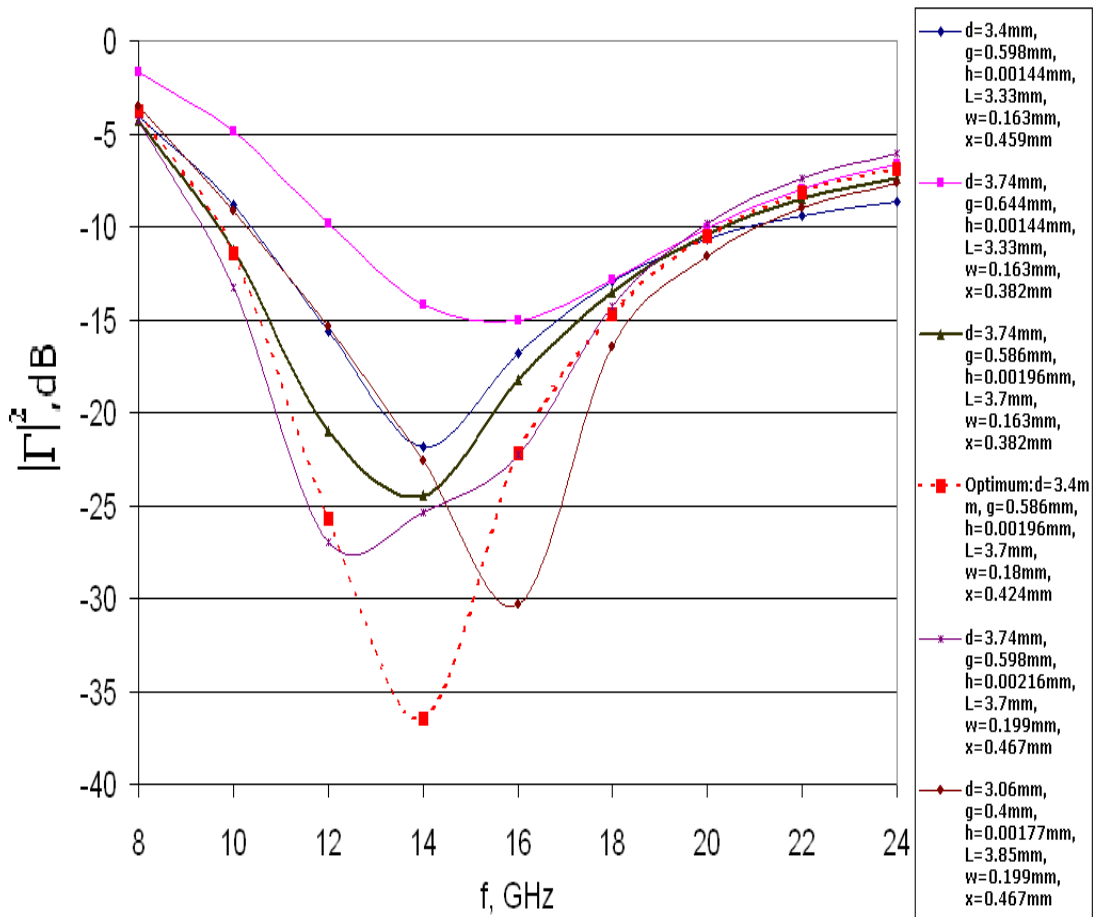
(b)

Fig 4.2 power Power reflection coefficient for varying values of spacer thickness d, offset between upper and lower Hilbert curve g, Hilbert curve thickness h, Hilbert curve side length L, Hilbert curve width w and spacing between top and bottom Hilbert curve x.a)Ex polarization b)Ey polarization.

From the results shown in Fig 4.2 it can be concluded that the design is robust and performance is not very sensitive to the variation in design parameters.

4.2.3 Effect of Conductivity

Furthermore, the effects of changing conductivity of the inclusion material has also been investigated, and the results are shown Fig. 4.3
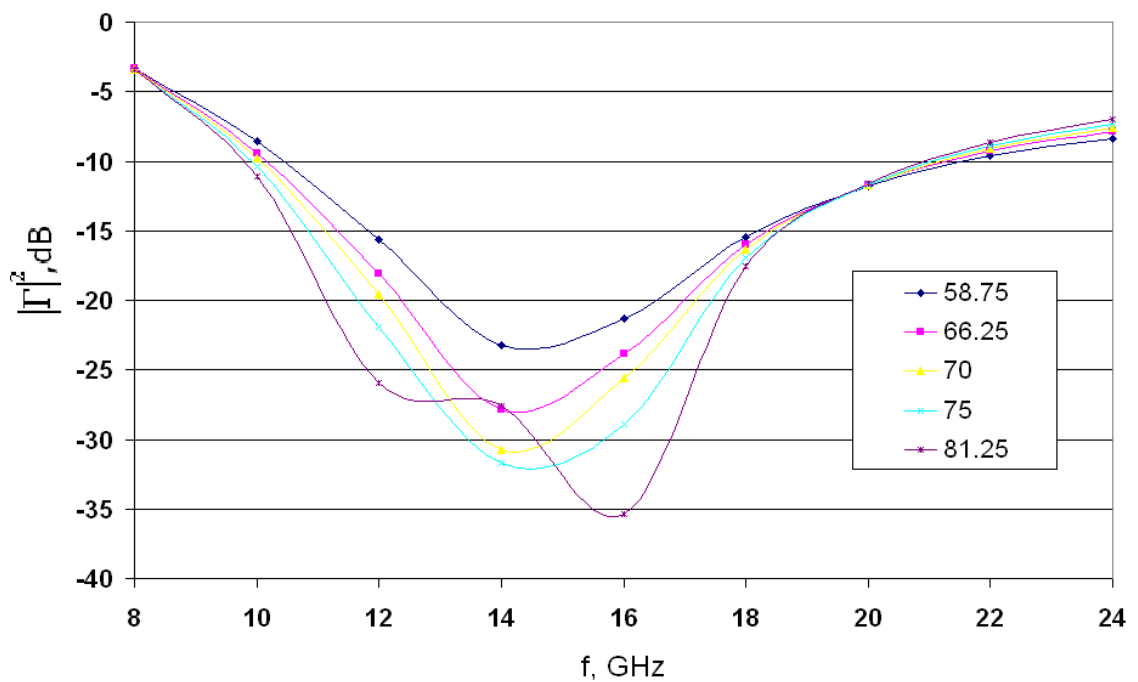
Fig 4.3 Power reflection coefficient for various values of Hilbert curve conductivities (KSm^{-1}).

As can be observed from the results the design is not very sensitive to the change in the conductivity of the Hilbert curve material. Even though change in conductivity will change the impedance of the Hilbert curve, the Power reflection coefficient will still be very low as long the net impedance of the structure is not very ifferent from that of the

free space. The reason for aforementioned fact has been discussed at the beginning of section 4.2.2

4.2.4 Larger Unit Cell for Low Frequency Absorber

In order to study the effects of scaling a larger structure was simulated. All the geometric parameters have been scaled by a factor of two, while keeping the same material for both the spacer and Hilbert curve. The only exception is the thickness of Hilbert curve which is kept the same at 0.0196mm. The reason was to keep the DC resistance of Hilbert curve at 400Ω, as scaling both the width and thickness of the Hilbert curve would have reduced the Hilbert curve resistance by a factor of two.

The result was absorption at lower frequency band, as expected. The results are shown in Fig 4.4.
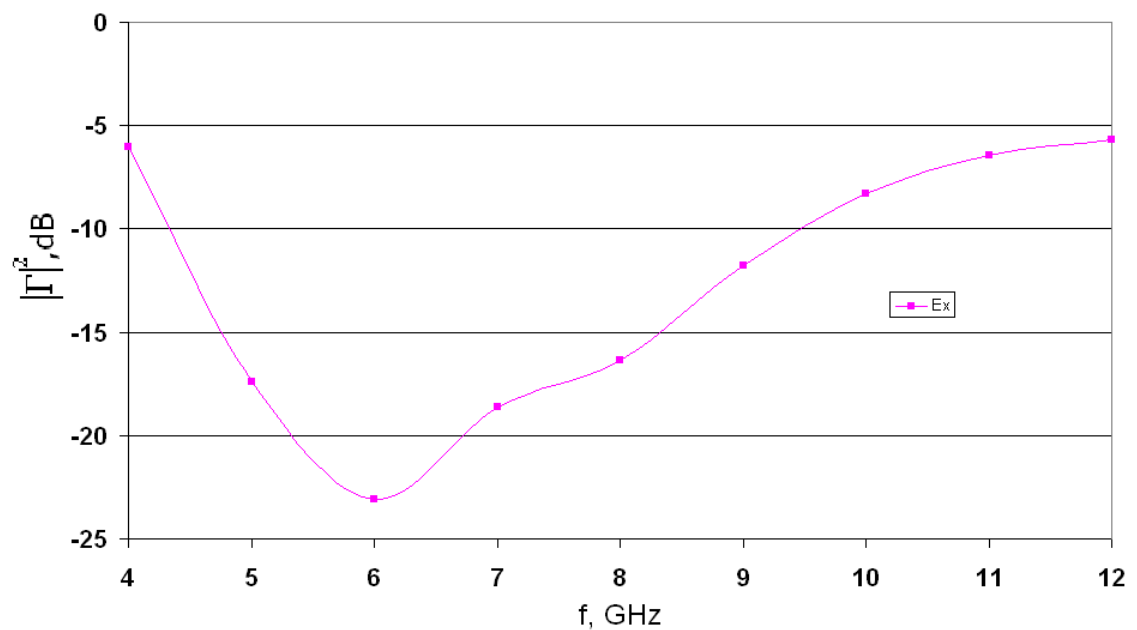
Fig 4.4. Power reflection coefficient for larger structure, E_x polarization.

Comparing Fig 4.4 and Fig 3.3, it can be observed that for E_x polarization, the absorption bandwidth has shifted from 8.5 GHz-19GHz band to 4.4GHz-9.5GHz band. This roughly corresponds to a shift of one octave, as would be expected from the scaling properties of Maxwell equations (as all the dimensions were doubled)

4.2.5 Spacer Permittivity

The absorber was simulated in HFSS for various spacer permittivities .
Incident wave direction was chosen to be normal. Results for E_x and E_y polarizations are shown in Fig. 4.6
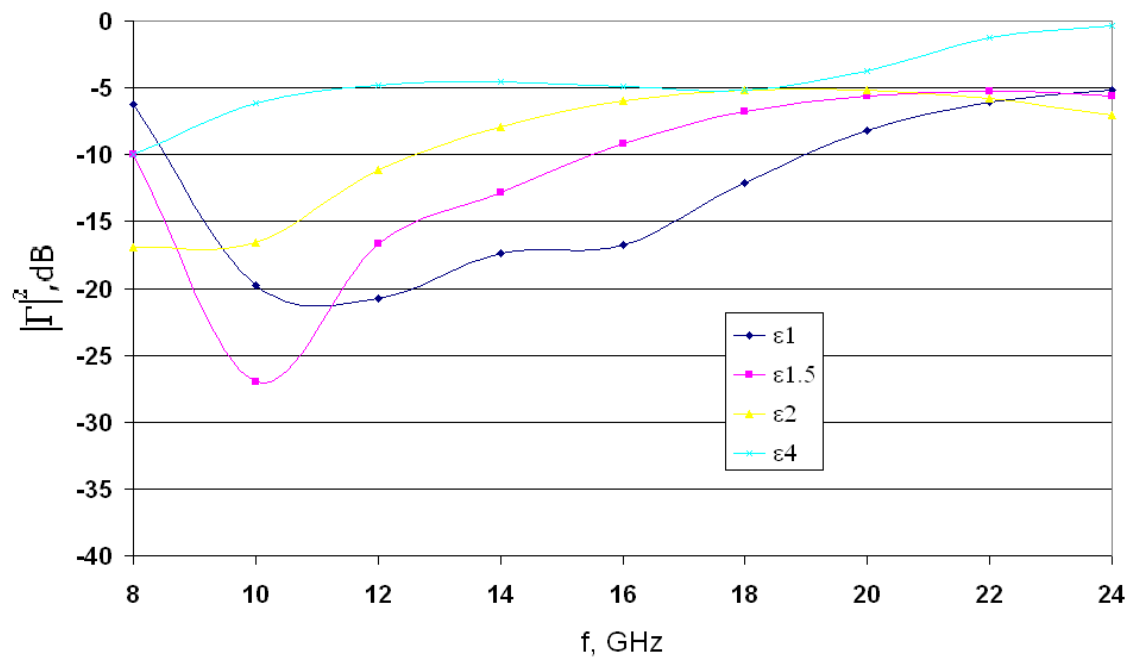
(a)
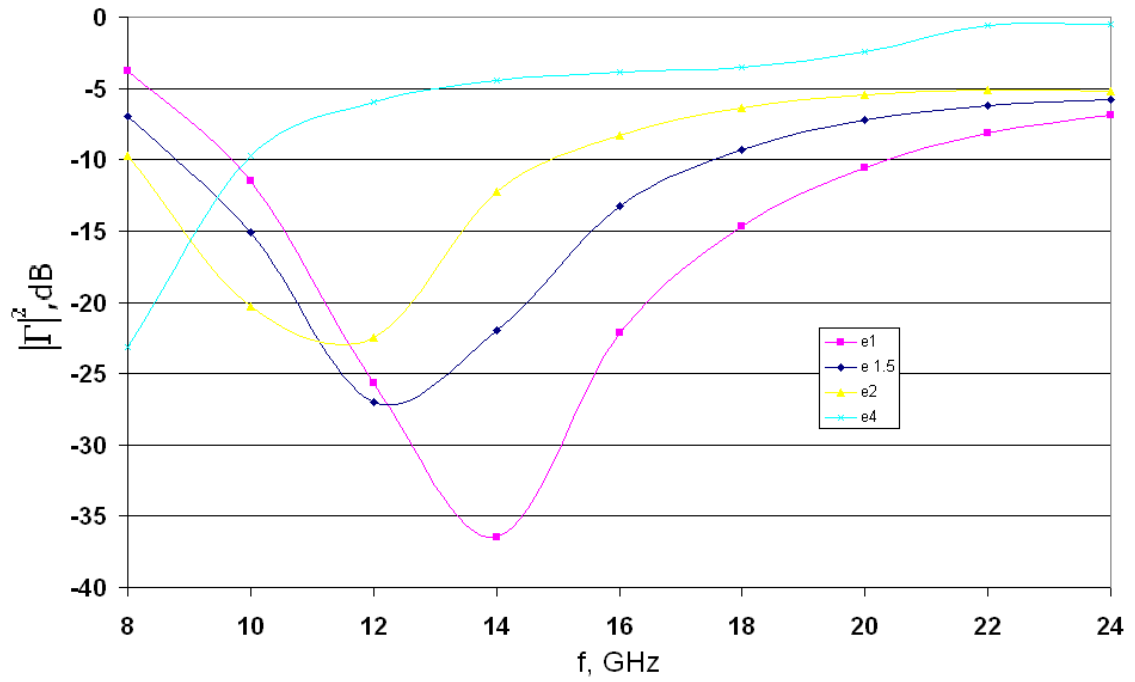
(b)

Fig.4.6. Power reflection coefficient for various values of spacer permittivity. a)E_x polarization b) E_y Polarization

It can be observed from Fig 4.6 that the widest bandwidth is achieved with the permittivity equal to that of free space the reason may be that for other values of the permittivity there will be an impedance mismatch at the dielectric- air interface. Moreover, it can be observed that the behaviour for the E_x polarization is not the same as that for the E_y polarization. The reason is that each of the two Hilbert curve has first resonance with orthogonal polarizations. Bottom Hilbert curve is immersed in the dielectric, and is sandwiched between PEC plan and top Hilbert curve; whereas top Hilbert curve lies on dielectric-air interface. This asymmetry results in dissimilar response to E_x and E_y polarized waves.

4.2.5 Cylindrical Hilbert Curve Absorber

When an absorber designed for planer surface is used on a cylindrical target, its performance depends on diameter of the cylinder in term of wavelengths[47]. If the diameter is more than 10λ the absorber gives same performance as it does for a planer surface. If however, the diameter is much less than 10λ the performance degrades[47].The concept of using an array of resistive Hilbert curves as absorber was extended to a PEC cylinder. Procedure similar to the case of PEC plane was repeated.

A section of the cylinder was defined as a unit cell of the cylindrical array. Cylinder axis was chosen along X axis, and length of unit cell was chosen to be 4.4mm. Cylinder diameter was 20mm. structure is shown in Fig 4.7
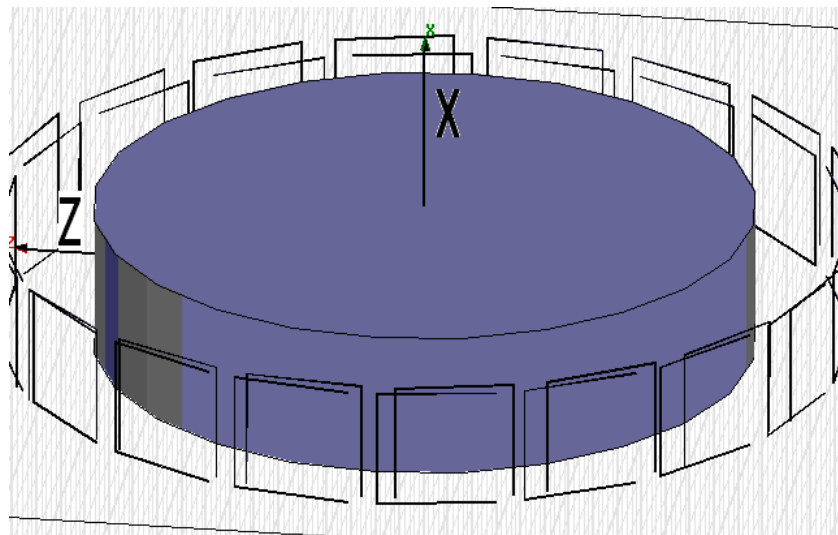
Fig 4.7 Unit Cell of Cylindrical cloak structure. PEC Cylinder surrounded by two layer Hilbert curve array shell. Cylinder axis along X

Two layers of cylindrical shell Hilbert curve array were placed around the cylinder. Radius of the cylinder was chosen to be 10mm.

Hilbert curves had length of each side equal to 3.6mm. The Hilbert curve was of square cross section with thickness of 0.02mm. Conductivity of the Hilbert curve material was chosen to be 80KSm^{-1}.

Inner layer was placed 12.7 mm from the axis or 2.7mm from the PEC surface. The Hilbert curve ring (section of cylindrical shell Hilbert curve array in a single unit cell) consisted of 18 Hilbert curves, each placed at uniform angular spacing 20° from adjacent curve, with open side of Hilbert curve lying along X axis (along cylindrical axis). Outer layer was 13.1mm from axis (3.1mm from cylinder surface). Outer layer was geometrically identical to inner layer, except that the open side of the Hilbert curve was lying along Φ (angular) direction. The outer layer was shifted by 3.7^o azimuthally (anti clockwise) and 0.4mm (+x axis) axially with respect to inner Hilbert curve layer, in order to reduce coupling between inner and outer curve arrays.

The structure was simulated using Ansoft's HFSS, by imposing periodic boundary conditions on the front and back surface of the unit cell, while the other boundaries were defined as radiation boundaries. K vector was along –Z axis. Frequency range was chosen to be 8-13GHz. This corresponds to cylinder diameter of 0.54-0.86λ over the given frequency range.

Monostatic RCS of the structure, was evaluated, and results are shown in Fig 4.8
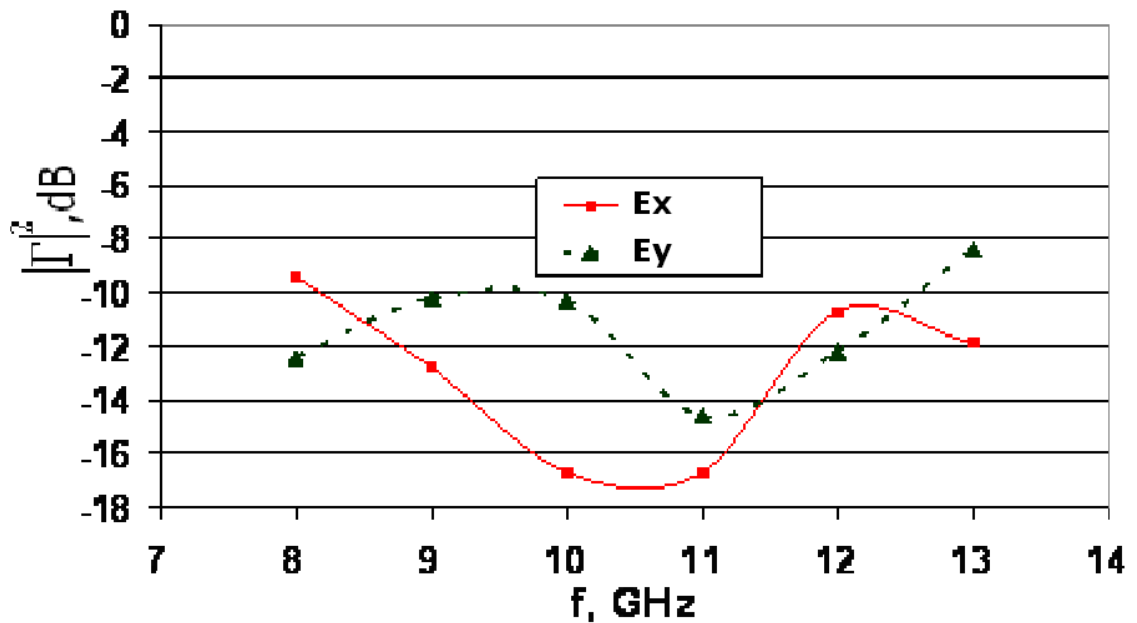
Fig 4.8 Power reflection coefficient for cylindrical Hilbert curve absorber

As shown in Fig 4.8, the Hilbert curve structure provides more than 10 dB reduction in monostatic RCS from 8.2 to 12.6 GHz, for both polarizations. This corresponds to a fractional absorption bandwidth of 42%. This performance is achieved with absorber thickness of only 0.11λ (at centre frequency). Furthermore the cylinder radius is smaller than the wavelength , hence an absorber designed for a planer surface will not usually work for this case[47]. However the Hilbert curve absorber gives good performance even for cylinder with diameter much less than a wavelength.

Fig 4.9 illustrates that electric field is concentrated in the cylindrical shell formed by Hilbert curves, resulting in strong absorption, hence considerable reduction in RCS.
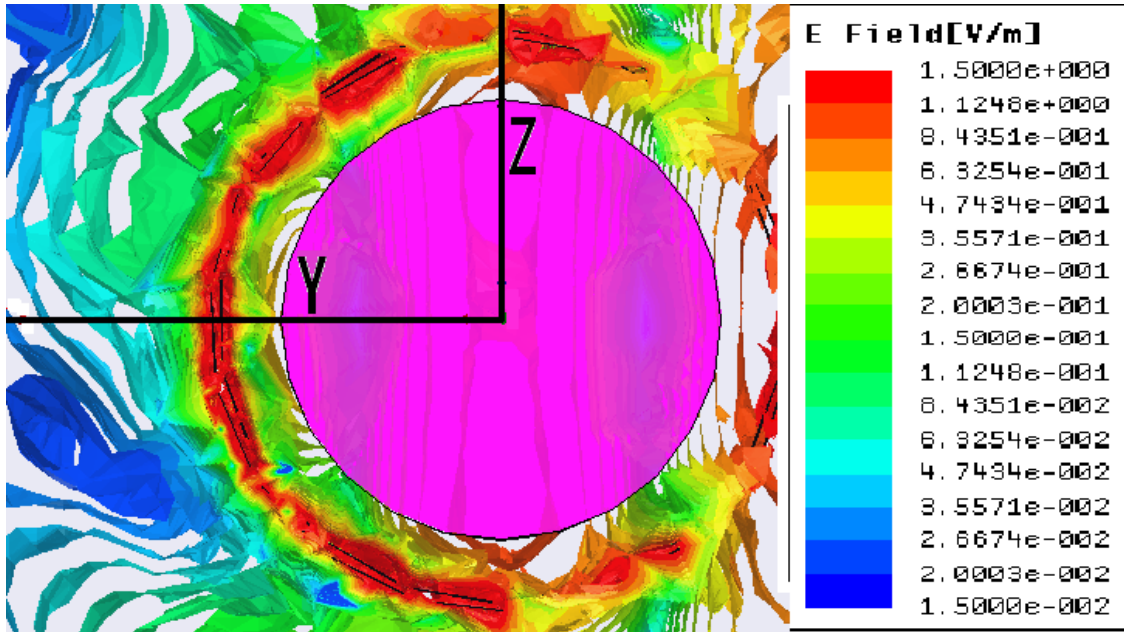
Fig 4.8 E field intensity (axial view) at 11GHz, Ex polarisation,

4.2.7 Parametric Analysis of Hilbert Curve Terahertz Absorber

To thoroughly study the Hilbert curve terahertz absorber discussed in the previous Chapter, sensitivity to variation in geometrical and material parameters, such as thickness and width of the curve, dielectric spacer thickness and permittivity, and conductivity of the ground plane were examined [21]. It must be noted that the Hilbert curve terahertz absorber discussed here is the same as one discussed in the previous Chapter. The Hilbert curve material in this case is always aluminium, so there is no compensation for change in the Hilbert curve cross section. The Hilbert curve resistance therefore changes with changing the thickness or width.

Fig 4.10 shows the absorption for three different widths of the Hilbert curves. It is clear that change in width (± 50%) has only a slight effect on the performance in terms of the peak absorption and bandwidth. Effect of change in Hilbert curve thickness is also examined and illustrated in Fig. 4.11 As in the case of width, change in thickness (± 30%) would affect the absorption only slightly. These two Figures reveal that the Hilbert curve is not particularly sensitive to the change of the width and thickness of the metal strip.

As the Hilbert curve material is kept the same, changing either thickness or width would change the Hilbert curve resistance and thus the impedance of the Hilbert curve absorber layer. Besides the resistance, change in geometry would also effect the reactances of the Hilbert curve.

The concept here is the same as that for the radar absorber, but the conditions are less stringent. As it is a part of detector, our requirement is only -3dB absorption. Absorption of more than -3dB means Power reflection coefficient of less than -3dB, a condition which can satisfied by relatively wide range of the absorber impedance. On a Smith chart it would mean the impedance should lie within 0.7r of the centre, where r is the radius of smith chart. This would mean that the absorber is not very sensitive to the change either in thickness or width .In the case of radar absorber , where a Power reflection coefficient of less than -10dB is required, the allowed range of absorber impedance becomes relatively narrow, as explained in 4.2.2
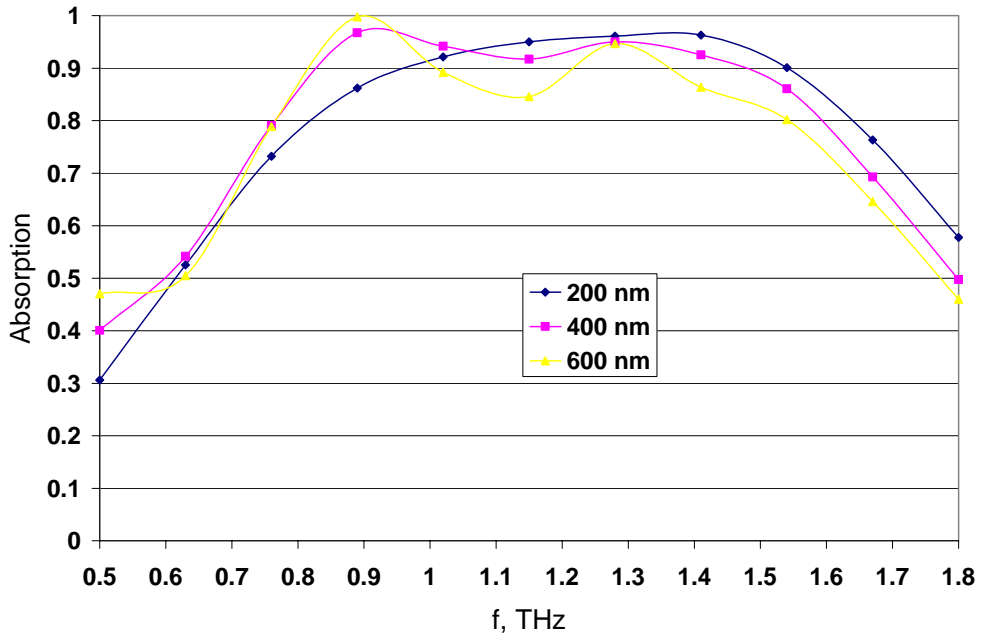
Fig 4.10 Absorption (fractional power absorbed) for various values of Hilbert curve width (normal incidence.
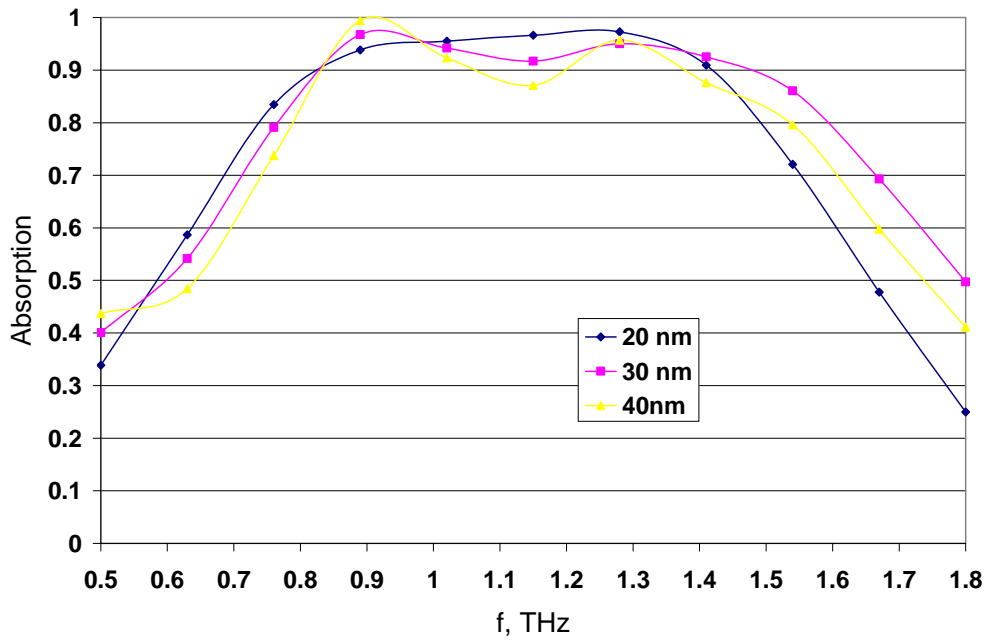
Fig 4.11 Absorption (fractional power absorbed) for various values of Hilbert curve thickness (normal incidence.

Effects of spacer parameters were analyzed next. First effect of permittivity was investigated, and numerical results are shown in Fig 4.12. From the results it can be observed that lower permittivity gives broader bandwidth. The reason probably is that at lower permittivity the spacer characteristic impedance is closer to that of free space. As it was observed in the case of radar absorber, free space permittivity gives maximum bandwidth.
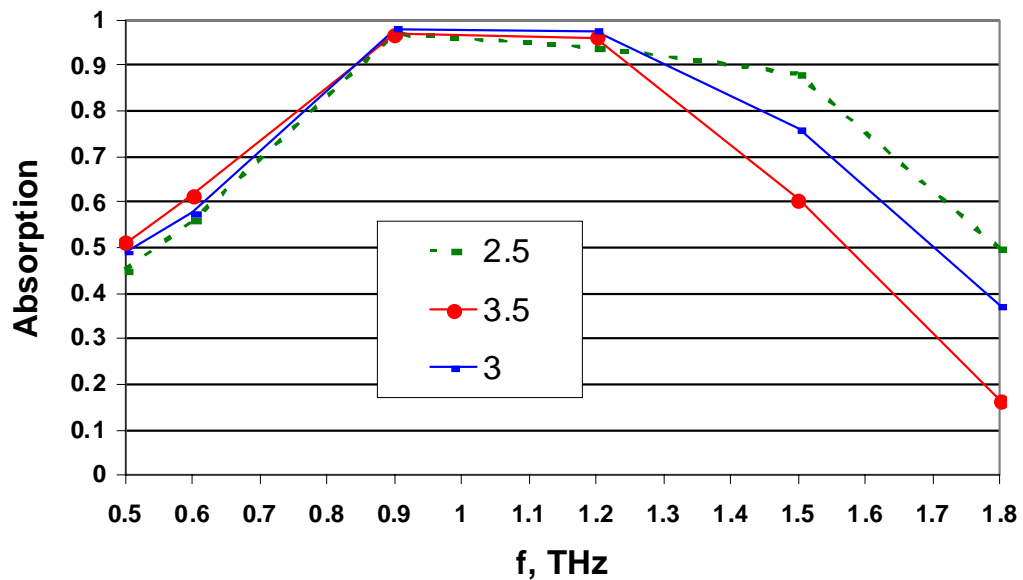
Fig 4.12 Absorption (fractional power absorbed) for various values of spacer permittivity (normal incidence)

Besides permittivity, influence of the dielectric thickness was investigated as well. From the results shown in Fig 4.13 it is clear that the absorption band shifts to higher

frequency as dielectric thickness is reduces. This is what would be expected theoretically from the scaling properties of Maxwell's equations.

Absorption bandwidth is slightly reduced when the thickness is varied from its design value because changing thickness of spacer changes the inductive admittance due to metal ground plane, which affects impedance matching of the structure to the free space.
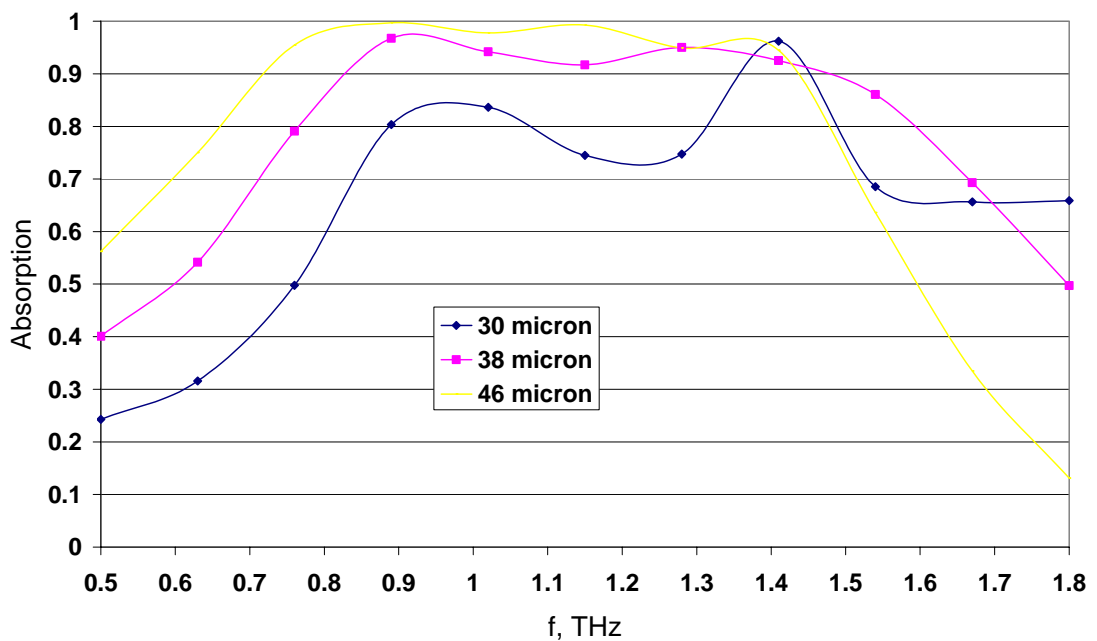
Fig 4.13 Absorption (fractional power absorbed) for various values of spacer thickness in µm (normal incidence

Finally effect of the ground plane conductivity was analyzed. Two cases were considered; copper with conductivity of 58 MSm^{-1}, and another fictitious material with conductivity of 1 MSm^{-1}. Results are shown in Fig 4.14
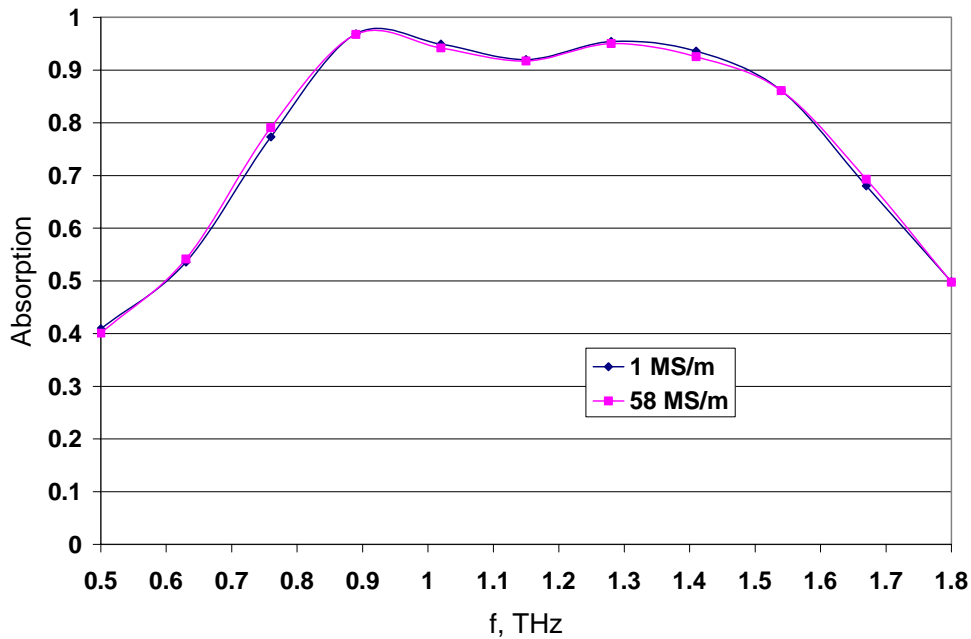
Fig 4.14 Absorption (fractional power absorbed) for copper(58 MSm^{-1})and 1MSm^{-1} ground planes(normal incidence)

The results show that ground plane conductivity has little influence on the performance. It must be noted that 1MSm^{-1} represents a rather poor conductor. Hence as long as the ground plane is constructed from a good conductor, precise value of conductivity is of little consequence.

The reason is simple, looking at the equation for a terminated transmission line in [24], one can observe that as long as the load impedance(in this case surface impedance of the ground plane) is much less than the characteristic impedance of the transmission line (in this case characteristic impedance of the dielectric spacer), the net impedance observed will the same as in the case of a short circuited transmission line (in this case the spacer terminating in a PEC plane)

4.3 Conclusion

Parametric analysis was carried out on the Hilbert curve microwave and terahertz absorbers. From the simulation results it was concluded that the Hilbert curve array absorber has a high tolerance to variations in the geometric parameters of the structure and dielectric parameters of the spacer. The only exception is the spacing between the ground plane and the Hilbert curve array.

Furthermore, it was also observed that it is possible to extend the concept to absorbers for subwavelength cylindrical targets, with reasonably good results.

In the case of the terahertz absorber the requirement was only 3dB absorption, which less stringent than 10dB absorption required for the radar absorber. Under this relaxed condition even the spacing between the ground plane and the Hilbert curve has only weak effect of the absorption bandwidth.

It can be thus said that besides good performance another important advantage of the proposed Hilbert curve absorber is its robustness in terms of tolerance to the variations in the design parameters.

Chapter 5

Plasmonic Cloaking for Subwavelength Objects with Various Geometric Shapes

5.1. Introduction

Cloaking of objects using artificial electromagnetic materials, also known as metamaterials, has been investigated over the last few years. There are basically three ways of concealing an object from electromagnetic waves, first to absorb the impinging signal [25-26], second to cancel out the scattered electric and magnetic fields of the object [28], and third to guide incoming waves around the object [29-31]. In the case of cancellation, mainly the spatial fundamental electric and magnetic dipole components of scattered field are cancelled [28,33].

Cloaking makes an object completely invisible to an observer by manipulating the fields around the object in such a way that the resulting field pattern is same as it would have been with out the target being present. An absorber on the other hand simply absorb the incoming radiation, and the target can still be detected from the shadow that it casts due to absorption. An example is an object covered with radar absorbing screen and placed between an airborne radar and the ground. Even though the object will absorb the electromagnetic wave, it will still be detected as it will cause a drop in the energy reflected from the ground due to absorption by target. The object

will thus appear as a shadow region to the radar. If however, instead of absorption cloaking is used, the object will be completely transparent to the radar, and radar will receive the radar signal reflected by the ground without any effect due to the target.

From the law of conservation of energy the radiation impinging on an object must be absorbed, scattered or diverted around the object. Cancellation of polarization doesn't involve any absorption, hence the cancellation must result in the incoming wave being diverted around the object in such a way that at the receiver the wave should appear to be coming undisturbed from the source. It can therefore be claimed that field cancellation is also a form of cloaking [33].

Metamaterials are interesting for cloaking purposes because their electromagnetic properties are not restricted like those of natural materials. For instance negative permeability or permittivity in natural materials can be found only in a narrow frequency bands, and the losses are very high.

Hiding a target from the radar by absorption is well established and extensively used[25,26] and has been discussed in the previous Chapters .The rest of the two techniques are however relatively new, and usually require use of metamaterials due to the required permittivities and permeabilities that are not easily available.

Guiding the electromagnetic waves around the target is accomplished through using a cloak with such a permittivity/permeability profile that the incoming wave is diffracted around the object instead being scattered or reflected [29]. A cloaking problem can be considered as coordinate transformation [29,31,101]. For instance, if a target is to be

cloaked using a hollow cloaking shell. From a geometric point of view the problem can be interpreted as the transformation of the space of hollow cloak to the free space so that the hollow region remains invisible to incoming radiation[29,31]. This transformation can be achieved by transforming Maxwell's equations, written for free space, to the new coordinates representing the cloak, which results in modification of the coefficients of Maxwell's equations, which in turn could be represented by modified values for the constitutive parameters [30].

Such an analysis was first performed initially to solve Maxwell's equations in a non homogeneous medium in [30]. Later a metamaterial cloak which worked on the principle of transforming a hollow sphere to free space was proposed and theoretically analysed [29]. and very recently such a cloak was experimentally implemented [31] using split ring resonators (SRRs) and thin wires to create a cloak with the required values of tensor constitutive parameters.

Radar signature reduction through coordinate transformation and cancellation of the incident fields was further considered analytically and numerically by many other researchers [109-119].

Cloaking can also be achieved through cancellation of the field generated by the target. This can be achieved mainly by two means; first to have a cloak with the polarizability equal and opposite to that of the target [28,102-104]; second to have a permittivity and permeability profile which will result in anomalous resonance either within the cloak or its vicinity [115]. Cloaking through anomalous resonance was first investigated in the case of a metamaterial hollow cylinder superlens, where it was realized that such a

lens would be invisible in the quasistatic limit (when the field gradient is low throughout the object) [115]. In both cases, the cloaking effect is achieved by having the net polarization equal to zero. Later it was shown that such a structure can cloak a collection of dipoles, provided that all the dipoles were within a certain radius [116].

Cloaking by cancellation of the target polarization using plasmonic metamaterial cover was first investigated theoretically in [28], where a mathematical model of such a cloak was presented. Later the same authors extended the concept to a collection of particles [32]. However, only spherical (including fused spheres) objects were analysed. Extension of studies on plasmonic metamaterial cloaking to other geometrical shapes is the subject of this work.

Metamaterial cloaks have also been implemented using inverse scattering element [117], superconductor based metamaterials for very low frequencies [118], and transmission line networks [119] .

5.2 Theoretical Analysis

Cloaking by simply having a cloaking shell with polarisation equal and opposite to the target is easy to understand. The idea is that the field generated by an object can be decomposed into spherical harmonics in spherical coordinates [28]. The lowest order spherical harmonics represent the electric and magnetic dipole terms, whereas the higher order terms represent the multipolar terms.

The spherical harmonics are Bessel functions combined with Legendre polynomials and sin/cosine functions. The radial dependence is given by the Bessel functions, whereas the other functions give angular and azimuthal dependence. If the object is small compared to the wavelength, then, on the boundary of the object, regardless of the exact geometrical shape, the higher order terms of the Bessel functions will be much smaller than the first order terms, and can thus be neglected. The first order terms represent electric and magnetic dipoles. Therefore it can be claimed that electric and magnetic fields generated by subwavelength objects are roughly the same regardless of there exact geometrical shape, with difference only in the strength of electric and magnetic dipole, which depends mainly on the dielectric properties of the object and surrounding material. For the reason explained above, the cloak parameters that have been obtained by A Alu and Engheta [33] for cloaking a metallic sphere, can also be used for other geometrical shapes, and this is central hypothesis of this work.

Consider a sphere made of material with permittivity of ε which is coated with a shell of different material with permittivity ε_c. The condition for cancelling electric dipoles of scattered radiation is given by [28,33].

$$
\begin{vmatrix}
j_n(ka) & j_n(k_c a) & y_n(k_c a) & 0 \\
[ka\,j_n(ka)]'/\varepsilon & [k_c a\,j_n(k_c a)]'/\varepsilon_c & [k_c a\,y_n(k_c a)]'/\varepsilon_c & 0 \\
0 & j_n(k_c a_c) & y_n(k_c a_c) & j_n(k_o a_c) \\
0 & [k_c a_c\,j_n(k_c a_c)]'/\varepsilon_c & [k_c a_c\,y_n(k_c a_c)]'/\varepsilon_c & [k_o a_c\,j_n(k_o a_c)]'/\varepsilon_o
\end{vmatrix} = 0
$$

(5.1a)

$$
\begin{vmatrix}
j_n(ka) & j_n(k_c a) & y_n(k_c a) & 0 \\
[ka\, j_n(ka)]'/\mu & [k_c a\, j_n(k_c a)]'/\mu_c & [k_c a\, y_n(k_c a)]'/\mu_c & 0 \\
0 & j_n(k_c a_c) & y_n(k_c a_c) & j_n(k_o a_c) \\
0 & [k_c a_c\, j_n(k_c a_c)]'/\mu_c & [k_c a_c\, y_n(k_c a_c)]'/\mu_c & [k_o a_c\, j_n(k_o a_c)]'/\mu_o
\end{vmatrix} = 0
$$

(5.1b)

where j_n and y_n are the spherical Bessel functions of order n, and apostrophe denotes differentiation with respect to the argument of the Bessel function. k_c and k are the wavenumbers of the electromagnetic wave in the cover and object respectively. *a* and a_c are radii of the object and cloak respectively. For a subwavelength object the higher order terms can be neglected [28,33]. The condition for cancellation of dipole terms can be obtained by putting n equal to one in the equations above. For small arguments i.e. less than one, the first order spherical Bessel functions can be approximated as [120].

$$
J_1(x) = \frac{x}{3}
$$

$$
y_1(x) = -\frac{1}{x^2}
$$

$$
\rightarrow [x j_1(x)]' = \frac{2x}{3}
$$

$$
\rightarrow [x y_1(x)]' = \frac{1}{x^2}
$$

(5.2)

Substituting (5.2) into (5.1a)

$$\begin{vmatrix} \dfrac{ka}{3} & \dfrac{k_c a}{3} & -\dfrac{1}{k_c^2 a^2} & 0 \\[2mm] \dfrac{2ka}{3\varepsilon} & \dfrac{2k_c a}{3\varepsilon_c} & \dfrac{1}{\varepsilon_c k_c^2 a^2} & 0 \\[2mm] 0 & \dfrac{k_c a_c}{3} & -\dfrac{1}{k_c^2 a_c^2} & \dfrac{k_0 a_c}{3} \\[2mm] 0 & \dfrac{2k_c a_c}{3\varepsilon_c} & \dfrac{1}{\varepsilon_c k_c^2 a_c^2} & \dfrac{2k_0 a_c}{3\varepsilon_0} \end{vmatrix} = 0$$

$$\rightarrow \dfrac{ka}{3}\begin{vmatrix} \dfrac{2k_c a}{3\varepsilon_c} & \dfrac{1}{\varepsilon_c k_c^2 a^2} & 0 \\[2mm] \dfrac{k_c a_c}{3} & -\dfrac{1}{k_c^2 a_c^2} & \dfrac{k_0 a_c}{3} \\[2mm] \dfrac{2k_c a_c}{3\varepsilon_c} & \dfrac{1}{\varepsilon_c k_c^2 a_c^2} & \dfrac{2k_0 a_c}{3\varepsilon_0} \end{vmatrix} - \dfrac{2ka}{3\varepsilon}\begin{vmatrix} \dfrac{k_c a}{3} & -\dfrac{1}{k_c^2 a^2} & 0 \\[2mm] \dfrac{k_c a_c}{3} & -\dfrac{1}{k_c^2 a_c^2} & \dfrac{k_0 a_c}{3} \\[2mm] \dfrac{2k_c a_c}{3\varepsilon_c} & \dfrac{1}{\varepsilon_c k_c^2 a_c^2} & \dfrac{2k_0 a_c}{3\varepsilon_0} \end{vmatrix} = 0$$

$$\rightarrow \begin{vmatrix} \dfrac{2k_c a}{3\varepsilon_c} & \dfrac{1}{\varepsilon_c k_c^2 a^2} & 0 \\[2mm] \dfrac{k_c a_c}{3} & -\dfrac{1}{k_c^2 a_c^2} & \dfrac{k_0 a_c}{3} \\[2mm] \dfrac{2k_c a_c}{3\varepsilon_c} & \dfrac{1}{\varepsilon_c k_c^2 a_c^2} & \dfrac{2k_0 a_c}{3\varepsilon_0} \end{vmatrix} - \dfrac{2}{\varepsilon}\begin{vmatrix} \dfrac{k_c a}{3} & -\dfrac{1}{k_c^2 a^2} & 0 \\[2mm] \dfrac{k_c a_c}{3} & -\dfrac{1}{k_c^2 a_c^2} & \dfrac{k_0 a_c}{3} \\[2mm] \dfrac{2k_c a_c}{3\varepsilon_c} & \dfrac{1}{\varepsilon_c k_c^2 a_c^2} & \dfrac{2k_0 a_c}{3\varepsilon_0} \end{vmatrix} = 0 \qquad (5.3)$$

$$\rightarrow \varepsilon\begin{vmatrix} 2a & a_c^2 & 0 \\ \varepsilon_c a_c & -\varepsilon_c a^2 & \varepsilon_0 \\ 2a_c & a^2 & 2 \end{vmatrix} - 2\begin{vmatrix} \varepsilon_c a & -\varepsilon_c a_c^2 & 0 \\ \varepsilon_c a_c & -\varepsilon_c a^2 & \varepsilon_0 \\ 2a_c & a^2 & 2 \end{vmatrix} = 0$$

After simplification one gets

109

$$a = \sqrt[3]{\frac{(\varepsilon_c - \varepsilon_o)(2\varepsilon_c + \varepsilon)}{(\varepsilon_c - \varepsilon)(2\varepsilon_c + \varepsilon_o)}} a_c \qquad (5.4)$$

The condition for cancellation of the magnetic dipole is then obtained by replacing ε with μ in the equations above. In the case of non ferromagnetic metals, the condition for the cancellation of the electric dipole term can be approximated as [28,33].

For metals in microwave region

$$\varepsilon = \varepsilon_0 \left(1 - j \frac{\sigma}{\varepsilon_0 \omega} \right)$$

$$\frac{\sigma}{\varepsilon_0 \omega} >> 1$$

$$\rightarrow |\varepsilon| >> |\varepsilon_0|$$

$$\rightarrow a = \sqrt[3]{\frac{(\varepsilon_o - \varepsilon_c)}{(2\varepsilon_c + \varepsilon_o)}} a_c \qquad (5.5)$$

(5.5) will give a realizable value of radius only if $\varepsilon_c < \varepsilon_0$. The required value of radius will either be imaginary (for $\varepsilon_c > \varepsilon_0$) or zero (for $\varepsilon_c = \varepsilon_0$) if this condition is not met [28,33].

Magnetic polarizabilities of subwavelength objects in which electromagnetic fields can't penetrate are negative [33]. Thus having a plasmonic cloak with positive magnetic permeability, it is possible to cancel out both the electric and magnetic dipole terms of the scattered field [33]. In [33] the required values of cloak radius, permittivity and permeability are calculated numerically, as analytical methods given above work one term at time only [33], however they do give a rough idea of the required parameters.

As explained earlier, the same concept can be extended to other geometrical shapes, provided they are much smaller than the wavelength of the incident wave.

In this Chapter cloaking of metallic sub-wavelength cube and cylinder objects by isotropic, homogeneous plasmonic cover is investigated and numerically analysed. Significant reductions in both monostatic and bistatic RCS have been observed even in the presence of losses. In the case of a cube object, oblique incidence is also considered. Furthermore, cloaking of a rectangular bar has also been investigated. The cloak in all these cases is a spherical plasmonic shell, but with losses. The simulation results reveal that a lossy shell slightly degrades the cloaking performance; nevertheless the reduction in RCS is still sufficient for potential practical applications.

Effects due to variation of dimensions parallel and normal to the electric field on RCS were studied in detail. RCS was numerically evaluated for various values of length and width, both with and without the cloak. It was observed that significant reduction in RCS can be obtained for rectangular objects with a wide range of target dimensions, using a cloak which is designed for cloaking a conducting sphere.

Further the bistatic RCS of a conducting sphere with radius equal to 0.2λ is compared with that of other uncloaked geometric objects. It was observed that the scattered fields of the cone, cylinder and cube are very similar, except in the direction parallel to the electric field polarization, which is not very important for cloaking purposes, as the scattered field in this direction is very weak(As the scattered field is dominated by electric dipole term), and thus has no significant effect as far as cloaking is concerned. Furthermore it can be observed from the RCS of the uncloaked objects that the scattered field is dominated by electric dipole component in all of the subwavelength cases, i.e. the field is nearly uniform in the H plane, and in the E plane it has two minima along the axis parallel to E field.

5.3   Simulations Setup and Results

In this study the investigation of cloaking a cube, a cylinder, and a cone has been carried out, and in the case of a cube object, oblique incidence has also been considered. The cloak in all these cases is spherical plasmonic shell. The values for the length (in case of cube), height, and radius (in case of cylinder) are chosen such that the object just fits into the cloaking shell. The parameters (inner and outer radii,

constitutive parameters, and losses) are the same as those proposed in [33] for cloaking a metallic sphere. The inner and outer radii of the cloak are however normalized to the operating wavelength (25 cm).

Cube, cone and cylinder were chosen for the investigation because they are representative of non spherical geometric shapes, whose all three longest dimensions, defined as three longest orthogonal lines that can fit into the object, are similar to that of a sphere. The idea is to use object with non spherical geometry, but with roughly same electrical and magnetic polarizabilities as the given sphere. Furthermore, the study of a fused sphere in [32] is extended to rectangular bar. In case of cloaking the bar, the parameters for cloaking shell inner and outer radii (normalized to operating wavelength) have been taken from [33]. The value of cloak permittivity given by (5.5) will work only to cancel out the electric dipole term. In order to cancel out both the electric and magnetic dipole terms a magneto-plasmonic cloak has to be used, with values obtained numerically, which has been done in [32,33]. The operating frequency chosen in this case is slightly lower (1.14 GHz rather than 1.2 GHz) than that used in the case of smaller objects, the reason is that frequency at which cloaking is most effective moves to slightly lower frequency [32]. The spacing between the centres of the cloaking shell is chosen arbitrarily.

Monostatic and bistatic RCS are evaluated using Ansoft HFSS , and compared to that of uncloaked objects. The operating frequency is selected to be 1.2 GHz (1.14 GHz in case of extended objects)

5.3. 1 Aluminium Cube

Fig. 1 shows an aluminium cube covered by a plasmonic metamaterial shell. The outer radius of the shell is 57.5 mm and the inner one is 50 mm (0.2λ at 1.2 GHz. The relative permittivity of the shell is 0.1 and the relative permeability is 5.1. Electric and magnetic loss tangents for lossy cloak are 0.15 and 0.1 respectively. The same constitutive parameters for the cloak have been used throughout this Chapter with the exception of the extended object. The dimensions of the cube are chosen such that it would just fit in the shell, i.e., the cube length of each side is 57.75 mm.
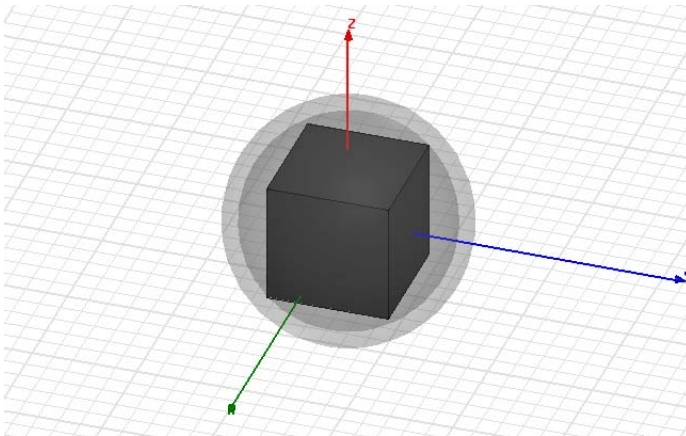
Fig 5. 1 Spherical cover shell (outer radius r_{out} = 57.5 mm and inner radius r_{in} = 0.2λ = 50 mm . ε_r(shell)=0.1 μ_r(shell)= 5.1,. k vector is along Y axis and E along Z axis.

The matematerial shell structure was investigated with and without the dielectric and magnetic losses. Dielectric and magnetic loss tangents for the lossy shell were 0.15 and 0.1 respectively. The k and E vectors were along the Y and Z axes respectively. Fig 5.2 illustrates that the monostatic RCS (normalized to the square of wavelength) is -4.4 dB without cloaking, -30.7 dB and -21.5 dB with lossless and lossy plasmonic shells respectively. Magnetic and dielectric loss tangents for the lossy cloaking shell

are 0.15 and 0.1 respectively. It can be observed that monostatic RCS with the lossless

plasmonic shell is 26 dB lower than that without cloaking, whereas for the lossy case,

reduction is 17dB. The simulated results are close to that reported in [7] for the

metallic sphere.
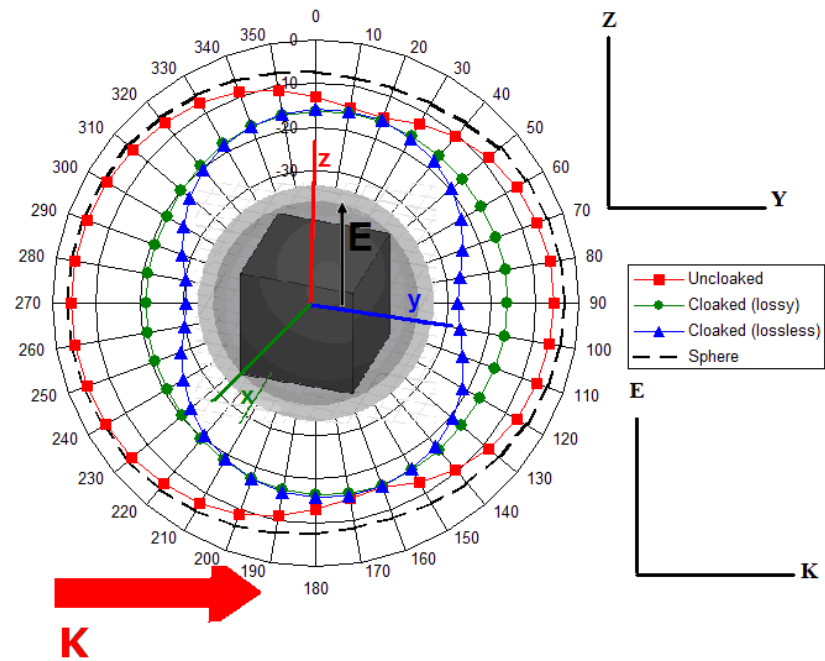
(a)
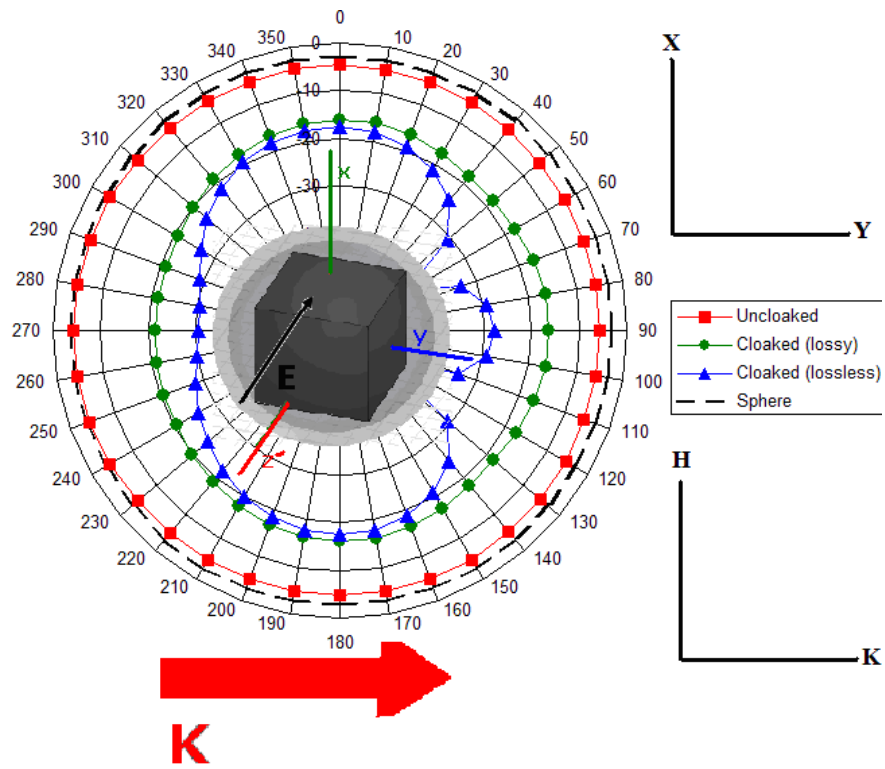
(b)
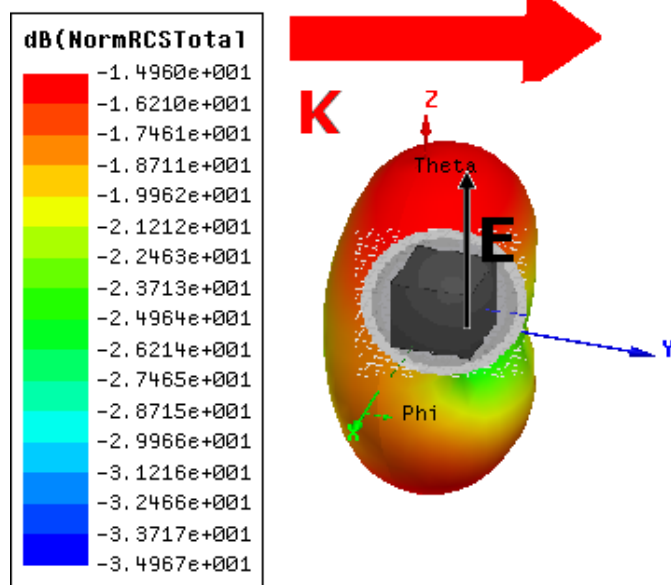
(c)

Fig 5.2 RCS (both monostatic and bistatic), dB(σ/λ^2),cube (cloak, δ_e=0.15, δ_m=0.1), (a) E plane (b) H plane (c) 3D view.

It is evident that significant cloaking has been achieved for the metallic cube. It also becomes clear that the effect of the dielectric and magnetic losses of the plasmonic shell is to degrade the RCS. By introducing dielectric and magnetic loss tangents of 0.15, and 0.1 respectively, the monostatic RCS has increased by 9 dB. Losses will change the permittivity and thus field generated by the cloak, resulting in poorer performance.

The maximum value of the bistatic RCS (normalized to the square of wavelength) for uncloaked and cloaked (lossy cloak) case is -4.4dB and -16dB respectively, meaning a reduction of 11.6 dB in the maximum bistatic RCS even in the presence of losses.

The effect of incident angle of the incident wave has also been examined by rotating the cube by 45 degrees, first around the Z axis and then 45 degrees around the X axis.

(a)

117
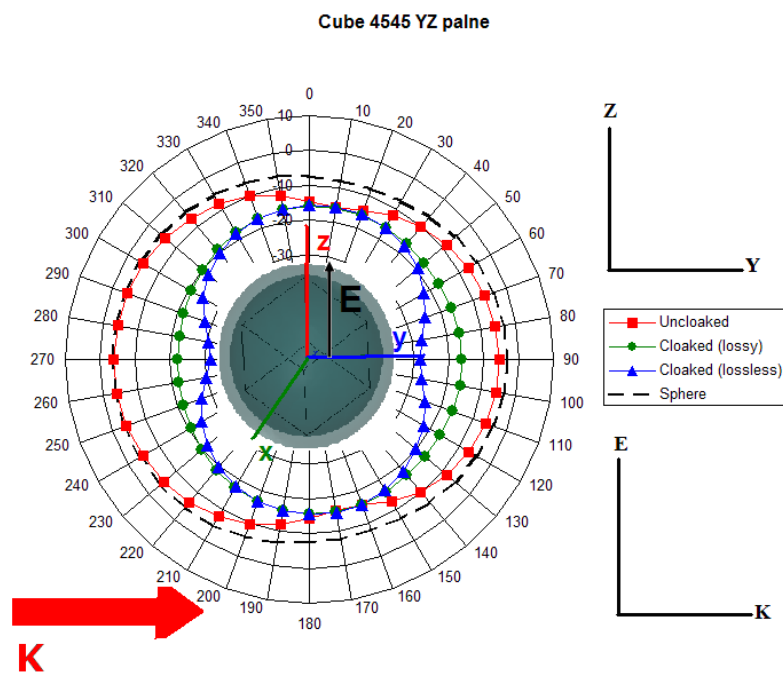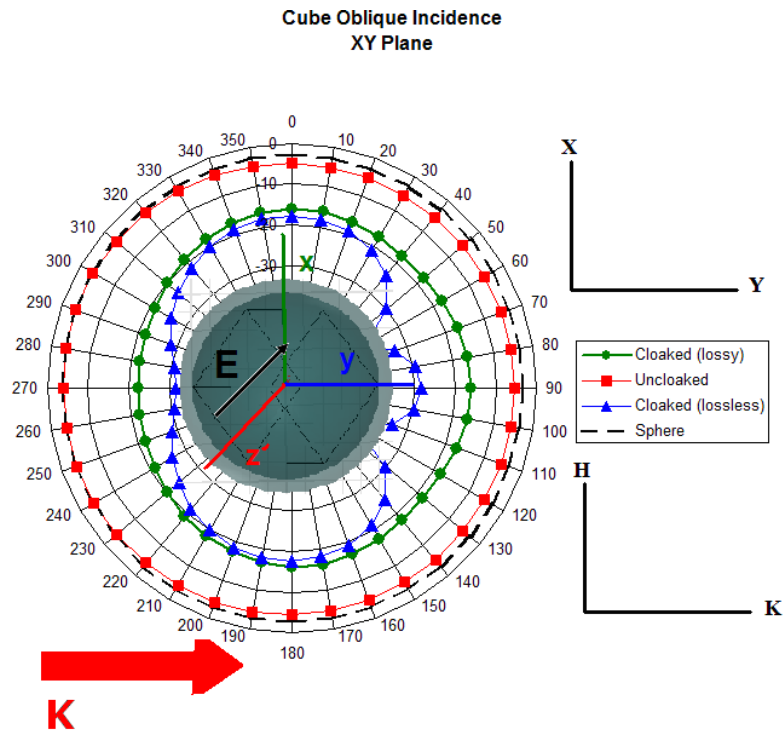
(b)

Fig 5.3 RCS (both monostaitic and bistatic) at oblique incidence ,dB(σ/λ^2), cube, 1.2 GHz (a) E plane (b) H plane .

From Fig 5.3 it can be observed that in the case of oblique incidence the monostatic RCS (normalized to square of wavelength) is -4.1 dB without cloaking, and is −22.4 dB with the lossy cloak. The monostatic RCS with lossy plasmonic shell is 18.3 dB lower than that without the shell. Moreover it can be concluded from the Fig 5.3 that maximum bistatic RCS has also decreased by 11.7 dB with the use of lossy plasmonic shell.

5.3. 2 Aluminium Cylinder

An aluminium cylinder with a height of 70 mm and a radius of 35mm was covered by the plasmonic shell with the same geometrical and material parameters as used in the cases above. The structure is shown in Fig 5.4.
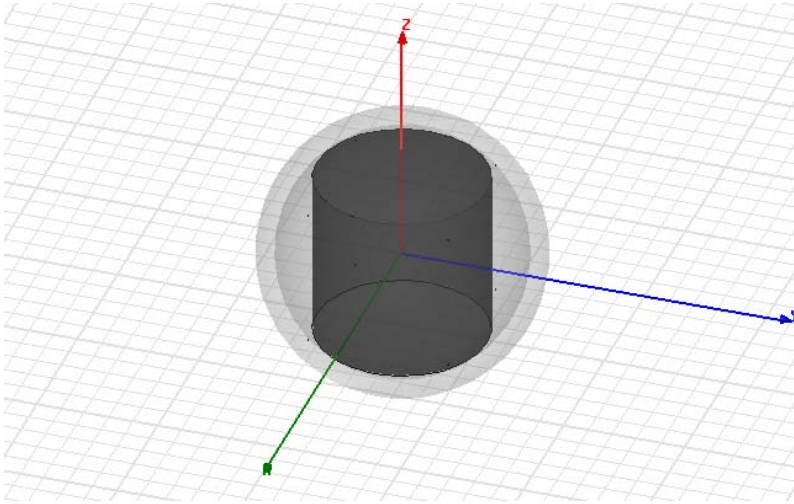
Fig 5.4 Spherical cover shell (r_{out} = 57.5 mm, r_{in} = 0.2λ = 50 mm, ε_r = 0.1, μ_r = 5.1) and covered cylinder, cloak (r=35mm, h=70mm). k vector is along Y axis and E along Z axis.

Far field patterns for cloaked and uncloaked cylinder are given in Fig 5.5. It can be observed that maximum bistatic RCS decreases by 13 dB. From Fig 5.5 it can be observed that for cylindrical metallic object too, the reduction in monostatic RCS is 17.9 dB even in presence of losses.

From the results above, it can be concluded that the exact shape of cloaked object plays a minor role in the cloaking phenomenon, as long as the object is small compared to the incident wave wavelength. It is assumed that any subwavelength conducting object will be cloaked, by the cloak designed for a sphere, as long as the longest dimensions of the object is same as diameter of the sphere (in case of cube they are lines joining opposite corners), the basic idea being that electric and magnetic dipole polarizabilities have to be roughly the same as that of the sphere.

(a)

(b)
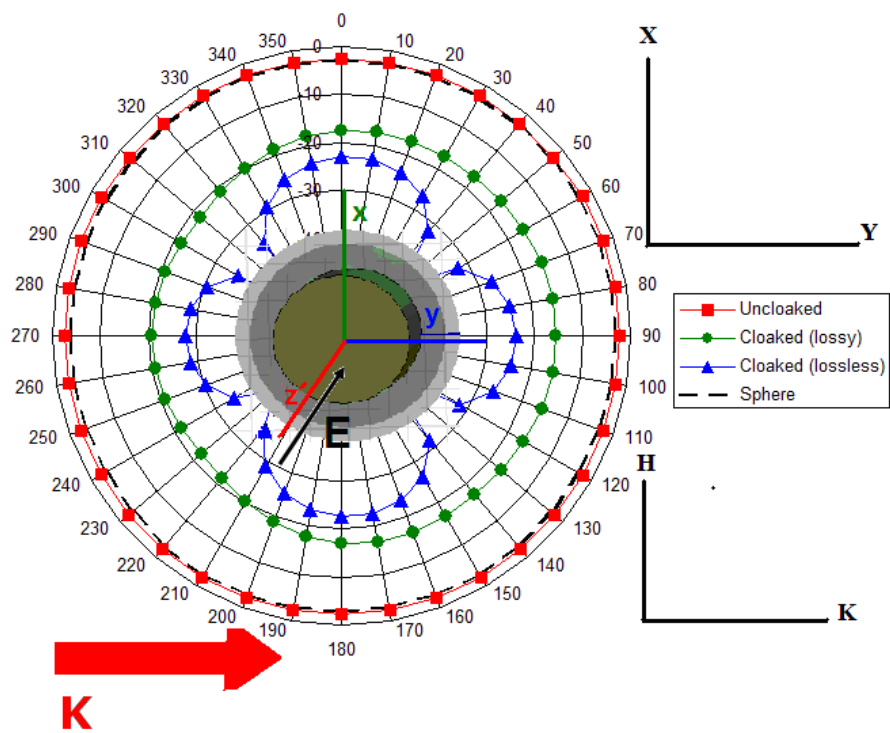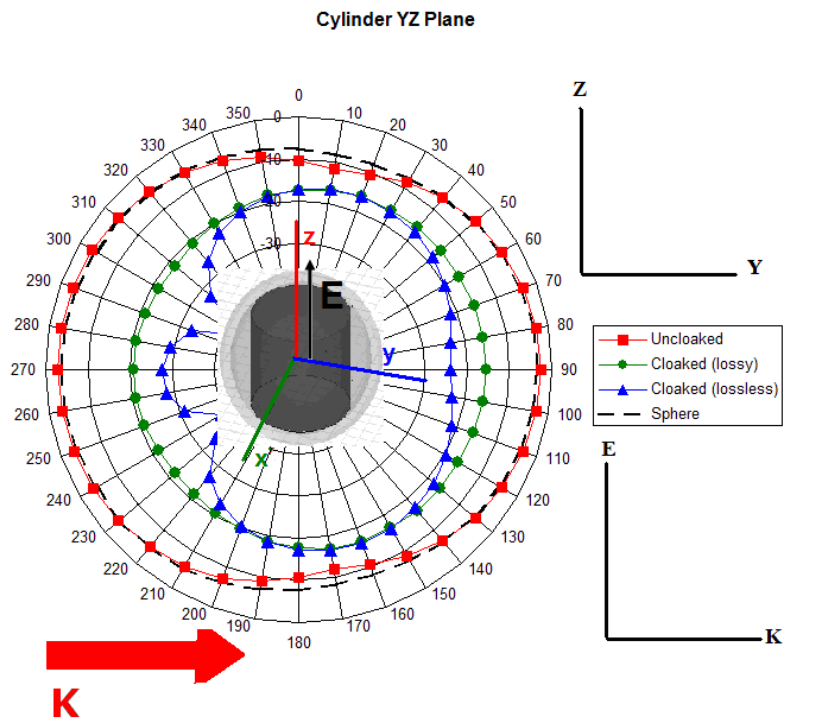
Fig. 5.5 RCS (both monstatic and bistatic),dB(σ/λ^2),Cylinder(Cloak,δ_e=0.15, δ_m=0.1),(a) E plane(b) H plane.

Furthermore the study shows that the cloaking is not very sensitive to the dielectric and magnetic losses. It must noted the dielectric and magnetic loss tangents for the lossy cloak are 0.15 and 0.1 in all the cases unless otherwise specified

5.3.3 Aluminium Cone

The simulation was then repeated with cone. Base diameter of the cone is chosen to be 50mm, and the height to be 75mm. Monostatic RCS reduces by 15.8 dB, whereas maximum bistatic RCS was reduced by 9.7dB as shown in Fig 5.7 and 5.8. These reductions in the RCS are obtained even in the presence of losses.
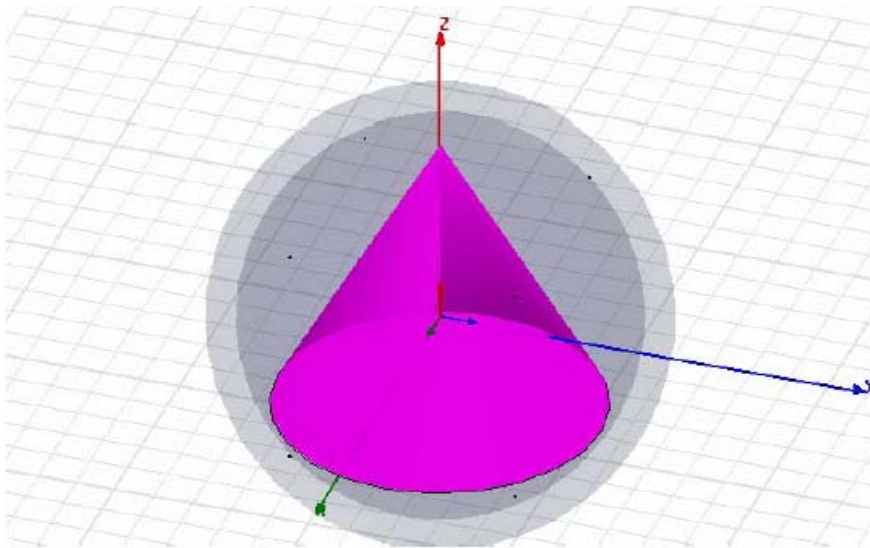
Fig 5.6 Cone with cloaking shell, ε_r= 0.1, δ_e=0.15, δ_m=0.1, μ_r=5.1, Axis of the cone is along Z axis, E field along Z axis, and k vector along Y axis.
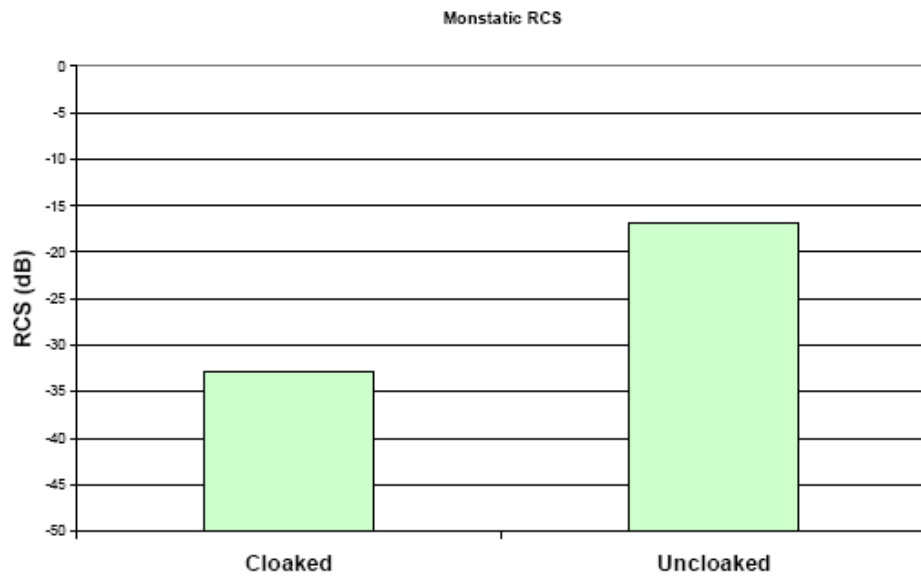
Fig 5.7 Monostatic RCS of cone with and without cloaking

(a)

Cone XY Plane

(b)
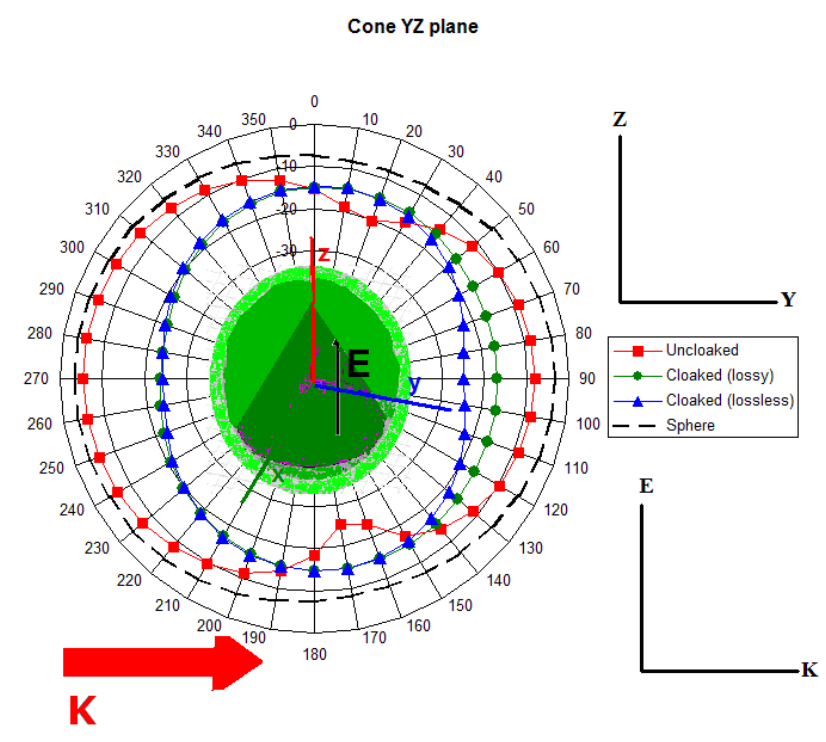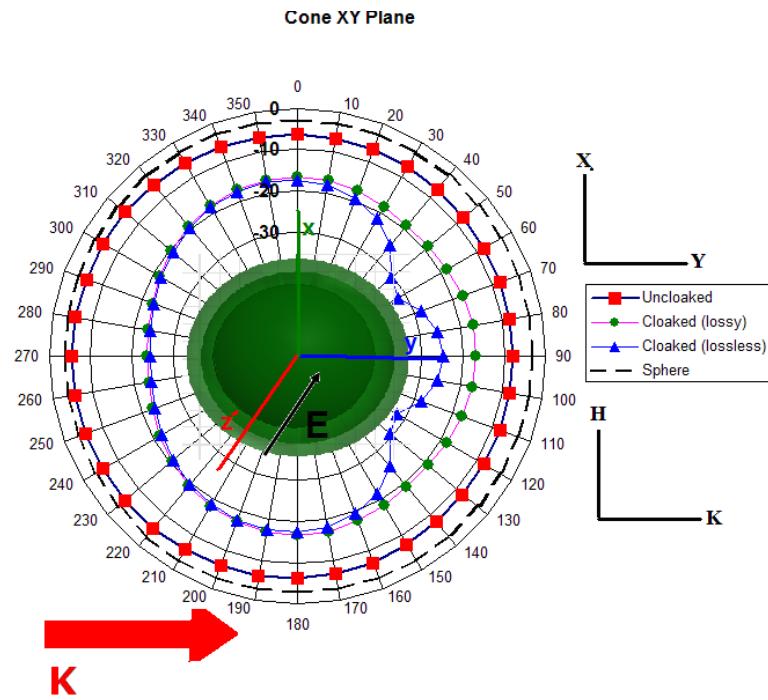
Fig 5.8 RCS dB(σ/λ^2), (a) E and (b) H plane plots for the cone.

5.3.4 Extended Object

The study has been extended to the case where cloaked object is long (length not smaller than wavelength) in one dimension. However unlike the structure studied in [32], the cloaked object was not fused spheres, but a rectangular bar.
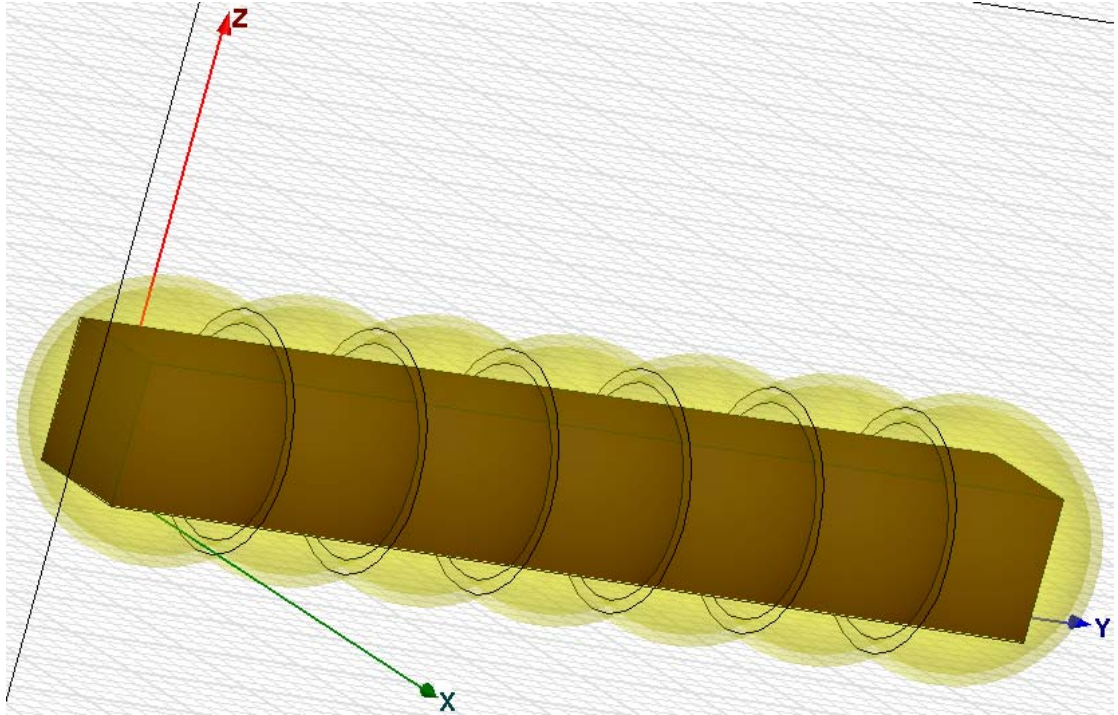
Fig 5.9 Long aluminium bar (length = 400 mm, width = height = 56 mm, PEC surface assumed), cloaking shell (outer radius: 54.5mm,: inner radius 50mm, separation of centres of spheres: 58 mm) , ε_r =0.1, μ_r=5.1 dielectric loss tangent 0.015, magnetic loss tangent 0.01

For this structure a low loss cloak was used. ε and μ were 0.1 and 5.1 respectively. Dielectric and magnetic loss tangents were 0.01 and 0.015 respectively. The cloak consisted of fused spheres with inner radius of 50mm, outer radius of 54.5mm, and distance between centres of adjacent spheres equal to 58mm.The aluminium bar was 400mm long and had a square cross-section 56mm by 56mm. The K vector was along –Z axis. The frequency used was 1.14 GHz instead of 1.2 GHz. The bistatic RCS is shown in Fig 5.10 and 5.11

As is evident from Fig 5.10and 5.11, good cloaking is achieved for E field polarization perpendicular to the bar (reduction in both monostatic RCS, and that maximum bistatic

RCS is 8.2 dB) , however for polarization parallel to the bar, the reduction in monostatic RCS is only 1 dB and that in maximum bistatic RCS is only 3dB. The reason is that for parallel polarization the dipole is long and the Quasistatic approximation doesn't hold.


(a)

(b)
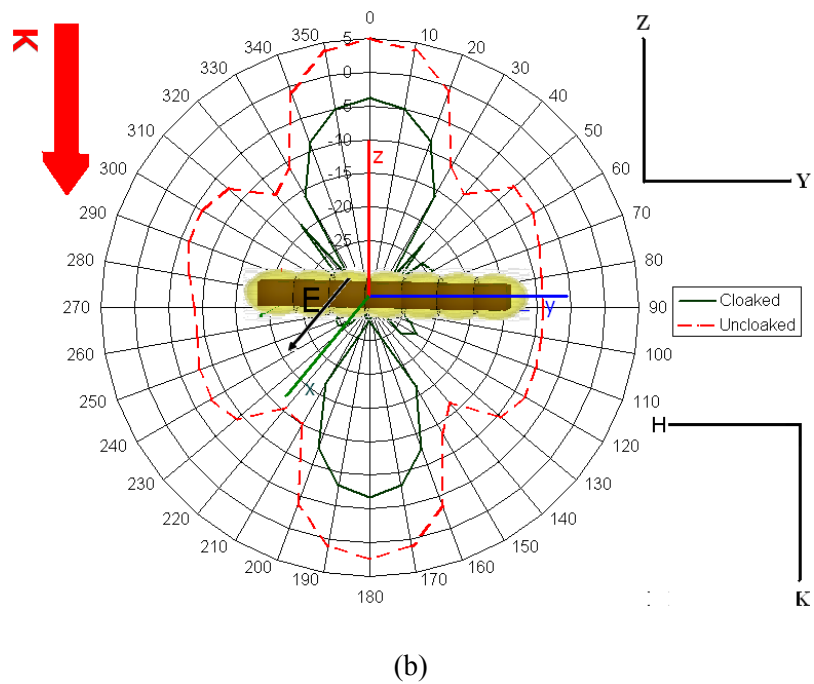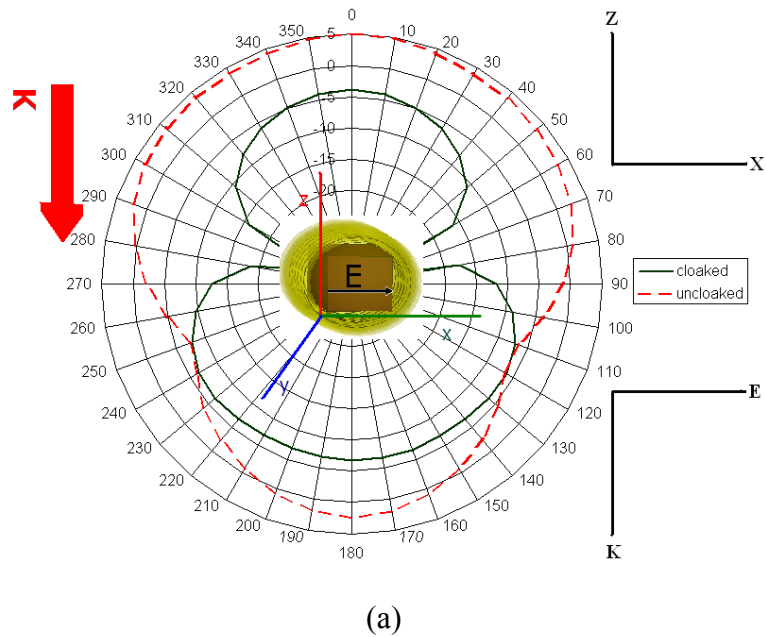
Fig 5.10 RCS (both monostatic and bistatic), dB(σ/λ^2), Bar (Cloak, δ_e=0.015, δ_m=0.01), E=Ex.),(a) E plane(b) H plane
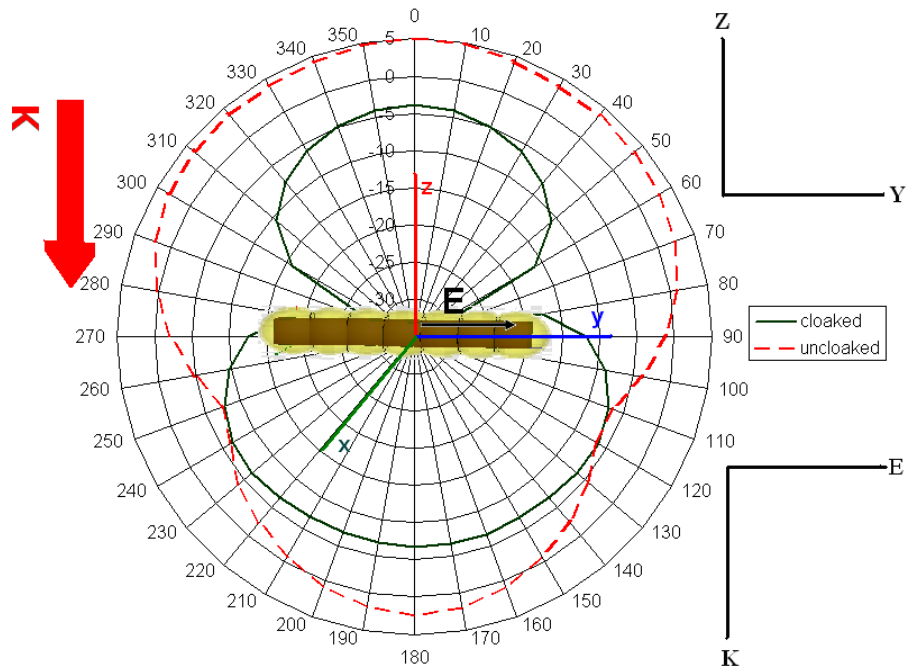
(a)
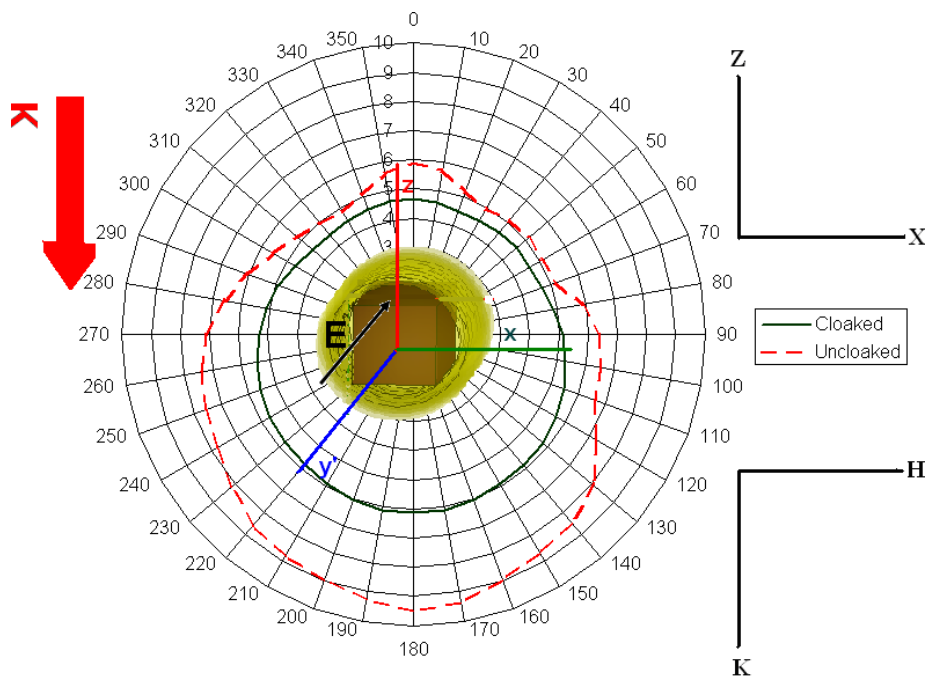
(b)

Fig 5.11 RCS (both monstatic and bistatic), dB(σ/λ^2), Bar (Cloak,δe=0.015, δm=0.01), E=Ey.),(a) H plane(b) E plane

5.3.5 Relative Size of the object and performance of the plasmonic cloak

Discussion in the theory section concerned objects considerably smaller than the wavelength. As the wavelength increases the theory will no longer hold. In order to investigate the limit of the theory discussed in this work, the simulation was repeated for relative size of the object and cloak up to 1.07λ. Results are shown in Fig 5.12
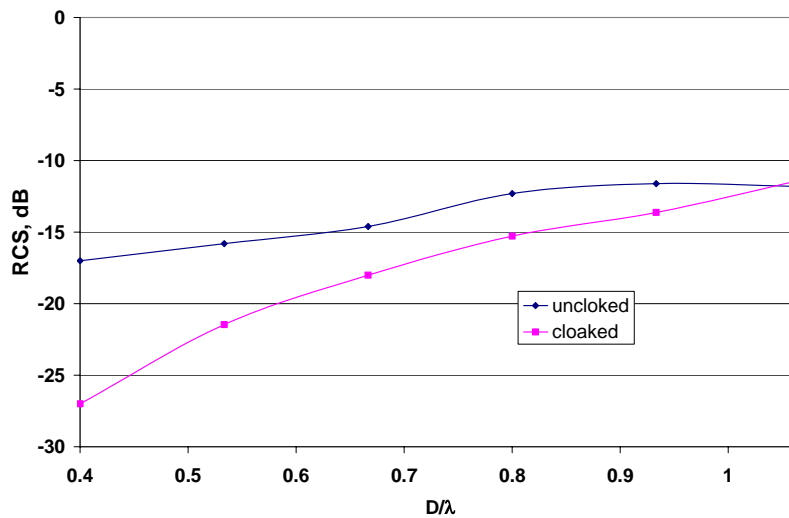
Fig 5.12 RCS dB(m^2), for varying relative size of the cube.

In Fig 5.12 D stands for the diagonal length of the cube and inner diameter of the cloak (as both are equal). From the results it can be observed that the performance of the cloak degrades as the relative size of the object increases, and for relative size of more than λ there is practically no reduction the scattered power. Furthermore increased scattering for the uncloaked is observed at relative size of 0.9 λ, which is probably due to resonances determined by the shape and geometry of the object.

5.3.6 Parametric Analysis

Furthermore, effect of change in target dimension and conductivity was analyzed as well.

In order to study the influence of target dimension, simulation was done by varying one dimension of a subwavelength bar at a time. Maximum value of each dimension was such that it would fit into the cloak. The E field was along Z axis and the K vector along Y axis. The frequency chosen was 1.2GHz. The cloak used was the same as was used for the subwavelength cube, the cylinder, and the cone

Fig5.13 and Fig 5.14 gives the monostatic RCS for the subwavelength aluminium bar, with and without the cloak. In this case E field is along the Z axis. It can be observed from these figures that good cloaking (i.e. reduction of 10dB or more in Monostatic RCS) can achieved as long as X&Y dimensions are above 30mm ,with Z dimension equal to 50mm. Similarly while keeping X & Y dimensions at 50mm, good cloaking can be achieved as long as the Z dimension is above 40mm. It should be noted that the cloak was actually designed for a sphere with diameter of 100mm (0.4λ).

Furthermore Fig 5.13 and 5.14 show the cloaking to be more sensitive to variation dimension along the E field polarization. This is probably because the induced dipole moment primarily depends on the length of object along the direction of E field.
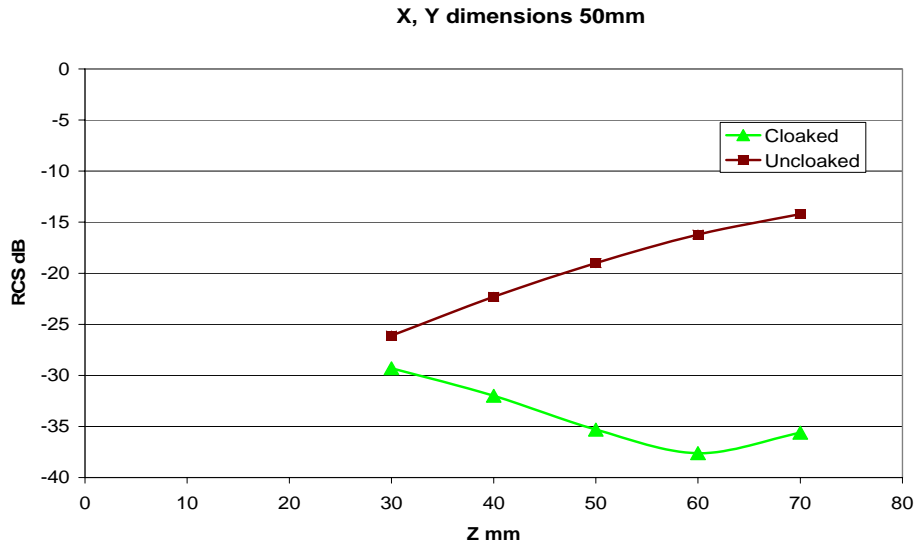
X, Y dimensions 50mm

Fig.5.13 Monostatic RCS for subwavelength aluminium bar Vs Z dimension, X&Y dimensions constant at 50mm
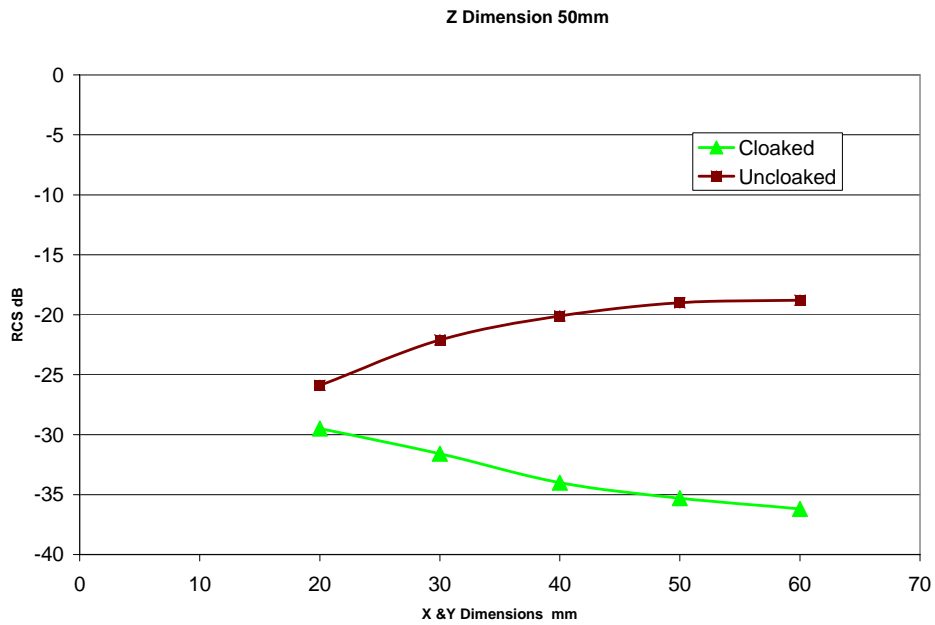
Z Dimension 50mm

Fig.5.14: Monostatic RCS Vs X & Y dimensions, (Z dimension constant at 50mm)

The Simulation was then repeated for various values of target conductivities, ranging from 0.01 Sm^{-1} to PEC. The target chosen this time was conducting sphere with radius of 50mm, i.e. equal to the inner radius of the cloak.

Values for Monostatic and maximum Bistatic RCS are shown in Fig 5.15 and 5.16. Values of RCS are given in m^2.
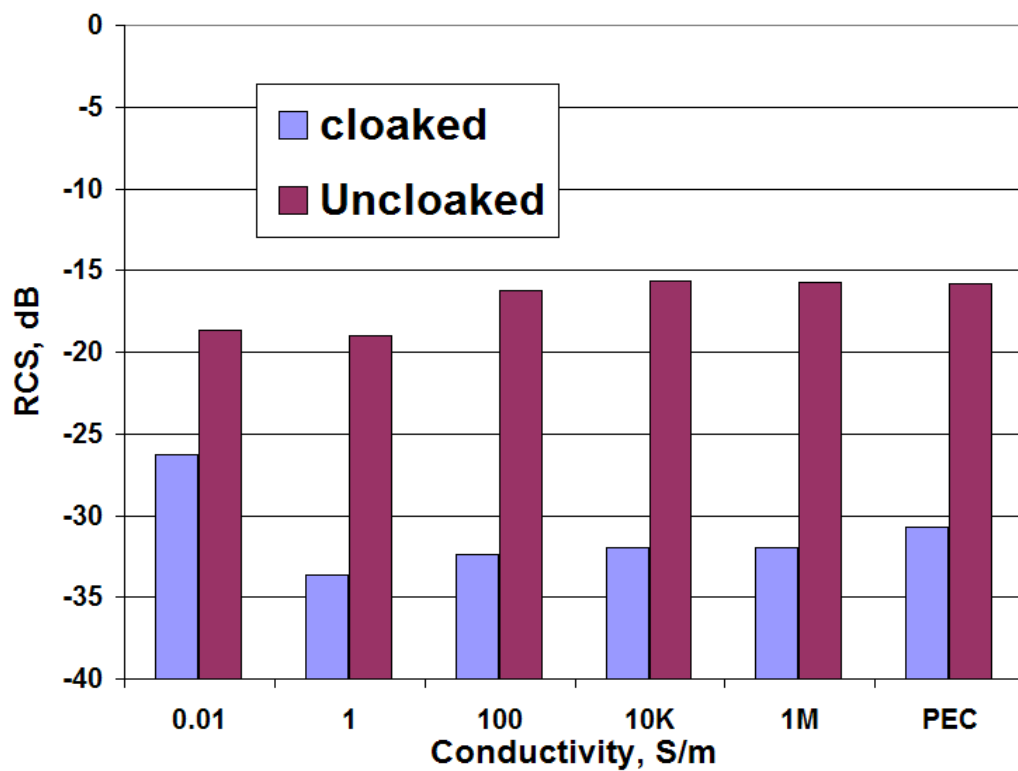
Fig. 5.15 Monostatic RCS with and without cloak for various values of target(inner sphere) conductivity
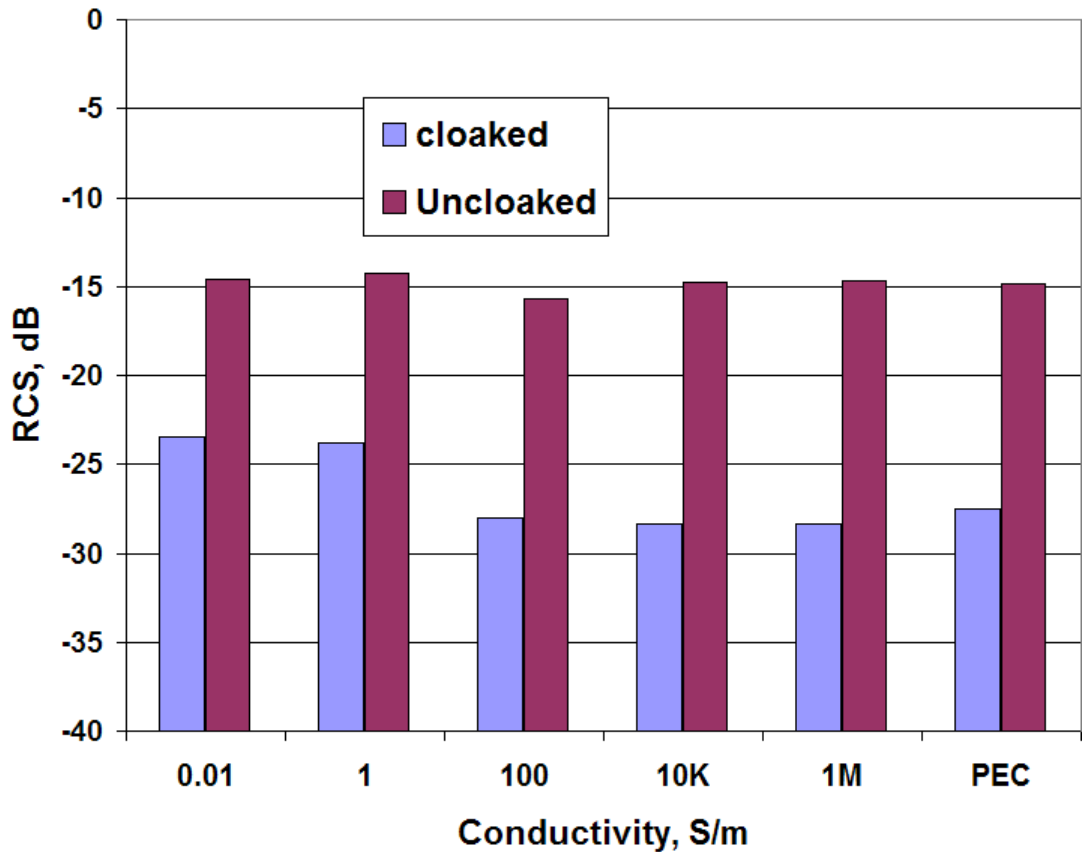
Fig. 5.16 Maximum bistatic RCS with and without cloak for various values of target (inner sphere) conductivity.

From Fig 5.15, it can be observed that, the plasmonic cloak designed for a sphere made of a good conductor, provides good performance for low conductivity sphere as well.

The reduction in monostatic RCS is roughly the same i.e. between 14.6dB and 16.3dB, for conductivities down to $1Sm^{-1}$. Even for conductivity of 0.01 Sm^{-1}, the plasmonic cloak provides a reduction of 7.6dB in monostatic RCS. This implies that the performance of the plasmonic cloak is not strongly affected by increased resistivity of the enclosed sphere.

In the Fig 5.16 simulation results showing values for maximum Bistatic RCS with and without cloak are shown. Results in Fig 5.15 imply that the plasmonic cloak performs quite well even in terms of reducing bistatic RCS.

The reduction in the maximum bistatic RCS is roughly the same i.e. between 12.3dB and 13.7dB for conductivities down to 100Sm^{-1}. Even for conductivity of 0.01 Sm^{-1}, the plasmonic cloak provides a reduction of 8.9dB in maximum bistatic RCS.

It's clear from the results above that the performance of a plasmonic shell cloak is not very sensitive to the conductivity of enclosed sphere, and good cloaking, both in terms of monostatic and bistatic RCS is obtained even for quite low values of sphere conductivity.

It may be noted that for conductivity of 100Sm^{-1}, skin depth at 1.2GHz is 1.4mm, which is tiny fraction of sphere radius (50mm). Therefore for conductivity of 100Sm^{-1} and above electric field doesn't penetrate deep into the sphere, and the sphere behaves like a conducting sphere. Not surprisingly, there is little change in reduction of monostatic or maximum bistatic RCS down to conductivity of 100Sm^{-1}.

However in the case of conductivity of 0.01 Sm^{-1}, skin depth is 140mm, which is more than the diameter of the sphere and the sphere thus behaves as a semi conducting object. But even in this case, plasmonic cloak provides good performance, though not as good as in the case of high conductivity spheres.

In case of a plasmonic cloak over a conducting sphere, the electric field is concentrated in the plasmonic shell [33]. In order to get further insight into effect of low conductivity on the above mentioned characteristic of the plasmonic cloak, electric field profiles were evaluated for two cases; PEC sphere, and sphere with conductivity of 0.01 Sm^{-1}. Results are shown in Fig 5.17 and 5.18.
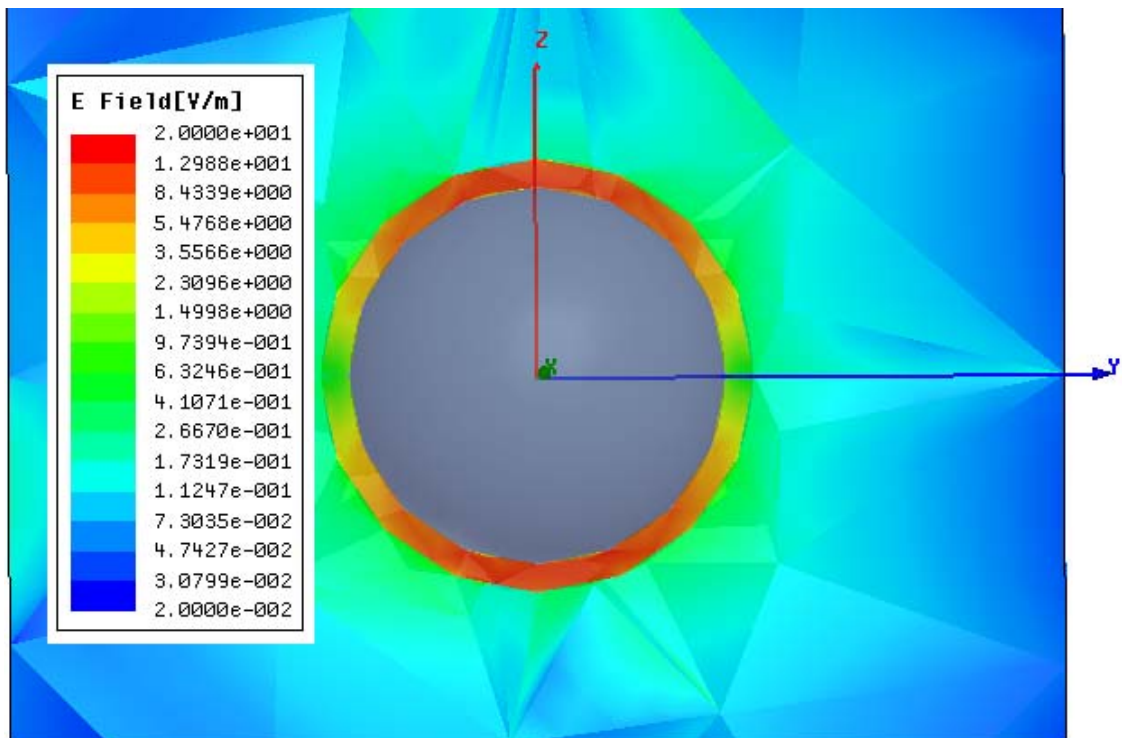
Fig 5.17 E field profile [V/m] for PEC sphere enclosed in plasmonic cloak in YZ (E plane) plane.
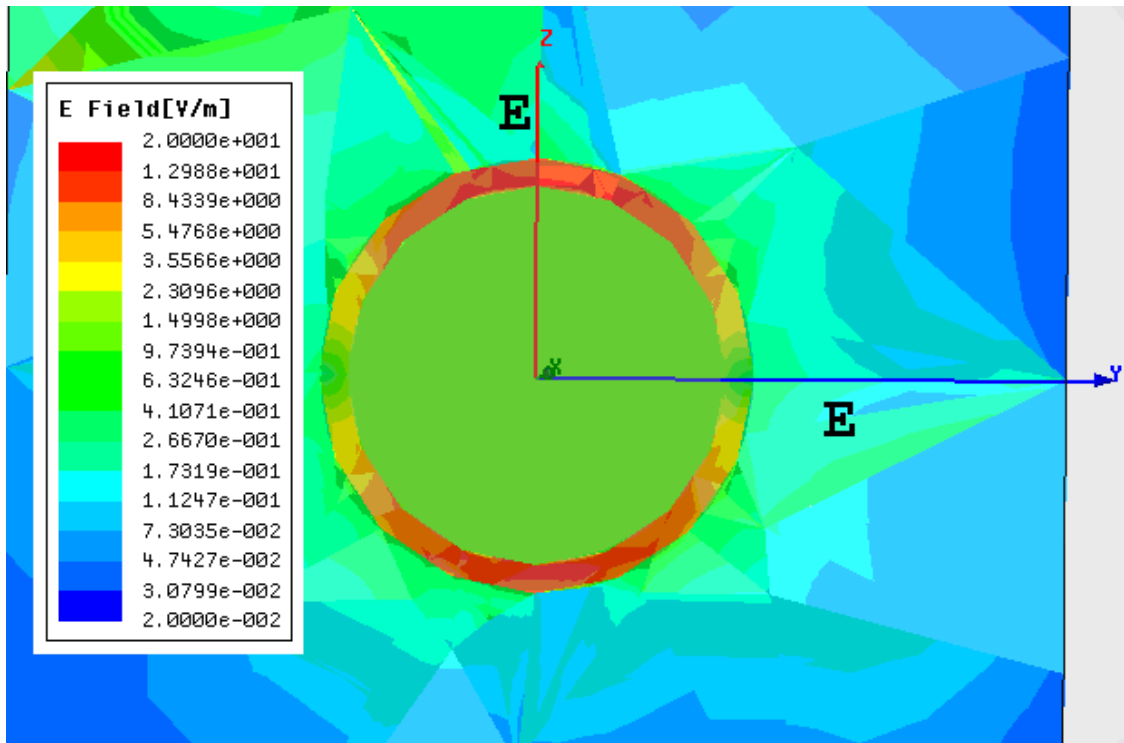
Fig. 5.18 E field profile [V/m] for 0.01 S/m conductivity sphere enclosed in plasmonic cloak in YZ (E plane) plane.

It can be observed from Fig 5.18, that even in case of sphere with very low conductivity, most of the energy is confined in the plasmonic shell, just as in the case of a PEC sphere. The confinement is however not as strong as in the case of a PEC sphere, as can observed by comparing Fig 5.17 and 5.18. The field in the cloaking shell outside 0.01Sm^{-1} cloaked sphere is weaker, indicating weaker confinement of incident field.

This implies that even in the case of low conductivity, the behaviour of the plasmonic cloak doesn't change fundamentally and most of the energy in concentrated in plasmonic shell and is diverted around the sphere, thus reducing the RCS.

5.4 Conclusion

From the results above, it can be concluded that for objects which are small compared to the operating wavelength, and hence can be modelled as superposition of electrical and magnetic dipole good cloaking can be achieved using hollow shell of magnetic plasmonic material. It is further evident that the geometry of the cloaked object is of little consequence, as long as the dimensions remain roughly the same, the reason being that in case of these small objects the only important parameters are electrical and magnetic dipole moment, which primarily depends on the dimensions in case of conducting objects. For the cube and cylinder, reduction in monostatic RCS was, even in presence of losses was 99%, whereas reduction in maximum Bistatic RCS for cube and cylinder was 92% and 95% respectively.

In the case of extended objects, cloaking was achieved as long as the E field was directed along dimension smaller than wavelength (8 dB reduction in maximum Bistatic RCS). For E-field directed along length of extended objects, cloaking effect is minimal (roughly 3dB).

Thus the hypothesis that subwavelength objects could be modelled as a short electric dipole, with the dipole strength mainly depending on the dimension along E field, stands verified, provided the other dimensions are not very small, and therefore, such objects could be cloaked by a plasmonic shell.

Performance of plasmonic cloak designed for conducting sphere was numerically evaluated for spheres with various values of conductivity; ranging from 0.01 Sm^{-1} to PEC. It was observed that the plasmonic cloak gives quite good performance even for very low values of conductivities. Reduction in monostatic and maximum bistatic RCS in case of sphere with conductivity of 0.01Sm^{-1} was 7.6dB and 8.9 respectively.

Furthermore field profile around 0.01Sm^{-1} cloaked object showed confinement of electric field inside the plasmonic shell just as it is the case with PEC sphere.

It is thus concluded the plasmonic cloak designed for conducting objects, gives good performance even for sphere constructed of low conductivity material, and the cloak performance is not very sensitive to cloaked object conductivity. The cloak gives reasonably good performance even when the skin depth is larger than the diameter of the sphere, and the sphere can thus no longer be considered as good conductor.

From results above, it can be claimed that the plasmonic cloak can give good performance for a wide range of cloaked object dimensions, shapes and conductivities. Furthermore the sensitivity is less if the variation in dimension is not along the E field polarization. The cloaking has thus high tolerance for variation in a cloaked object's dimensions.

Chapter 6

Negative Group Velocities and Extraordinary Transmission in Artificial Plasmonic Structures

6.1 Introduction

One of the most exiting discoveries in the area of electrodynamics in recent years has been the artificial of artificial surface plasmons on textured metallic surfaces and bulk plasma waves in thin wire arrays [121,122]. Plasmonic waves are a type of surface wave [123]. Surface waves are those waves which travel along the interface of two materials [124].

Plasmonic waves occur naturally on the surfaces of materials with negative permittivity. The most common example of a negative permittivity material is a metal close to its plasma resonance frequency [125].

Plasmonic structures have several interesting applications. The reason is that plasmonic waves can be confined to a region smaller than the diffraction limit, and also plasmonic modes can create very strong electric fields [126-144]. Plasmonic structures are useful for Raman spectroscopy [127- 129]. The reason is that normally a Raman scattering signal is quite weak. Plasmonic modes increase the field strength in certain regions of the plasmonic structure. The sample can then be placed where the

electric field is strong, which will result in the amplification of the radiation emitted by the sample [127-129].

Other important areas of application for plasmonic waveguides are high speed inter connects [130-137], subwavelength lithography [138-141], and subwavelength imaging [24, 25]. In the case of lithography the main obstacle is the lower limit imposed on the feature size due to the diffraction limit [142,143]. A similar problem is encountered in fabricating closely placed optical interconnects, i.e. a minimum limit on the beam diameter, making it impossible to place two optical waveguides very close to each other. Plasmonic structures overcome these problems as they can focus electromagnetic fields below the diffraction limit [130-144]. Field confinement due to plasmonic modes also improves the performance of optical detectors [144]

The problem with natural plasmonic materials is that they are available only in the visible and ultra violet bands. For lower frequencies artificial plasmonic structures are used [3] .

Most common source of artificial plasmonic waves is a textured metallic surface [145-157]. Usually such a structure consists of apertures drilled into a metal surface [145-149] or corrugated surfaces and wires [155]. Surface plasmons can also be present on the surfaces on photonic crystals [158].

An interesting feature of a aperture array plasmonic surfaces is near unity transmission of the incident light [1,2,4]. Furthermore our simulations of aperture array artificial plasmonic surfaces revealed regions of negative and super luminous group velocities

for normally incident waves. Both of these are discussed in the theory and result sections.

Study of aforementioned phenomenon are very interesting theoretically. The reason is that these phenomenon involve questions of relativity and causality. Superluminal and negative group velocity appear to violate relativistic (information should not propagate with superluminal velocity) and pre relativity causalities (cause should precede the effect) respectively. However careful examination reveals that causality is preserved, as the actual information velocity is still luminal or subluminal, as would be explained in the theory section below.

6.2 Theory

Plasmonic waves are a type of surface waves [123,124] . Surface waves were first investigated by Zenneck [124] in the case of radio waves travelling along the surface of the Earth. In order to get insight into plasmonic mode the characteristics of plasmonic waves in general are analyzed. In the case of ordinary waves, all the components of the wavevector k are real. The wavevector for an ordinary propagating wave has the following form. Similar treatments could be found in standard electrodynamics text books such as [123,159].

$$\overline{k} = k_x \hat{x} + k_y \hat{y} + k_z \hat{z} \qquad\qquad (6.1)$$

From the Maxwell equations the magnitude of vector k is defined by the permittivity and permeability of the material. Therefore in case of an interface between two materials, the following condition has to be satisfied on both sides of the interface (assuming one side of the interface is free space).

$$\left| \overline{k} \right| = k_0$$
$$\rightarrow \sum k_i^2 = k_0^2$$

(6.2)

where $k_0 \ldots k_i$ are the components of vector k.

As all the components are real, the following condition is imposed by (6.2) on any k_i

$$k_i \leq k_0$$

(6.3)

An upper limit on the value of k translates into a lower limit on the area in which the electromagnetic field can be confined, as the k vector represents the fields in the reciprocal space.

Plasmonic waves have on the other hand at least one of the components of the k vector imaginary. A typical plasmonic mode has the following form of the k vector.

$$\bar{k} = k_x \hat{x} + k_y \hat{y} + ik_z \hat{z} \tag{6.4}$$

The condition on maximum value of any component is no longer given by (6.3). The new condition can be derived using (6.4), as follows.

$$k_0{}^2 = k_x{}^2 + k_y{}^2 - k_z{}^2$$
$$\rightarrow k_x{}^2 + k_y{}^2 = k_0{}^2 + k_z{}^2 \tag{6.5}$$
$$\rightarrow (k_x, k_y) \leq \sqrt{k_0{}^2 + k_z{}^2}$$

There is no upper limit on the values of k_x and k_y, as along as value of k_z is sufficiently high. hence plasmonic modes can be confined to an arbitrarily small region.

There are two types of plasma wave on such structures; Localized surface plasmons and surface plasmon polaritons.

Localized surface plasmons are generated by the modes inside apertures. These apertures act as metallic waveguides. A waveguide's effective permittivity is negative below the cut off frequency. An array of waveguides would therefore support localized plasmonic modes below the cut off frequency of the apertures [121-125].

Surface plasmon polaritons are generated by the periodic variation in the surface constitutive parameters. For example a periodic array of apertures in a metallic surface. Periodicity of the array results in periodicity of the fields near the surface as expected from the Floquet theorem for periodic structures.

If the spacing between the apertures is much smaller than the wavelength then the same periodicity will be imposed on the fields near the surface, as is the case of fields in a periodic structure. Smaller than wavelength spacing will mean value of k_x and k_y higher than k_o, (with exception of zeroth order Floquet mode) which will result in a plasmonic wave on the surface.

Normally it is not possible to couple a freely propagating incident wave to a plasmonic wave, as the transverse component of the k vector wouldn't match. However in the periodic structure a mode can couple to another mode if their k vectors differ only by a multiple of the reciprocal lattice vector (obtained by taking Fourier transform of the lattice vector). For simplicity an artificial plasmonic surface constructed from either a periodic array of aperture or corrugations, or any other periodic texturing is assumed.

An incident wave can be coupled to the plasmonic modes of Floquet order n and m on the surface, provided [123]

$$\overrightarrow{k_{sp}} = \overrightarrow{k_x} + n\overrightarrow{G_x} + m\overrightarrow{G_y} \qquad\qquad (6.6)$$

where k_{sp} is wavevector of the plasmonic mode, k_x the x component of the incident wavevector, G_x and G_y are the x and y components of the reciprocal lattice vector of the plasmonic surface.

An interesting feature of these structures is the near complete transmission of the incident wave. From the standard electrodynamics point of view sub wavelength apertures have very low transmittance [24]. However it has been observed that an array of such apertures gives extraordinarily high transmission [121]. This results from the tunnelling of the incident wave through the subwavelength apertures assisted by the surface plasmon polaritons [121,122]. The modes inside the subwavelength apertures are localized plasmons, as explained in the theory section, and tunnelling of the electromagnetic waves is due to these modes [122]. This tunnelling is enhanced due to surface plasmon polaritons [122].

6.2.2 Negative and Superluminal Group Velocities.

Group velocity is usually considered to be the speed at which information and energy travel through a medium. Mathematically it's defined as [24].

$$v_g = \frac{d\omega}{dk} \qquad (6.7)$$

Group velocity can be also written in terms of phase delay as below [44].

$$\phi = kx$$

$$\rightarrow \frac{d\phi}{d\omega} = x\frac{dk}{d\omega}$$

$$\rightarrow \frac{d\phi}{d\omega} = \frac{x}{v_g} \qquad (6.8)$$

$$\rightarrow v_g = x\frac{d\omega}{d\phi}$$

When considering phase it's more convenient to use group delay, the time for information in a signal to travel from one point to another. From the equation above, relation for a group delay can derived as follows.

$$G_d \equiv \frac{x}{v_g}$$

$$\rightarrow G_d = \frac{d\phi}{d\omega} \qquad (6.9)$$

Obtaining group delay is then very easy from the S parameters, as the phase of the S_{21} gives the phase delay from input to output.

For certain dispersive media the group velocity can be superluminal or negative, depending on how the phase delay ϕ varies with frequency [160-162]. This situation is very interesting as it appears to violate the principle of causality. However in all of these cases the frequency range over which the group velocity is negative is very narrow. From the theory of Fourier transform this would mean the pulse would have to be very wide if negative group delay is desired. Furthermore for reliable transmission of information the distortion should not very high. This means that the group velocity doesn't change very much over the frequency band of the input signal. This further reduces the available bandwidth and increases the minimum pulse width for which negative group velocity could be obtained. Group delay basically gives the time taken by the peak of the signal to travel from one point to another point. If the pulse is much wider than the negative group delay, then it simply means that the signal peaks at the output before it does at the input [163-165]. The front of the pulse will still travel at luminal or subluminal velocity thus observing relativistic causality. It is the front of the pulse which conveys the information, and the speed at which this travels is always less than or equal to the speed of light [163-165]

6.3 Structures

In this work structures similar to that reported in [149] are investigated, and another different array of cylindrical coaxial apertures for anomalous high transmission and negative group velocities. In all of the structures, the apertures are in a 0.1mm thick aluminium sheet The structures are Sierpinski arrays of simple square apertures, coaxial square apertures and an array of coaxial cylindrical apertures with each unit

cell containing two small and two large apertures. The last structure is basically a modified Apollonian gasket. The structures are shown in Fig. 6.1.

Structure geometry was chosen such that the frequency range investigated here is just below the cut off of the apertures in order to have maximum transmission while still remaining the stop band.

Besides these two structures, another one based on an array of coaxial cylindrical apertures is also investigated. This structure is interesting as it exhibits negative group velocity with reasonably low transmission loss i.e. around -3dB.

The first two structures give high transmission, most probably due to having same material i.e. on both sides of the structure, as the modes on both sides of the surface will be the same, improving coupling from one side to the other. In case of having one material on one side and another material on the second side would result in dissimilar surface mode structure on top and bottom surface of the structure.
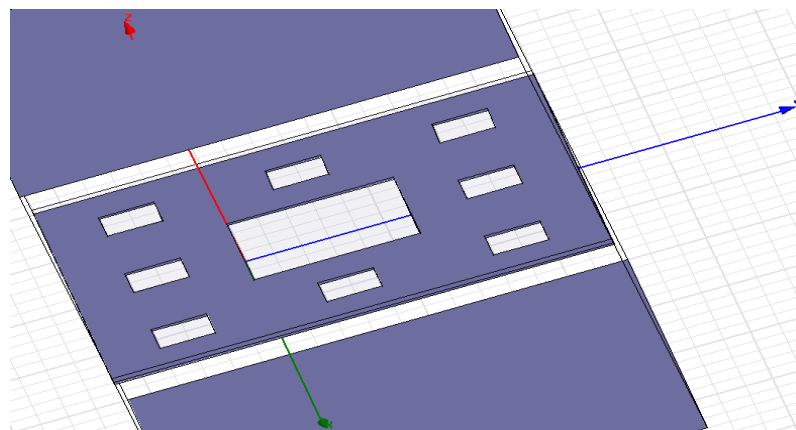
(a)
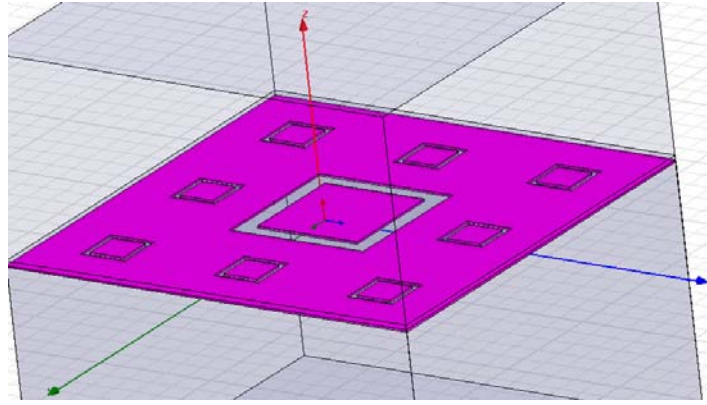
(b)
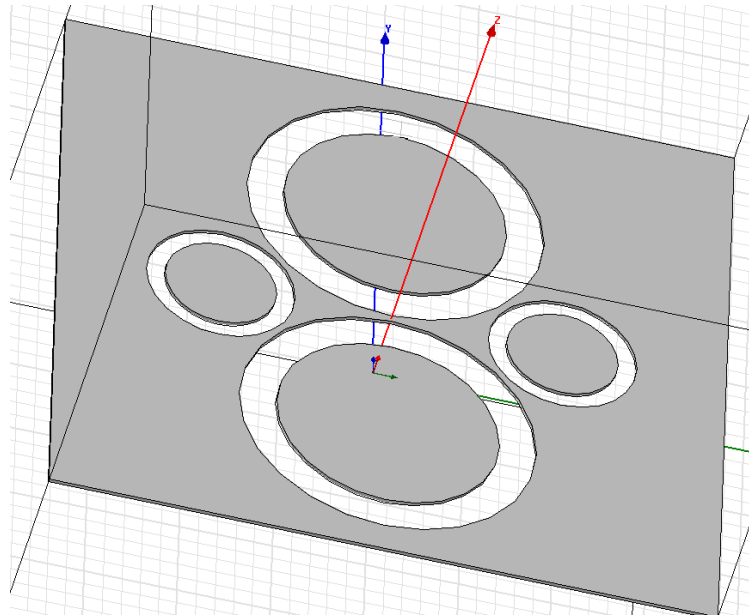
(c)

Fig. 6.1 a) Sierpinski array of square apertures , unit cell size 18mm by 18mm b) same as a, but simple square apertures replace by annular square apertures with length of inner square being 3/4th of the outer square c) Modified Apollonian gasket, Same unit cell size as a&b. centres of the large apertures located 4.1mm from the centre of the cell, outer and inner radii are 4mm and 3mm respectively, smaller apertures located at distance of 4.6mm from the centre , with outer and inner radii of 2mm and 1.5mm respectively.

6.4 Simulations and Results

The structure was analyzed in HFSS, using periodic boundary conditions and Floquet ports. The structure was assumed to be immersed in vacuum.

The incident wave was modelled as a Floquet port above the structure. In order to evaluate transmitted power a second Floquet port was defined below the structure. The whole unit cell is 18mm by 18mm, large square has dimension of 6mm by 6mm, whereas the inner square inside the large square has dimension of 4.5mm. Smaller squares are scaled by 1/3. Structure has thickness of 0.1mm, and is constructed from Aluminium. Unit cell of the Structure is shown in Fig 6.1. Inner squares are absent in case of simple rectangular apertures. Numerical results for transmission are shown in Fig6.2
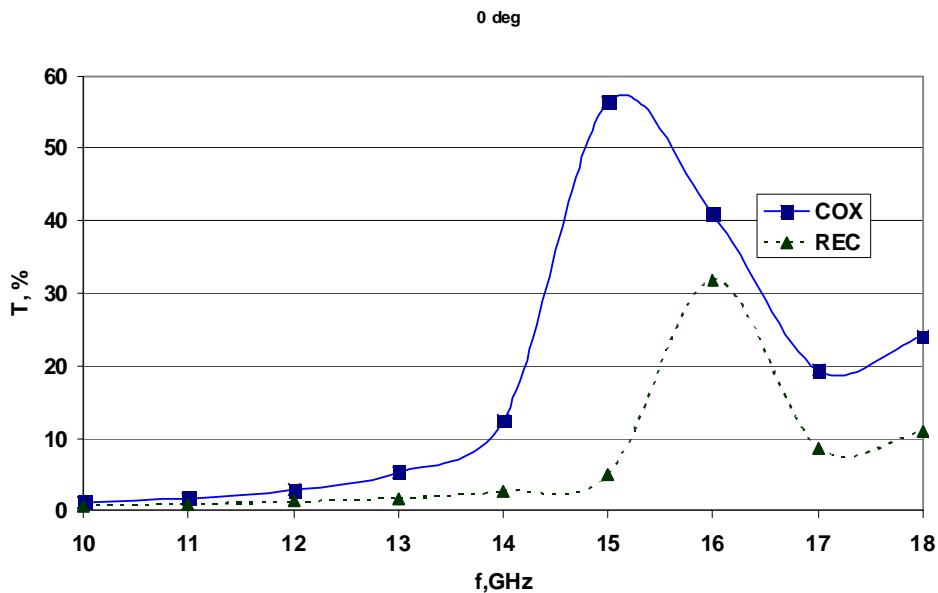
Fig 6.2   Transmission of normally incident wave through Sierpinski carpet array of rectangular(square) and coaxial (annular) apertures

The transmitted power is evaluated as sum of powers coupled to all the propagating modes on the other side. The results clearly show extraordinarily high transmission of the incident wave. In the case of coaxial apertures the transmission reaches above 57%. The structure reported in this work has vacuum on both sides. This symmetry is likely to help transmission of the incident wave. Symmetry of the structure means that the same plasmonic modes are present on both sides of the surface, which enhance the coupling between the top and bottom modes and thus the transmission of the incident waves.
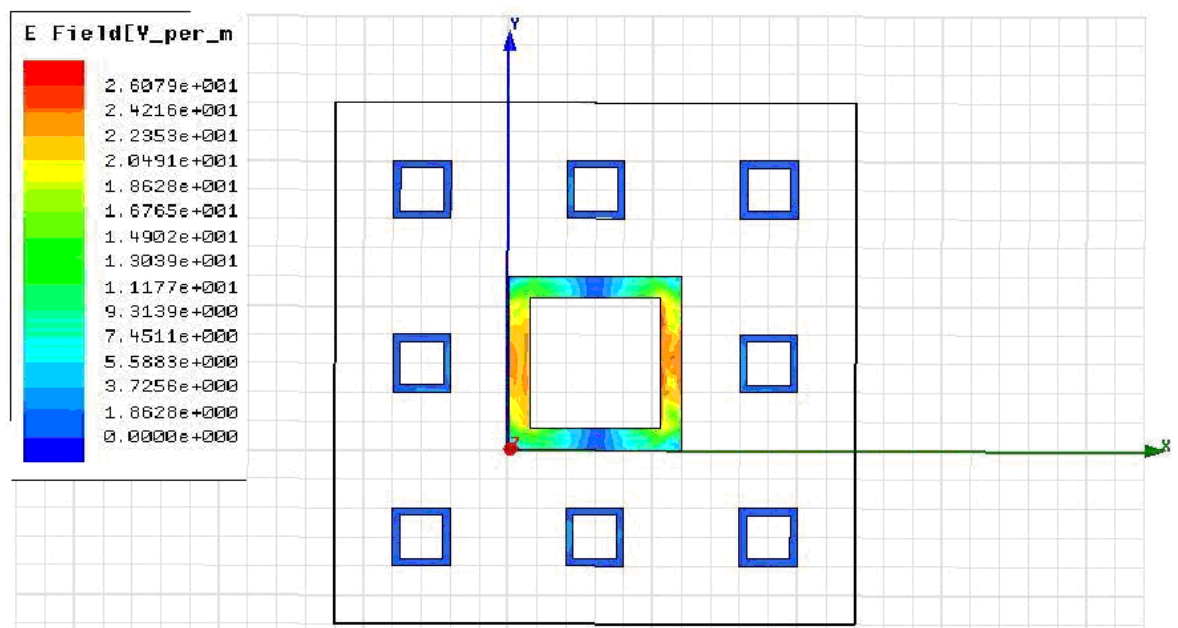
Fig 6.3 Field patterns in the apertures of the Sierpinski carpet array

Fig 6.3 shows electric field density in the Sierpinski array of annular/coaxial square apertures. The result shows a field enhancement of 26 times (incident field intensity was set at 1V/m). This electric field enhancement is another hallmark of an aperture array supporting plasmonic waves.

In the next step negative and superluminous group velocities were investigated. In the case of the Sierpinski carpet array the negative group velocity region had extremely low transmission i.e. below -20dB so is of little interest. The third structure based two large and two small coaxial cylindrical apertures unit cell showed a negative and superluminous group velocity regions where the transmission was around -3dB. This makes the structure very interesting as most of the negative group velocity structures have strong decay [164], but the structure presented here has attenuation of only around -3dB. Results for group delay and transmission for both the polarizations are shown in the Fig 6.4 and 6.5. Distance between the upper and lower Floquet ports is 20mm. The structure in 6.1c was analyzed both in HFSS and CST in order to be more confident about the results, and can be observed from Fig 6.4 and 6.5 they are in good agreement.

From the results in Fig 6.4 and 6.5 it can be observed that for Ey polarization the transmission is between -3dB and -3.4 dB. In this case the transmission band of the structure nearly coincides with the negative group velocity zone. In the case of Ex polarization the negative group velocity band lies well within the stop band. As can be observed from Fig 6.5 the transmission is less than -18dB throughout the negative group velocity zone. This asymmetry between different polarization is expected from the asymmetry of the structure. As the behaviour of an aperture array based plasmonic

structure depends on the interaction of artificial surface Plasmon polaritons and the localized plasmonic modes in the aperture, changing the aperture dimension would also change the response.

As for the frequency bands with superluminous group velocities, they lie on the edges of the negative group velocity band. At points where the group delay switches from positive to negative, it would cross point of zero group delay, which means infinite group velocity.

(a)
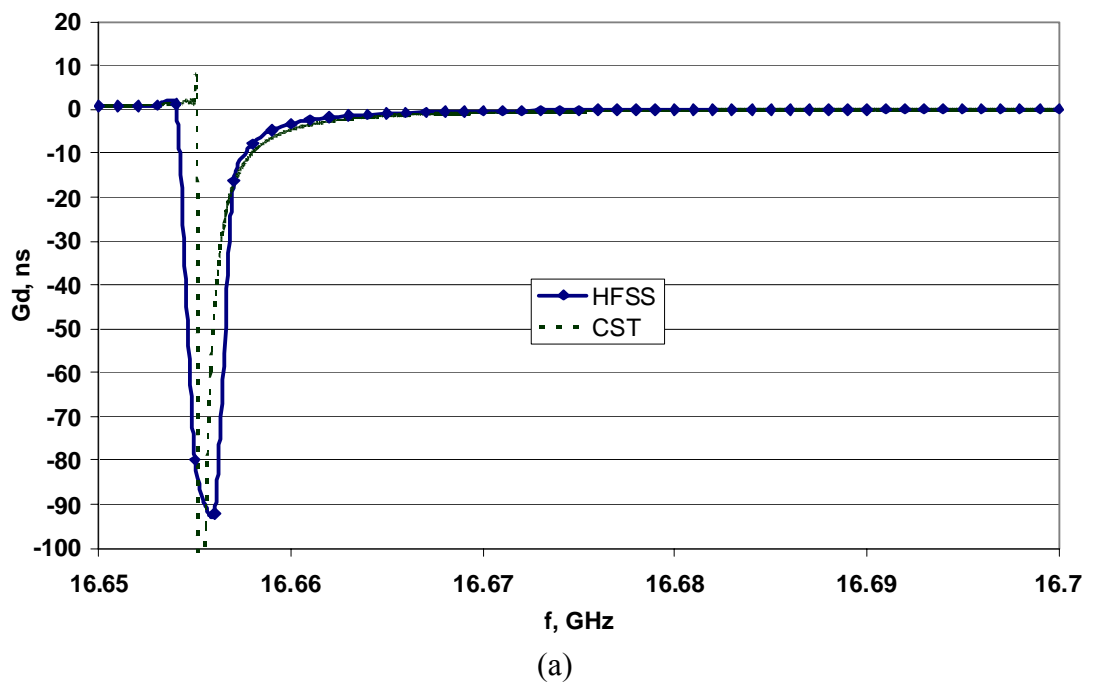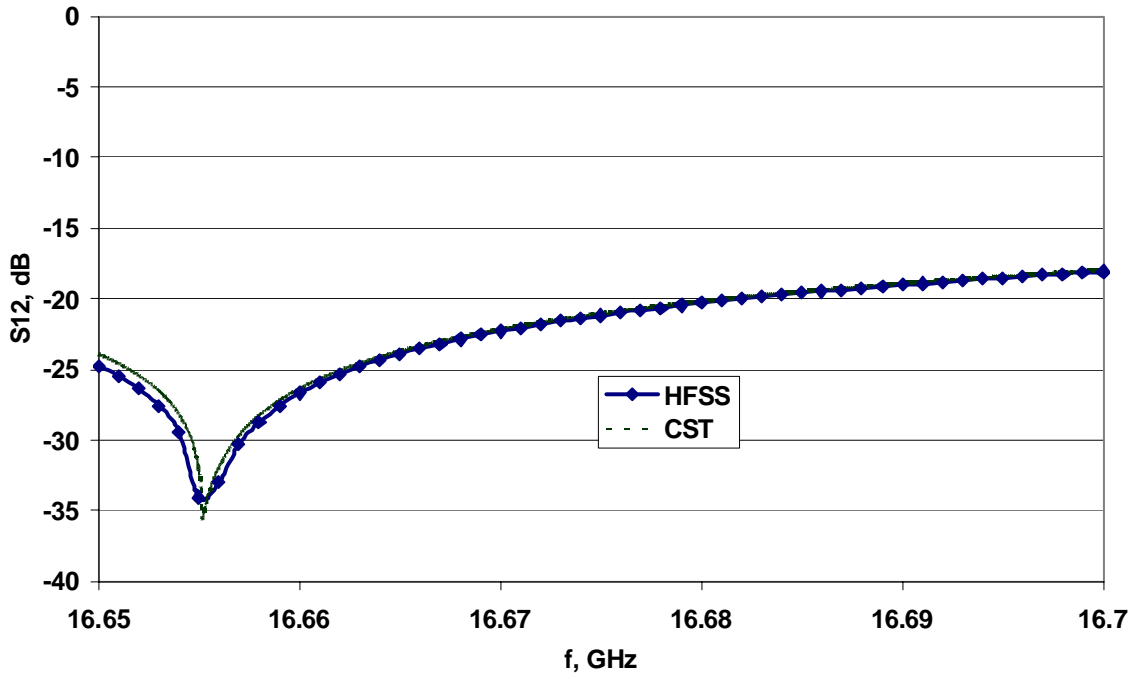
(b)

Fig 6.4 Results for Ex polarization for the structure shown in Fig 6.1c a) Group delay b) transmission .
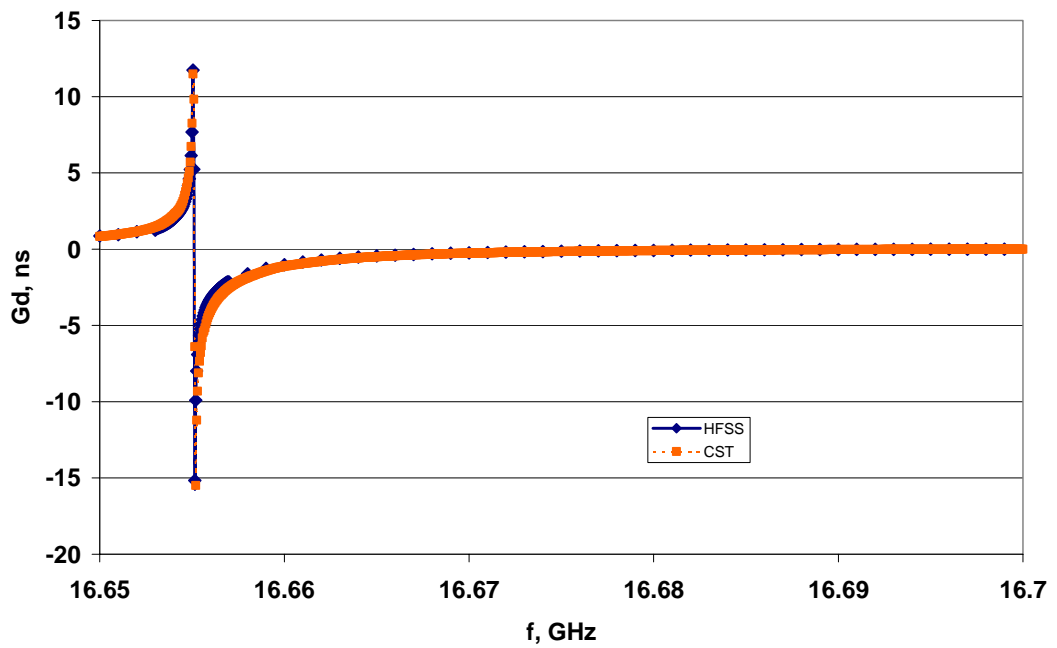
(a)
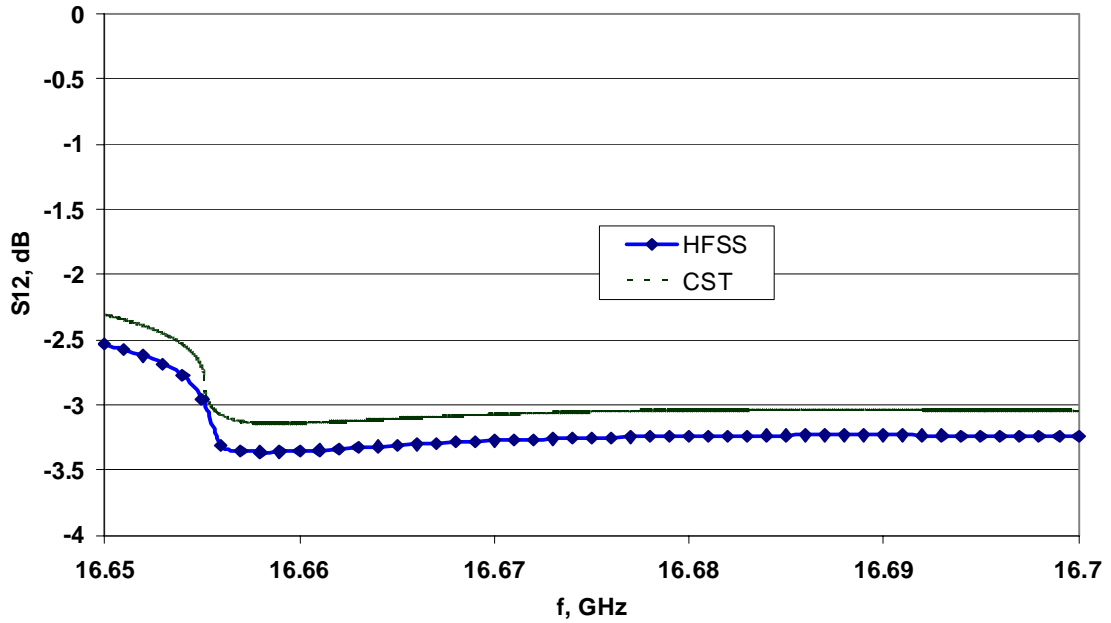
(b)

Fig 6.5 Results for Ey polarization for the structure shown in Fig 6.1c a) Group delay b) transmission

Another important point that must be noted here is that the bandwidth over which group delay occures (Ey polarization) is less than 30MHz, which translates into a minimum pulse width of about 30nS. The pulse width is much wider than the negative group delay. This means as discussed in the theory section that in such a case negative or superluminal group velocities don't imply violation of causality and relativity.

For the Ex polarization, the bandwidth is less than 15MHz giving a pulse width of at least 60nS. The group delay however varies very rapidly with the frequency. If the relatively flat group delay region is to be used then the negative group delay is 1nS at the most, which is much smaller than the pulse width.

6.5 Plasmonic Surface Radar Absorber

A radar absorber based on a waveguide array plasmonic structure was simulated. The array consists of holes of 5mm by 5mm with a period of 8mm in a material of 1.7S/m conductivity. Thickness of the structure is 5mm. Holes are filled with a dielectric with relative permittivity of 4. As the hole dimensions are below half wavelength, the modes inside the holes are below cut-off, and thus plasmonic. Unit cell of structure and results are shown below
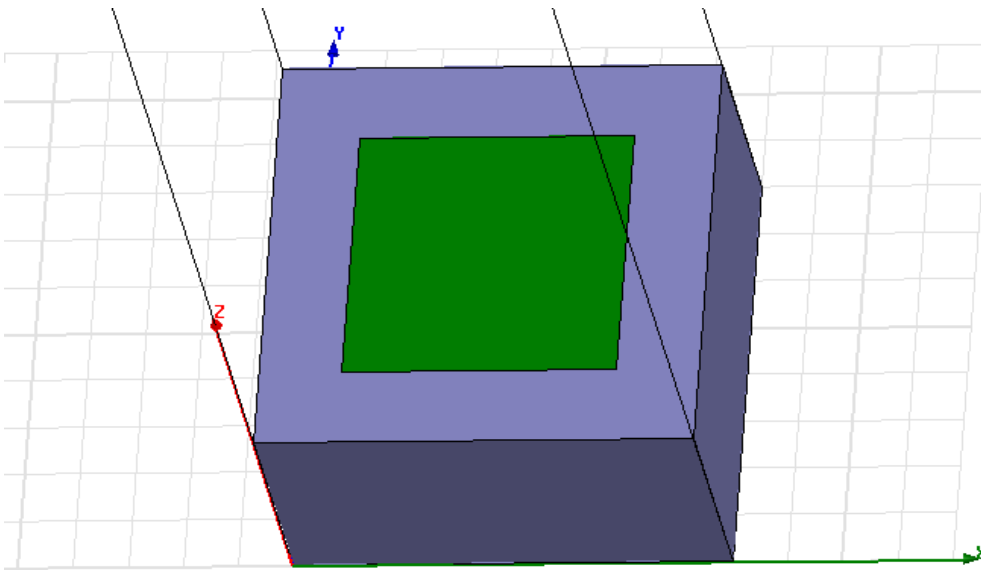
Fig 6.6. Unit cell of plasmonic absorber.

In the results below RCS of a PEC plane covered by the array is compared to that of a PEC plane covered by simple layer of the same lossy material with the same thickness.

From the results it can be observed that the structure gives -10dB of absorption bandwidth from 6.9GHz to 13.2 GHz. It can also be observed from the results that the structured plasmonic gives much better results than a simple layer of same material with the same thickness. This implies role of plasmonic modes in absorption, i.e. that the likely dominant loss mechanism is coupling of the incident wave to lossy plasmonic modes.
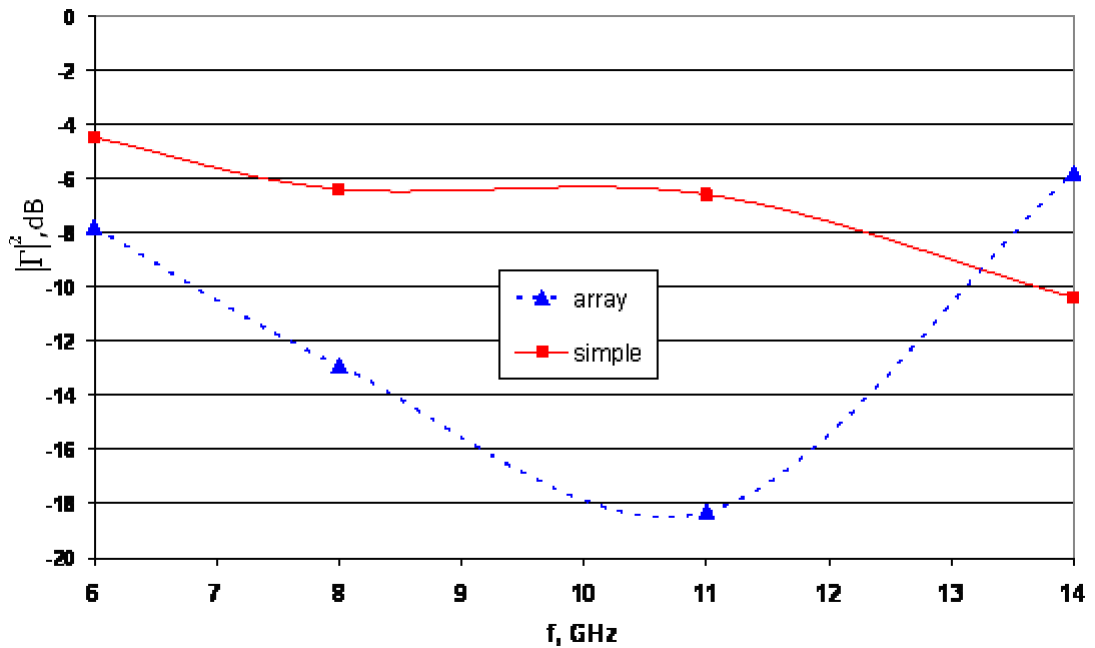
Fig 6.7. Power reflection coefficient for the array and simple layer of lossy material.

To further investigate the performance of the absorber, reflection data was obtained for oblique incidence as well. Results are shown in Fig 6.8
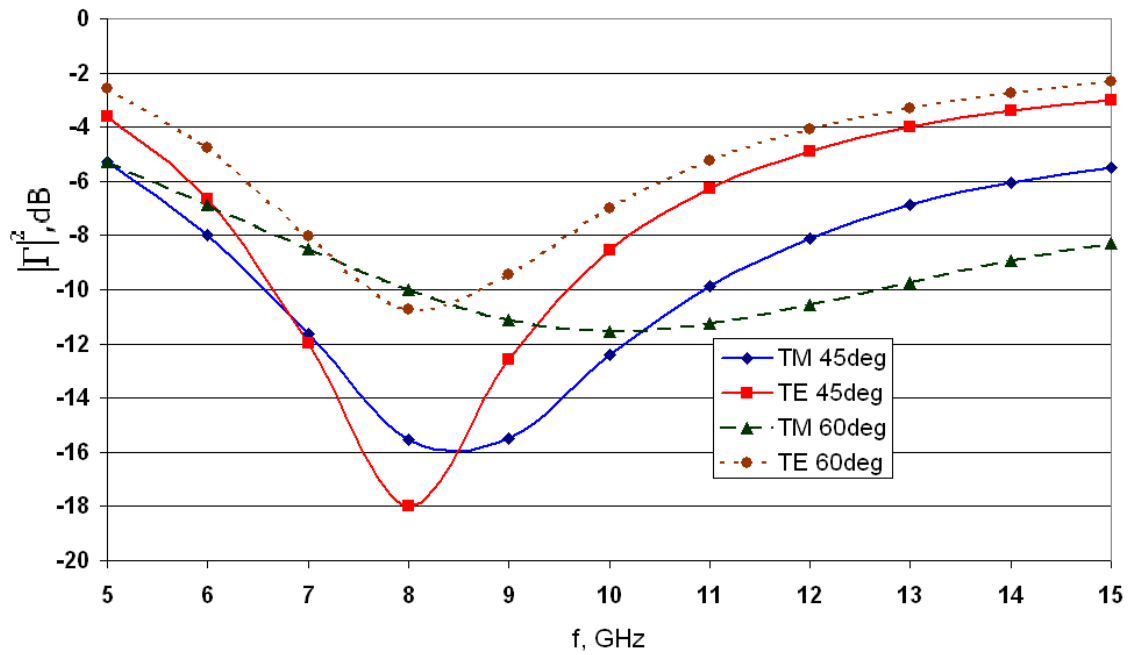
Fig 6.8. Reflection coefficient for the oblique incidence.

From the results it is observed that the proposed absorber not only given good absorption for normal incidence but also for oblique incidence. Moreover low reflection for oblique incidence implies strong attenuation of the surface waves.

6.6 Conclusion

Two plasmonic structures were investigated for both evanescent and regular propagating waves. Numerical results good transmission over a wide bandwidth for both the structures and for both evanescent and propagating waves. The coaxial aperture array gives much higher transmission for regular propagating wave.

It can be inferred from the results that using symmetrical background i.e. have the same material will results in higher transmission.

Furthermore it was observed that certain plasmonic surfaces can give negative group delay with reasonably good transmission for normally incident wave. The structure would be very interesting for studying the interesting phenomenon of superluminous and negative group velocities, and it's implications for the issues like causality and relativity. The trick for realizing a plasmonic structure giving negative and superluminous group delays with good transmission is to bring the transmission band of the structure close to the negative group velocity band.

Finally a radar absorber based on lossy artificial plasmonic structure was investigated. It was observed that such structure gave -10dB absorption bandwidth of nearly one octave.

Chapter 7

Conclusions and Future Works

In this thesis metamaterial based absorbers and plasmonic structures were investigated.

After an overview of the metamaterials, metamaterial absorbers were investigated in Chapters 3 and 4. A novel metamaterial absorber based on the resistive Hilbert curve array was proposed and analyzed [20]. It has been demonstrated that the two layer metamaterial Hilbert curve array constructed from resistive material can act as a thin wideband radar absorbing screen. One of the advantages of using the Hilbert curve over traditional circuit analogue radar absorbing screen is the smaller unit cell size, resulting in the elimination of the coupling to higher order radiating Floquet modes and hence the diffraction effects, which in turn reduces reflection at oblique angles of incidence. The resistive Hilbert curve array gives much wider bandwidth than the conductive space filling curve based absorbing screen. Moreover it gives very good performance even at oblique angles. Furthermore the structure is simpler than a typical circuit analogue radar absorbing screen.

Numerical results showed -10dB absorption bandwidth of nearly one octave, and even at oblique angles of incidence the absorber gave a wide absorption bandwidth. The aforementioned results indicated that smaller unit cell size of the absorber has suppressed diffraction lobes.

Furthermore the concept was extended to terahertz frequencies, and a wideband, wide angle terahertz absorber based on resistive Hilbert curve array was also proposed and

analyzed numerically [21]. The simulation results show a wide absorption fractional bandwidth of more than 100% for normal incidence. The structure also works well for oblique incidence. For the 60° and 45° angles of incidence the -3 dB absorption bandwidths are still of more than 90%, which is much wider than any other terahertz absorbers reported to date. The peak absorption is also very high i.e. 98% for normal incidence and varies from 86% to 94% for oblique incidence. Furthermore the proposed structure is shown to have high tolerance for variation in design parameters

In Chapter 5 plasmonic cloaking was investigated [22, 23]. The plasmonic cloak originally designed for a spherical target was used to cloak non spherical objects. From the results it was concluded that for objects which are small compared to the operating wavelength, and hence can be modelled as superposition of electrical and magnetic dipole, good cloaking can be achieved using hallow shell of magnetic plasmonic material. It was also evident that the geometry of the cloaked object is of little consequence, as long as the dimensions remain roughly the same, the reason being that in case of these small objects the only important parameters are electrical and magnetic dipole moment, which primarily depends on the dimensions in case of conducting objects. For the cube and cylinder, reduction in monostatic RCS, even in the presence of losses was 99%, whereas reduction in maximum Bistatic RCS for cube and cylinder was 92% and 95% respectively. Furthermore limitation of the quasistatic approximation was also investigated and the cloak was analyzed for increasing target size in order to study the limitation of the concept. From the numerical results it was concluded that the cloak provides good cloaking when the object size is less than about 0.6λ, and there is no reduction in the target radar signature once the object becomes larger than the wavelength.

In the case of extended objects, cloaking was achieved as long as E field was directed along the dimension smaller than wavelength (8 dB reduction in maximum Bistatic RCS). For E-field directed along the length of extended objects, cloaking effect is minimal (roughly 3dB only).

Thus the hypothesis that the subwavlength objects could be modelled as combination of electric and magnetic dipoles, with the dipole strength mainly depending on the dimension along E field, stands verified, provided that the other dimensions are not very small, and therefore, such objects could be cloaked by a plasmonic shell.

Furthermore the performance of plasmonic cloak designed for conducting sphere was numerically evaluated for spheres with various values of conductivity; ranging from 0.01 Sm^{-1} to PEC. It was observed that the plasmonic cloak gives quite good performance even for very low values of conductivities. Reduction in monostatic and maximum bistatic RCS in case of sphere with conductivity of 0.01Sm^{-1} was 7.6dB and 8.9 respectively.

Furthermore field profile around 0.01Sm^{-1} cloaked object showed confinement of electric field inside the plasmonic shell just as it is the case with PEC sphere.

It is thus concluded the plasmonic cloak designed for conducting objects, gives good performance even for sphere constructed of low conductivity material, and the cloak performance is not very sensitive to cloaked object conductivity. The cloak gives

reasonably good performance even when the skin depth is larger than the diameter of the sphere, i.e. when the sphere can no longer be considered as good conductor.

From results above, it can be claimed that the plasmonic cloak can give good performance for a wide range of cloaked object dimensions, shapes and conductivities. Furthermore the sensitivity is less if the variation in dimension is not along the E field polarization. The cloaking has thus high tolerance for variation in cloaked object's dimensions.

In Chapter 6 two plasmonic structures based on the Sierpinski carpet array were investigated for extraordinary transmission of the incident wave. Numerical results show a good transmission over a wide bandwidth for both the structures.

A novel plasmonic structure based on an array of modified Apollonian fractal was investigated for negative group velocity. It was observed that the structure gives negative group delay with reasonably good transmission for a normally incident wave, the structure has much higher transmission that a typical negative group velocity structure, as discussed in the previous Chapter. The structure would be very useful for studying the interesting phenomenon of superluminous and negative group velocities, and is very interesting for its implications for the issues like causality and relativity. The trick for realizing a plasmonic structure giving negative and superluminous group delays with good transmission is to bring the transmission band of the structure close to the negative group velocity band.

Finally a radar absorber based on lossy artificial plasmonic structure was investigated in Chapter 6. It was observed that such structure gave -10dB absorption bandwidth of nearly one octave. The structure was constructed from array of lossy waveguides at frequency range below the cutoff. One of the possible absorption mechanisms is coupling of the incident wave to the lossy plasmonic modes.

In summery a novel metamaterial absorber based on resistive Hilbert curve array is proposed and analyzed [20]. The objective was to realize a thin broad band metamaterial absorber which is not sensitive to the variation in design parameters, and gives good performance even at oblique incidence. The structure gave a wide absorption bandwidth [20]. The structure has a unit cell much smaller than the wavelength hence diffraction effects are eliminated [20]. In addition to the microwave absorber a terahertz absorber based on the same resistive Hilbert curve array concept was proposed and analyzed. The absorber provided much wider bandwidth than the standard absorbers [21].

Both the microwave and terahertz absorber were also analyzed for oblique incidence and sensitivity to the variations in design parameters. From the results it was observed that the absorber performance is not very sensitive to the variations in the design parameters and has wide absorption bandwidth even at oblique angles of incidence.

The objective of realizing a thin wide band radar absorber not sensitive to the variation in the design parameters was thus achieved.

The concept of plasmonic cloak was extended for the first time to non spherical subwavelength objects [22,23] and limitation of subwalength approximation was also investigated. The objective was to cloak non spherical subwavelength objects using plasmonic cloak designed for spherical targets and to have an understanding of the limitation of the subwavength approximation for the purpose of plasmonic cloaking in terms of the target size.

Cloaked targets of various sized and geometric shapes were analyzed in HFSS and from the results it was it was observed that a simple plasmonic cloaks works as long as the object is smaller than the wavelength. The objectives of extending the cloaking concept to non spherical object was thus achieved

Furthermore work on artificial plasmonic structure gave interesting results. The objective of work on the artificial plasmonic material was to realize plasmonic structures for wideband extraordinary transmission, negative group velocity, and plasmonic absorbers. Wide band extraordinary transmission band was observed for proposed plasmonic structure. Moreover a completely novel artificial plasmonic structure based on array of Apollonian fractal array of aperture in a conducting surface was analyzed and the results showed the interesting phenomenon of negative group velocity. Finally a novel plasmonic radar absorber was proposed and analyzed and the results showed a wide absorption bandwidth for the plasmonic radar absorber for normal and oblique incidence.

The objective of realizing novel plasmonic structures for extraordinary transmission, negative group velocity and wide band plasmonic absorber was thus achieved.

7.2 Future Work

Metamaterials are very promising for constructing absorbers and studying exotic electromagnetic phenomenon such as negative group velocity. It will be interesting to extend the work presented in the thesis further.

More work can be done on plasmonic cloaking for example studying multilayer cloaks for non spherical objects like cubes and cones, comparing it with performance of these cloaks with spherical targets.

In the case of metamaterial absorbers, new structures based on other fractal such as Peano curve can be designed and investigated. Other option would be combine a Dallenbach screen with a Hilbert curve absorber to make the absorber even more broad band.

The phenomenon of negative group velocity is also very interesting and can be investigated further. For example a periodic waveguide can be constructed by stacking the plasmonic surface, and inserting gain stages between them in order to compensate for the attenuation. Such structures will be interesting from relativistic point of view i.e. what consequences such structures will have for the issue information speed and causality.

References

1. G. V. Eleftheriades, and K. G. Balmain, "Negative-Refraction Metamaterials: Fundamental Principles And Applications," Wiley-IEEE Press, 2005.

2. R.A. Shelby, D.R. Smith, and S. Schultz, "Experimental verification of a negative index of refraction," Science, vol. 292, no. 5514, pp. 77–79, 2001.

3. J. B. Pendry, A. J. Holden, W. J. Stewart, and I. Youngs, "Extremely low frequency plasmons in metallic meso structures," Phys. Rev. Lett., vol. 76, pp. 4773–4776, 1996.

4. J. B. Pendry, A. J. Holden, D. J. Robbins, and W. J. Stewart, "Magnetism from conductors and enhanced nonlinear phenomena," IEEE Transactions on Microwave Theory and Techniques, vol. 47, no. 11, pp. 2075-2084, Nov 1999.

5. J. D. Baena, J. Bonache, F. Martín, R. M. Sillero, F. Falcone, T. Lopetegi, M. A. G. Laso, J. García–García, I. Gil, M. F. Portillo, and M. Sorolla, "Equivalent-Circuit Models for Split-Ring Resonators and Complementary Split-Ring Resonators Coupled to Planar Transmission Lines," IEEE Transactions on Microwave Theory and Techniques, vol. 53, issue 4, pp. 1451-1461, April 2005

6. C. Caloz, H. Okabe, T. Iwai, and T. Itoh, "Transmission line approach of left-handed (LH) materials," in USNC/URSI National Radio Science Meeting, vol. 1, San Antonio, TX, p. 39, June 2002.

7. G. V. Eleftheriades, A. K. Iyer, and P. C. Kremer, "Planar negative refractive index media using periodically L-C loaded transmission lines," IEEE Transactions on Microwave Theory and Techniques, vol. 50, pp. 2702–2712, Dec. 2002.

8. A. Grbic, and G. V. Eleftheriades, "Periodic Analysis of a 2-D Negative Refractive Index Transmission Line Structure," IEEE Transactions on Antennas and Propagation, vol. 51, no. 10, pp. 2604-2611 Oct 2003.

9. C. Caloz "Dual Composite Right/Left-Handed (D-CRLH) Transmission Line Metamaterial, " IEEE Microwave and Wireless Components Letters, vol. 16, no. 11, pp. 585-587, Nov 2006.

10. S. Lim, C. Caloz, , and T. Itoh, Fellow, IEEE, "Metamaterial-Based Electronically Controlled Transmission-Line Structure as a Novel Leaky-Wave Antenna With Tunable Radiation Angle and Beamwidth," IEEE Transactions on Microwave Theory and Techniques, vol. 52, no. 12, pp. 2678-2690, Dec 2004.

11. R. S. Kshetrimayum, L. Zhu, "Guided-Wave Characteristics of Waveguide Based Periodic Structures Loaded With Various FSS Strip Layers," IEEE Transactions on Antennas and Propagation, vol. 53, no. 1, pp. 120-124, Jan 2005.

12. D. J. Kern, D. H. Werner, and M. Lisovich, "Metaferrites: Using Electromagnetic Bandgap Structures to Synthesize Metamaterial Ferrites," IEEE Transactions on Antennas and Propagation, vol. 53, no. 4, pp. 1382-1389, April 2005.

13. C.L. Holloway , E.F. Kuester, J. Baker-Jarvis , P. Kabos, "A double negative (DNG) composite medium composed of magnetodielectric spherical particles embedded in a matrix," IEEE Transactions on Antennas and Propagation, vol. 51, Issue 10, pp. 2596 – 2603, Oct. 2003.

14. B. Seo, T. Ueda, T.Itoh, and H. Fetterman, "Isotropic left handed material at optical frequency with dielectric spheres embedded in negative permittivity medium," Appl. Phys. Lett. 88, 161122, 2006.

15. A. Rennings, C. Caloz, and I. Wolff, "A Novel Clustered Dielectric Cubes Metamaterial (CDC-MTM)", IEEE International Symposium on Antennas and Propagation, pp. 483-486, 2006.

16. J.D. Shumpert, WJ Chappell, and LPB Katehi "Parallel-plate mode reduction in conductor-backed slots using electromagnetic bandgap substrates", IEEE Transactions on Microwave Theory and Techniques, vol. 47, no. 11, pp. 2099-2104 ,NOVEMBER 1999.

17. J. B. Pendry, L. Martin-Moreno, and F. J. Garcia-Cidal "Mimicking surface plasmons with structured surface", Science,vol 305, pp. 847-848, Aug. 2004.

18. N. Engheta, "Thin absorbing screens using metamaterial surfaces," in IEEE AP-S Int. Symp, vol. 2, San Antonio, TX, pp. 392–395, June 16–21 2002.

19. V. G. Veselago, "The Electrodynamics Of Substances With Simultaneously Negative Values Of ε And μ," Soviet Physics Uspekhi , vol. 10, no. 4, pp. 509-514, January-February 1968.

20. A. Noor, and Z. Hu, "Dual polarised wideband metamaterial radar absorbing screen based on resistive Hilbert curve array," Electronic Letters, vol. 45, Issue 2, pp. 130-131, Jan 2009.

21. A. Noor and Z.Hu, "Study of Wideband, Wide Angle, Polarization Independent Metamaterial Hilbert Curve Absorbing Screen for Terahertz Bolometers," Journal of Infrared, Millimeter and Terahertz Waves (Springer), vol. 31, no.7, pp. 791-798, 2010

22. .A. Noor, and Z. Hu, "Cloaking of Sub-wavelength Metallic Objects by Plasmonic Metamaterial Shell in Quasistatic Limit", IET Microwaves Antennas & Propagation, vol.3, Issue 1, pp. 40-46, , Feb 2009.

23. A. Noor, and Z. Hu, "Effect of Target conductivity on Plasmonic Cloak," in LAPC 2009(Loughborough Antennas & Propagation Conference), pp. 273-276, 2009.

24. D.M. Pozar, "Microwave Engineering," 2nd Ed, John Wiley & Sons, 1999.

25. W. W. Salisbury, "Absorbent body for electromagnetic waves," US Patent 2599 944, filed May 11 , 1943, granted June 10, 1952.

26. W. H. Emerson, "Electromagnetic wave absorbers and anechoic chambers through the years," IEEE Transactions on Antennas and Propagation, vol. 21, no. 4, pp. 484-490, July 1973.

27. Y. Zhang, R. Mittra, B.-Z. Wang and N.-T. Huang, "AMCs for ultra-thin and broadband RAM design," Electronics Letters, 45(10), pp. 484-5, 2009.

28. A. Alù, and N. Engheta, "Achieving transparency with plasmonic and metamaterial coatings," Phys. Rev. E, 72, 016623, 2005.

29. J. B. Pendry, D. Schurig, D. R. Smith, "Controlling electromagnetic fields," Science, vol. 312, no. 5781, pp. 1780 - 1782, 23 June 2006.

30. A. J. Ward and J. B. Pendry, "Refraction and geometry in Maxwell's equations," Journal Of Modern Optics, vol. 43, no.4 , pp. 773-793, 1996.

31. D. Schurig, J. J. Mock, B. J. Justice, S. A. Cummer, J. B. Pendry, A. F. Starr, and D. R. Smith, "Metamaterial Electromagnetic Cloak at Microwave Frequencies," Science, vol 314,. no. 5801, pp. 977 - 980, 10 November 2006 .

32. A. Alù and N. Engheta, "Cloaking and transparency for collections of particles with metamaterial and plasmonic covers," Optics Express, vol. 15, no. 12, pp. 7578-7590, 11 June 2007.

33. A. Alù and N. Engheta, "Plasmonic materials in transparency and cloaking problems: mechanism, robustness, and physical insights," Optics Express, vol. 15, no. 6, pp. 3318-3332, 19 March 2007.

34. M. A. Antoniades, and G. V. Eleftheriades, "Compact Linear Lead/Lag Metamaterial Phase Shifters for Broadband Applications," IEEE Antennas And Wireless Propagation Letters, vol. 2, pp. 103-106, 2003.

35. E. L. Ginzton, W. R. Hewlett, J. H. Jasburg, and J. D. Noe, "Distributed amplification," in Proc. IRE, vol. 36, pp. 956-969, 1948.

36. C. Caloz, F. P. Casares-Miranda, and C. Camacho-Peñalosa, "Active Metamaterial Structures and Antennas," in IEEE MELECON 2006, Benalmádena (Málaga), Spain. (Invited paper) , pp. 268-271, May 16-19 2006.

37. A. Grbic and G. V. Eleftheriades, "A backward-wave antenna based on negative refractive index L-C networks," in Proc. IEEE Antennas Propagat. Soc. Int. Symp. Dig., vol. 4, pp. 340–343, Jun. 2002.

38. L. Lei, C. Caloz, and T. Itoh, "Dominant mode leaky-wave antenna with backfire-to-endfire scanning capability," Electronics Letters., vol. 38, no. 23, pp. 1414–1416, Nov. 2002.

39. A. Grbic and G. V. Eleftheriades, "Experimental verification of backward-wave radiation from a negative refractive index metamaterial", Journal Of Applied Physics, vol. 92, no. 10, pp. 5930 – 5935, 15 November 2002.

40. J. R. James and P. S. Hall, "Handbook of Microstrip Antennas". London, U.K. Peter Peregrinus, 1989.

41. M. Pozar and D. H. Schaubert, "Microstrip Antennas: The Analysis and Design of Microstrip Antennas and Arrays," New York: IEEE Press, 1995.

42. S. Maci, G. Biffi Gentili, P. Piazzesi, and C. Salvador, "Dual-band slot-loaded patch antenna," Proc. Inst. Elect. Eng. Microw. Antennas Propag., vol. 142, no. 3, pp. 225–232, Jun. 1995.

43. R. Porath, "Theory of miniaturized shorting-post microstrip antennas," IEEE Transactions on. Antennas and Propagation, vol. 48, no. 1, pp. 41–47, Jan. 2000.

44. A. Alù , F. Bilotti, N. Engheta, and L. Vegni, "Subwavelength, Compact, Resonant Patch Antennas Loaded With Metamaterials", IEEE Transactions On Antennas And Propagation, vol. 55, no. 1, pp. 13-25, January 2007

45. Chambers B, "Optimum design of a Salisbury screen radar absorber," Electronics Letters, 30, pp. 1353-1354, 1994.

46. Chambers B, and A. Tennant, "Characteristics of a Salisbury screen radar absorber covered by a dielectric skin," Electronics Letters vol. 30 no. 21, pp.1797-1799, 13th October 1994.

47. E. F. Knott, and K. B. Langseth, "Performance Degradation of Jaumann Absorbers due to Curvature," IEEE Transactions On Antennas And Propagation, vol. 28, no. 1, pp. 137-139, January 1980.

48. A. Cheldavi, and M. Kamarei, "Optimum Design of N sheet capacitive Jaumann Absorber using Genetic Algorithm," in IEEE International Symposium on Antennas and Propagation , Digest, vol. 4, pp. 2296-2299, 1997.

49. H. Severin, "Nonreflecting absorbers for microwave radiation," IRE Transactions On Antennas And Propagation., vol. AP4, pp. 385-392, July 1956.

50. W. Dallenbach, and W. Kleinsteuber, "Reflection and Absorption of Decimetre-Waves by Plane Dielectric Layers," Hochfreg Eleklroak, vol. 51, pp. pp. 152-156, 1938.

51. S. Chamaani, S. Mirtaheri, and M. Shooredeli "Design of very thin wide band absorbers using modified local best particle swarm optimization," Int. J. Electron. Commun. (AEÜ) 62, pp. 549 – 556, 2008.

52. K. Matouˇs and G. J. Dvorak, "Optimization of Electromagnetic Absorption in Laminated Composite Plates," IEEE Transactions on Magnetics, vol. 39, no. 3, pp.1827-1835 , MAY 2003

53. Oh JH, Oh KS, Kim CG, and Hong CS, "Design of radar absorbing structures using glass/epoxy composite containing carbon black in X-band frequency ranges," Compos Part B,35, pp.49–56, 2004.

54. W. Chin, D. Lee, "Development of the composite RAS (radar absorbing structure) for the X-band frequency range," Composite Structures 77, pp. 457–465, 2007.

55. Micheli, D., and R. Pastore, "Carbon based nanomaterial composites in RAM and microwave shielding applications," 2009 9th IEEE Conference on Nanotechnology (IEEE-NANO 2009), pp. 226-235, 26-30 July 2009.

56. P Zhihua, P Jingcui, P Yanfeng, O Yangyu, and N Yantao, "Complex permittivity and microwave absorption properties of carbon nanotubes/polymer composite: a numerical study," Physics Letters A 372(20), pp. 3714-3718, 2008.

57. B. T. Caudle1, G. T. Flowers, M. E. Baginski1, S. M. Wentworth1, and S. M. Rao, "Recent developments in radar absorbing paints and the zinc oxide tetrapod whisker," 2009 IEEE International Conference on Microwaves,

Communications, Antennas and Electronics Systems - COMCAS, pp.1-4, 9-11 Nov. 2009.

58. H. Zhang, J. Zhang, and H. Zhang, "Computation of radar absorbing silicon carbide foams and their silica matrix composites," Computational Materials Science 38, pp. 857–864, 2007.

59. N. Roy, "Berechnung und Messung von dunnen Einschicht und Zweischichtabsorben fur elektromagnetische Wellen im Frequenzbereich von 4–200 MHz'' Z. Angew. Phys, vol 19, no. 4, pp. 303–310, 1965.

60. Y. Fan , H. Yang , X. Liu , H. Zhu and G. Zou, "Preparation and study on radar absorbing materials of nickel-coated carbon fiber and flake graphite," Journal of Alloys and Compounds 461(1-2), pp. 490-494, 2008.

61. S. Liu, L. Zhang, J. Zhou, and R. Wu, "Structure and properties of cellulose/Fe2O3 nanocomposite fibers spun via an effective pathway," Journal of Physical Chemistry C 112(12), pp. 4538-4544, 2008.

62. E. Naito, K. Suetake, H. Matsumura,, and E. Fuziwara, "Matching Frequencies of Ferrite-Based Microwave Absorbers," Densi Tsusin Gakkai Rombunsi, vol. 52B, no. 7, pp. 398–404, 1969.

63. Lv, D., C. Tong, and J. Wang "RCS simulation of plasma-coated targets modeled by NURBS surfaces," in IEEE Asia Pacific Microwave Conference (APMC 2009), pp. 673-676, 7-10 Dec. 2009.

64. Yeo, J. and D. Kim , "Novel tapered AMC structures for backscattered RCS reduction," Journal of Electromagnetic Waves and Applications, 23(5-6), pp. 697-709 , 2009.

65. Q.-R. Zheng, Y.-M. Yan, X.-Y. Cao, and N.-C. Yuan, "High impedance ground plane (HIGP) incorporated with resistance for radar cross section (RCS)

reduction of antenna," Progress in Electromagnetics Research 84, pp. 301-13, 2008.

66. J. McVay, N. Engheta, and A. Hoorfar, "Thin Absorbers Using Space-Filling-Curve High-Impedance Surfaces," IEEE Antennas and Propagation Society International Symposium, 3-8 July 2005, vol. 2A, pp. 22- 25, 2005.

67. B. Zheng and Z. Shen, "Wideband radar absorbing material combining high-impedance transmission line and circuit analogue screen," Electronics Letters, vol. 44 no. 4, pp. 318-319, 14th February 2008.

68. W. Tang and Z. Shen, "Simple design of thin and wideband circuit analogue absorber," Electronics Letters, vol. 43 no. 12, pp. 689-691, 7th June 2007.

69. J. Yang and Z. Shen, "A thin and broadband absorber using double-square loops," IEEE Antennas and Wireless Propagation Letters, vol.6, pp.388-391, Dec 2007.

70. E.F. Knott and C.D Lunden, "The two-sheet capacitive Jaumann absorber," IEEE Transactions on Antennas and Propagation, vol. AP- 43, no.11, pp. 1339 – 1343, 1339-1343, Nov. 1995.

71. Z. Shen and H. Wang, "On the Optimum Design of a Thin Absorbing Screen," in IEEE Antennas and Propagation Society International Symposium, pp. 6039-6042, 2007.

72. P. V. Wright, B Chambers, A Barnes, K Lees and A Despotakis, "Progress in smart microwave materials and structures," Smart Mater. Struct. 9, pp. 273–279, 2000.

73. G. I. Kiani, K. L. Ford, K. P. Esselle, A. R. Weily, and C. J. Panagamuwa ,"Oblique Incidence Performance of a Novel Frequency Selective Surface

Absorber," IEEE Transactions on Antennas and Propagation, vol. 55, no. 10, pp. 2931-2934, October 2007.

74. S. Simms and V. Fusco, "Chessboard reflector for RCS reduction," Electronics Letters, vol. 44, no. 4, pp. 316-317, 14th February 2008.

75. J. McVay, N. Engheta, and A. Hoorfar, "High impedance metamaterial surfaces using Hilbert-curve inclusions," IEEE Microwave and Wireless Components Letters, vol. 14, no. 3, pp. 130-132, , March 2004.

76. A. Ishimaru "Electromagnetic Wave Propagation, Radiation and Scattering," Prentice Hall, 1991.

77. P. Z. Peebles, "Radar principles," Wiley Interscience, 1998.

78. K.N. Rozanov and S.N. Starostenko , "Numerical study of bandwidth of radar absorbers", Eur. Phys. J. AP 8, pp. 147-151 (1999).

79. E Knott, " Radar Cross section," 2nd Ed, SciTech Pub, 2004.

80. E Knott, "Radar cross section reduction using cylindrical segments," IEEE Transactions on Antennas and Propagation, November, vol.24, issue 6, pp. 882-884, 1976.

81. K.J. Vinoy, K.A. Jose, V.K. Varadan, and V.V. Varadan, "Resonant Frequency of Hilbert Curve Fractal Antennas," in IEEE International Symposium on Antennas and Propagation , vol.3, pp.648-651, 2001.

82. S. A. Tretyakov and S. I. Maslovski , "Thin absorbing structure for all incidence angles based on the use of a high-impedance surface", Microwave And Optical Technology Letters , vol. 38, no. 3, pp. 175-178, August 5 2003.

83. H. Tao, C. M. Bingham, A. C. Strikwerda, D. Pilon, D. Shrekenhamer, N. I. Landy, K. Fan, X. Zhang, W. J. Padilla, and R. D. Averitt, "Highly flexible

wide angle of incidence terahertz metamaterial absorber: Design, fabrication, and characterization," Physical Review B, 78, 241103(R), 2008.

84. N. I. Landy, C. M. Bingham, T. Tyler, N. Jokerst, D. R. Smith, and W. J. Padilla "Design, theory, and measurement of a polarization-insensitive absorber for terahertz imaging, " Physical Review B, 79, 125104,2009.

85. Tao H, Landy NI, Bingham CM, Zhang X, Averitt RD, Padilla WJ., "A metamaterial absorber for the terahertz regime: design, fabrication and characterization," Optics Express 16(10), 7181-8, 2008.

86. M. Diem, T Koschny, and C. M. Soukoulis, "Wide-angle perfect absorber/thermal emitter in the terahertz regime," Physical Review B (Condensed Matter and Materials Physics) 79(3): 033101 (4 pp.), 2009.

87. Qi-Ye Wen, Huai-Wu Zhang, Yun-Song Xie, Qing-Hui Yang, and Ying-Li Liu, "Dual band terahertz metamaterial absorber: design, fabrication, and characterization," Applied Physics Letters 95(24): 241111 (3 pp.), 2009.

88. M. Tonouchi, "Cutting-edge terahertz technology," Nature Photon., vol. 1, pp. 97–105, 2007.

89. I. Kaˇsalyna, A.J.L. Adam, T. O. Klaassen, J. N. Hovenier, G. Pandraud, V.P. Iordanov, and P. M. Sarro, "Design and Performance of a Room-Temperature Terahertz Detection Array for Real-Time Imaging", IEEE Journal of Selected Topics in Quantum Electronics, vol. 14, no. 2, pp. 363-369, March/April 2008.

90. D. P. Neikirk and D. B. Rutledge, "Air-bridge microbolometer for farinfrared detection," Appl. Phys. Lett., vol. 44, pp. 153–155, 1984.

91. P. L. Richards, "Bolometers for infrared and millimeter waves," J. Appl. Phys., vol. 76, no. 1, pp. 1–24, Jul. 1994.

92. Taino, T., and H. Ishii et al "Terahertz electromagnetic-wave detector using Nb-based superconducting tunnel junction on LiNbO3 substrate absorber," Physica C: Superconductivity and its applications, vol. 463-465: pp. 1119-22, 2007

93. Ariyoshi, S., T. Taino. A. Dobroiu, H. Sato, H. Matsuo, and C. Otani, "Terahertz detector based on a superconducting tunnel junction coupled to a thin superconductor film," Applied Physics Letters 95(19): 193504 (3 pp.), 2009.

94. Stevenson, T. R., and J. S. Adams et al, "Superconducting films for absorber-coupled MKID detectors for sub-millimeter and far-infrared astronomy," IEEE Transactions on Applied Superconductivity 19(3): 561-4, 2009.

95. Teperik T. V., Garcia de Abajo F. J., Popov V. V. and Shur M. S. , "Strong terahertz absorption bands in a scaled plasmonic crystal," Applied Physics Letters 90(25): 251910-1, 2007.

96. E. A. Shaner, M. C. Wanke1, A. D. Grine1, S. K. Lyo1, J. L. Reno1, and S. J. Allen, "Enhanced responsivity in membrane isolated split-grating-gate plasmonic terahertz detectors.," Applied Physics Letters 90(18): 181127-1, 2007.

97. H. Hashiba, V. Antonov, L. Kulik, A. Tzalenchuk, P. Kleinschmidt, S. Giblin, and S. Komiyama, "Isolated quantum dot in application to terahertz photon counting," Phys. Rev. B, Condens. Matter, vol. 73, no. 8, pp. 081 310(R), Feb. 2006.

98. P. Kleinschmidt, S. P. Giblin, V. Antonov, H. Hashiba, L. Kulik, A. Tzalenchuk, and S. Komiyama, "A Highly Sensitive Detector for Radiation in

the Terahertz Region,", IEEE Transactions On Instrumentation And Measurement, vol. 56, no. 2, pp. 463-467, APRIL 2007.

99. H. Hashiba, V. Antonov, L. Kulik, S. Komiyama, and C. Stanley, "Highly sensitive detector for submillimeter wavelength range," Appl. Phys. Lett., vol. 85, no. 24, pp. 6036–6038, Dec. 2004.

100. E. Perret, N. Zerounian, S. David, and F. Aniel, "Complex permittivity characterization of benzocyclobutene for terahertz applications," Microelectronic Engineering, 85 , pp. 2276–2281, 2008

101. Shalaev, and G.W. Milton, "Nonmagnetic cloak with minimized scattering", Appl. Phys. Lett. 91, 111105 ,2007.

102. Alu, A. and N. Engheta, "Multifrequency optical invisibility cloak with layered plasmonic shells," Physical Review Letters 100(11): 113901-1, 2008

103. F. Bilotti., S. Tricarico, and L. Vegni , "Plasmonic metamaterial cloaking at optical frequencies," IEEE Transactions on Nanotechnology 9(1), pp. 55-61, 2010.

104. M. G. Silveirinha, A. Alu, and N. Engheta , "Infrared and optical invisibility cloak with plasmonic implants based on scattering cancellation," Physical Review B (Condensed Matter and Materials Physics) 78(7), 075107-1, 2008.

105. Wang, H. and X. Zhang "Achieving multifrequency transparency with cylindrical plasmonic Cloak," Journal of Applied Physics 106(5), 053302 (6 pp.), 2009.

106. Alu, A. and N. Engheta , "Peculiar and anomalous cloaking features of plasmonic materials," 2009 International Conference on Electromagnetics in Advanced Applications. ICEAA 2009, Piscataway, NJ, USA, IEEE, 14-18 Sept. 2009.

107. S. Tricarico, F. Bilotti, L. Vegni, "Plasmonic and non-plasmonic layered structures for cloaking applications at visible frequencies," Microwave and Optical Technology Letters 51(11), pp. 2713-17, 2009.

108. M. G. Silveirinha, A. Alù, and N. Engheta, "Cloaking mechanism with antiphase plasmonic satellites," Physical Review B (Condensed Matter and Materials Physics) 78(20), 205109 (9 pp.), 2008.

109. A. Greenleaf, Y. Kurylev, M. Lassas and G. Uhlmann, "Electromagnetic Wormholes and Virtual Magnetic Monopoles from Metamaterials," Phys. Rev. Lett, vol. 99, 183901, 2007.

110. W. Cai, U. K. Chettiar, A. V. kildishev and V. M. Shalaev, "Optical cloaking with metamaterials," Nature Photonics 1, vol. 1, pp. 224-227 , April 2007.

111. F. Zolla, S. Guenneau, A. Nicolet, J. B. Pendry, "Electromagnetic analysis of cylindrical invisibility cloaks and the mirage effect," Optics Letters, vol. 32, no. 9, pp. 1069-1071, May 1 2007.

112. H. Chen and C. T. Chan, "Transformation media that rotate electromagnetic fields", Applied Physics Letters, 90, 241105 , 2007.

113. F. L. Teixeira, "Closed-Form Metamaterial Blueprints for Electromagnetic Masking of Arbitrarily Shaped Convex PEC Objects," IEEE Antennas and Wireless Propagation Letters, vol. 6, pp. 163-164, 2007.

114. Nicorovici, N. A., McPhedran, R. C. & Milton, G. W, "Optical and dielectric properties of partially resonant composites," Phys. Rev. B (Solid State), 490, pp. 8479–8482,1994.

115. Graeme W. Milton , Nicolae-Alexandru , and P. Nicorovici, "On the cloaking effects associated with anomalous localized resonance," Proc. R. Soc. A, 462, pp. 3027-3059, 2006.

116. N. A. Nicorovici, G. W. Milton, R. C. McPhedran, and L. C. Botten, "Quasistatic cloaking of two-dimensional polarizable discrete systems by anomalous resonance," Optics Express 15(10), pp. 6314-22, 2007.

117. A. Hakansson, "Cloaking of objects from electromagnetic fields by inverse design of scattering optical elements," Optics Express, vol. 15, no. 7, pp. 4328-4334, 2 April 2007.

118. B. Wood and J. B. Pendry, "Metamaterials at zero frequency," J. Phys Condens. Matter, 19, 076208 , 2007.

119. P. Alitalo, O. Luukkonen1, L. Jylh, J. Venermo, and S. Tretyakov, "Transmission-line networks cloaking objects from electromagnetic fields," arXiv, 0706.4376v1, 29 June 2007.

120. Constantine A. Balanis., "Advanced Engineering Electromagnetics," John. Wiley & Sons, New York, 1989.

121. A. Digeron and T.W.Ebbesen , "The role of localized surface plasmon modes in the enhanced transmission of periodic subwavelength apertures," J. Opt. A: Pure Appl. Opt, 7 , S90–S96, 2005.

122. L.Martín-Moreno, F.García-Vidal, H. J.Lezec, K. M.Pellerin, T.Thio, J.B. Pendry, and T.W.Ebbesen, "Theory of Extraordinary Optical Transmission through Subwavelength Hole Arrays," Physical Review Letters, 86, pp. 1114 – 1117, 2001.

123. A. Ishimaru "Electromagnetic Wave Propagation, Radiation and Scattering," Prentice Hall, 1991.

124. Zenneck, J. "Propagation of plane electromagnetic waves along a plane conducting surface and its bearing on the theory of transmission in wireless telegraphy," Annalen der Physik, 23(5), pp. 846-866, September 1907.

125. E. Kretschmann, " Bestimmung optischer Konstanten von Metallen durch Anregung von Oberflächenplasmaschwingungen, " Zeitschrift für Physik A Hadrons and Nuclei, vol. 241, no. 4, pp. 313–324, , Aug. 1971.

126. S. Nie and S.R. Emory, "Probing single molecules and single nanoparticles by surface-enhanced Raman scattering," Science, vol. 275, no. 5303, pp. 1102–1106, Feb. 1997.

127. H. Xu, E. J. Bjerneld, M.Käll, and L Börjesson "Spectroscopy of Single Hemoglobin Molecules by Surface Enhanced Raman Scattering," Phys. Rev. Lett, 83, pp. 4357 – 4360, 1996.

128. C. J. L. Constantino, T. Lemma, P. A. Antunes, and R. Aroca "Single-Molecule Detection Using Surface-Enhanced Resonance Raman Scattering and Langmuir−Blodgett Monolayers," Anal. Chem., 2001, 73 (15), pp. 3674–3678.

129. Wu. J.-J Yang T.-J, and Shen. L.F, "Subwavelength microwave guiding by a periodically corrugated metal wire," Journal of Electromagnetic Waves and Applications, 23(1), pp. 11-19 , 2009.

130. M.-H. Lee , "40 Gbit/s light signal transmission in long-range surface plasmon waveguides," Appl. Phys. Lett., vol. 9,. 171117., Oct. 2007.

131. Dionne. J.A., Sweatlock. L.A, Sheldon. M.T., Alivisatos. A.P, and Atwater. H.A, "Silicon-based plasmonics for on-chip photonics," IEEE Journal of Selected Topics in Quantum Electronics, 16(1), pp. 295-306, 2010.

132. J. T. Kim, J. J. Ju, S. Park, M-su Kim, S. K. Park, and M-H Lee, "Chip-to-chip optical interconnect using gold long-range surface plasmon polariton waveguides," Optics Express, vol. 16, Issue 17, pp. 13133-13138, 2008

133. P. Berini, "Plasmon-polariton waves guided by thin lossy metal films of finite width: Bound modes of symmetric structures," Phys. Rev. B, 61, pp. 10484-10503, 2000.

134. A Alu, P. A. Belov, and N Engheta, "Parallel-chain optical transmission line for a low-loss ultraconfined light beam," Physical Review B (Condensed Matter and Materials Physics, 80(11): 113101 (4 pp.) , 2009.

135. T. Nikolajsen, K. Leosson, I. Salakhutdinov, and S. I. Bozhevolnyi , "Polymer-based surface-plasmon polariton stripe waveguides at telecommunication wavelengths," Appl. Phys. Lett., 82, pp. 668-670, 2003.

136. T. Tsuchizawa, T. Watanabe, K. Yamada, H. Fukuda, S. Itabashi, J. Fujikata1, A.Gomyo, J. Ushida1, D. Okamoto1, K. Nishi, and K. Ohashi, "Low-loss silicon oxynitride waveguides and branches for the 850-nm-wavelength region," Japanese Journal of Applied Physics, 47(8), pp. 6739-6743, 2008.

137. J. J. Ju, S. Park, M. Kim, J. T. Kim, S. K. Park, Y. J. Park, and M. Lee, "Polymer-based long-range surface plasmon polariton waveguides for 10-Gbps optical signal transmission applications," Journal of Lightwave Technology, 26(11), pp. 1510-1518, 2008.

138. W. S., N. Fang, C. Sun, Q. Luo, and X. Zhang, "Plasmonic Nanolithography," NANO LETTERS, vol. 4, no. 6, pp.1085-1088, 2004.

139. X. Luo and T. Ishihara, "Surface plasmon resonant interference nanolithography technique," Appl. Phys. Lett, 84, pp. 4780-4782, 2004.

140. X. Guo, J. Du, Y. Guo, and J. Yao, "Large-area surface-plasmon polariton interference lithography," Optics Letters, vol. 31, Issue 17, pp. 2613-2615, 2006.

141. N. Feth, C. Enrich, M. Wegener, and S. Linden, "Large-area magnetic metamaterials via compact interference lithography," Optics Express, vol. 15, Issue 2, pp. 501-507 , 2007.

142. Ahmadi, A. and H. Mosallaei , "The image performance of a negative index slab and a layered slab using coupled surface modes," Journal of Applied Physics, 106(6): 064502 (7 pp.) , 2009.

143. C. Wang, C. Du, and X Luo, "Surface plasmon resonance and super-resolution imaging by anisotropic superlens," Journal of Applied Physics, 106(6): 064314 (4 pp.) , 2009.

144. Akbari, A. and P. Berini, "Schottky contact surface-plasmon detector integrated with an asymmetric metal stripe waveguide," Applied Physics Letters, 95(2): 021104 (3 pp.) , 2009.

145. M Zhang, C Huang, G Wang, and Y Zhu, "Theory of extraordinary light transmission through sub-wavelength circular hole arrays," Journal of Optics (UK), 12(1): 015004 (5 pp.), 2010.

146. X R Huang, R W Peng, Z Wang, F Gao, and SS Jiang , "Charge-oscillation-induced light transmission through subwavelength slits and holes," Physical Review A (Atomic, Molecular, and Optical Physics, 76(3), pp. 1-4, 2007.

147. A. Krishnan, T. Thio, T.J. Kim, H.J. Lezec, T.W. Ebbesen, P.A. Wolff, J. Pendry, L. Martin-Moreno, and F.J. Garcia-Vidal, "Evanescently coupled resonance in surface plasmon enhanced transmission," Optical Communication, , 200, pp. 1-7, 2001

148. Yang, S.-H. and P. R. Bandaru, "Effect of surface texture and geometry on spoof surface plasmon dispersion," Optical Engineering, 47(2): 029001-1, 2008.

149. Y-J Bao, H-M Li, X-C Chen, R-W Peng, M Wang, X Lu, J Shao, and N-B Ming, "Tailoring the resonances of surface plasmas on fractal-featured metal film by adjusting aperture configuration," Appl. Phys. Lett., 92, 151902-3, 2008

150. Talebi, N. and M. Shahabadi, "Spoof surface plasmons propagating along a periodically corrugated coaxial waveguide," Journal of Physics D: Applied Physics, 2010, 43(13): 135302 (8 pp.)

151. Fernandez-Dominguez, A. I., Martin-Moreno, L., Garcia-Vidal, F. J., Andrews, S. R., and Maier, S. A., "Spoof surface plasmon polariton modes propagating along periodically corrugated wires," IEEE Journal on Selected Topics in Quantum Electronics, 14(6), pp. 1515-21, 2008.

152. Z Fu, Q Gan, YJ Ding, and FJ Bartoli , "From waveguiding to spatial localization of THz waves within a plasmonic metallic grating," IEEE Journal on Selected Topics in Quantum Electronics, 14(2), pp. 486-90, 2008.

153. B. Bai, X. Meng, J. Laukkanen, T. Sfez, L. Yu, W. Nakagawa, H. P. Herzig, L. Li, and J. Turunen, "Asymmetrical excitation of surface plasmon polaritons on blazed gratings at normal incidence," Physical Review B (Condensed Matter and Materials Physics, 80(3): 035407 (11 pp.),2009.

154. Kuznetsova, T. I. and V. S. Lebedev, "Transmission of evanescent modes through a subwavelength aperture of a cylindrical waveguide. 1. Ideal metal approximation," Quantum Electronics, 39(5), pp. 455-62 , 2009.

155. Tserkezis. C , Papanikolaou. N , Almpanis. E, and Stefanou. N, "Tailoring plasmons with metallic nanorod arrays," Physical Review B (Condensed Matter and Materials Physics, 80(12): 125124(9pp.), 2009.

156. T. Okamoto, I. Yamaguchi and T. Kobayashi, "Local plasmon sensor with gold colloid monolayers deposited upon glass substrates," Optics. Letters.,vol.25 , no. 6, pp. 372-374, 2000.

157. W Fan, S Zhang, B Minhas, KJ Malloy, and SRJ Brueck, "Enhanced Infrared Transmission through Subwavelength Coaxial Metallic Arrays," Physical Review Letters, 94(3): 0339029(4pp.) , 2005.

158. Ishizaki, K. and S. Noda, "Manipulation of photons at the surface of three-dimensional photonic crystals," Nature, 460(7253), pp. 367-70 , 2009.

159. J. Stratton, "Electromagnetic Theory," McGraw Hill, 1941

160. M Zamboni-Rached, F Fontana, and E Recami, "Superluminal localized solutions to Maxwell equations propagating along a waveguide: the finite-energy case," Physical Review E (Statistical, Nonlinear, and Soft Matter Physics) , 67(3): 36620-7, 2003.

161. Y. Japha, and G. Kurizki , "Superluminal delays of coherent pulses in nondissipative media: a universal mechanism," Physical Review A (Atomic, Molecular, and Optical Physics, 53(1), pp. 586-90, 1996.

162. W. M. Robertson, "Transmission-line matrix modeling of superluminal electromagnetic-pulse tunneling through the forbidden gap in two-dimensional photonic band structures," Journal of the Optical Society of America B (Optical Physics), 14(5), pp. 1066-73, 1997.

163. L. Brillouin, "Wave Propagation and Group velocity," Academic Press, New York, 1960.

164. M. Mojahedi, K.J. Malloy, and G.V. Eleftheriades, "Abnormal wave propagation in passive media," IEEE Journal on Selected Topics in Quantum Electronics, 9(1), pp. 30-39 , 2003.

165. M. Mojahedi, E Schamiloglu, F. Hegeler, and K.J. malloy, "Time-domain detection of superluminal group velocity for single microwave pulses," physics Review E, vol.62, pp. 5758-5766, 2000.

166. A. Noor, and Z. Hu, "Metamaterial Dual Polarized Resistive Hilbert Curve Array Radar Absorber," IET Microwaves Antennas and Propagation, 2010, vol. 4, Issue. 6, pp. 667–673.